Theoretical Study of non-equilibrium transport in Kondo quantum dots

Raphaël van Roermund

THÈSE

présentée par

RAPHAËL VAN ROERMUND

pour obtenir le grade de

DOCTEUR DE L'UNIVERSITÉ DE GRENOBLE
SPÉCIALITÉ : PHYSIQUE

THEORETICAL STUDY OF NON-EQUILIBRIUM TRANSPORT IN KONDO QUANTUM DOTS

Soutenue le 20 octobre 2010 devant la Commission d'Examen :

Pr.	Frank Hekking	Président
Pr.	Hans Kroha	Rapporteur
Dr.	Christophe Mora	Rapporteur
Pr.	Mihail Kiselev	Examinateur
Dr.	Mireille Lavagna	Directrice de thèse

MÉMOIRE PRÉPARÉ AU SEIN DU SERVICE DE PHYSIQUE STATISTIQUE,
MAGNÉTISME ET SUPRACONDUCTIVITÉ, INAC, CEA GRENOBLE

Contents

Acknowledgments

I would like to thank Mireille Lavagna for her kindness and her patience during these three years. I am also quite grateful to Sean (Shiue-yuan to be more precise) Shiau, who taught me the EOM technique and read all the notes I sent him. I am also thankful to Leonid Glazman for devoting me part of his precious time for what will remain the richest exchanges I had in physics these last three years. I also had the chance to share fruitful discussions with Durga Nandini, Hector Mera, Serge Florens, Sabine Andergassen and Adeline Crépieux. I also enjoyed exchanging ideas with great physicists as Benjamen Doyon, Natan Andrei, Takis Kontos and Denis Feinberg. If I started a PhD in physics, I should mention two fantastic physics teachers, Daniel Baye and Marc Haelterman, who certainly influenced me in that direction by transmitting me their passion. I would like to cite my advisors during my master thesis, Pascal Vanlaer and Pierre Marage, with whom I enjoyed my first research experience and from whom I learned many things that still help me today. Finally, I would like to thank my pencil that always lent an ear to my ideas.

As strange as it could sound from a theorist, I could not live without a social life. I had the chance to meet fantastic persons that I hope will stay life-long friends. I would like to mention Sean again for tolerating me for two years in his office even when my papers started overflowing on his desk side. I do appreciate your conversation a lot and your open-minded viewpoint on many issues. I spent fantastic moments with Pierre-Éric too, as much inside or outside CEA. I enjoyed a lot discussing with you on so many subjects I could fill in another thesis. I would never have known so much on beans agriculture or cases in Tagalok without you. It has also been a pleasure to spend time with other PhDs or post-docs in the lab such as Martin, Vincent, Alejandro, Yu, Caroline, Driss, Cyril and Vitaly. I also enjoyed the arrival of new permanents as Xavier, Manuel and Julia who gave a new soul to this theory group. Eventually I had the chance to spend time with many nice people outside CEA such as Oana, Ioan, Danny, Germain, Leaticia, Claudia, Benoît, Paul, Daniel, Andrei, Lauranne and so many others. Thanks to all of you for those nice moments.

Finally I should thank the two most important persons in my life without whom I would not be here. Florence who never complained when I came back late in the evening or when I worked on week-ends. Florence whose unfailing tolerance influenced me and gave me the strength to go over these three years. Florence for all the nice moments we had and will have. I finish with my mother who transmitted me her energy and her

faith in the future. Thank you for supporting me when I changed from electricity to physics. In that way, this work is also yours.

Abstract

In the absence of exact theoretical methods, many questions related to the non-equilibrium Anderson model have remained unsolved and are at the origin of an intense research activity. In this thesis I discuss transport through quantum dots put in the Kondo regime by means of an equations-of-motion method that was developed in order to account for the non-equilibrium effects and in particular the decoherence of the virtual spin-flip processes involved in the Kondo effect. I compare my results to previous approximations and show the improvements brought by the new decoupling scheme, which solves pathologies at the particle-hole symmetric point and enables the description of the system over a wide range of parameters. A decoherence rate is derived for the excitations which is shown to involve a crossover from the strong- to the weak-coupling regime when either the temperature or the bias voltage or the magnetic field is increased. In the light of this result, I conclude on the applicability of the present equations-of-motion scheme out of equilibrium. I also discuss observables out of equilibrium; the differential conductance exhibits a zero-bias peak reaching a maximum value $G = 2e^2/h$. Its low-energy behavior turns out to be universal after the bias voltage is normalized by the Kondo temperature. I finally show that a finite magnetic field splits the zero-bias peak in the differential conductance. The actual distance between the peaks is discussed in the light of recent experiments for which I give a phenomenological explanation. A new experimental setup is proposed in order to verify my assumptions.

Résumé

En l'absence de méthodes théoriques exactes, beaucoup de questions liées au modèle d'Anderson hors d'équilibre n'ont pas encore trouvé de solution, engendrant une intense activité de recherche. Dans cette thèse, je discute le transport à travers des boîtes quantiques placées dans le régime Kondo au moyen d'une méthode d'équations du mouvement développée afin de tenir compte des effets de non-équilibre, et en particulier de la décohérence des processus virtuels de spin-flip impliqués dans l'effet de Kondo. Je compare mes résultats aux approximations précédentes, et montre les améliorations apportées par le nouveau schéma de découplage, qui résout les pathologies au point de symétrie particule-trou et permet la description du système dans une vaste gamme de paramètres. Je dérive un taux de décohérence pour les excitations, et montre son implication dans le passage du régime de couplage fort à celui de couplage faible sous l'effet d'une différence de potentiel, de la température ou d'un champ magnétique. À la lumière de ce résultat, j'étudie l'applicabilité des équations du mouvement hors d'équilibre. Je discute ensuite l'évolution d'observables hors d'équilibre ; la conductance différentielle présente un pic centré autour d'une différence de potentiel nulle et atteignant une value maximale $G = 2e^2/h$. Son comportement à basse énergie se révèle universel lorsque la différence de potentiel est normalisée par la température Kondo. Je montre finalement qu'un champ magnétique divise le pic dans la conductance différentielle. La distance exacte entre les deux sommets est discutée à la lumière d'expériences récentes, pour lesquelles je donne une explication phénoménologique, et je propose un nouveau schéma expérimental pour vérifier mes hypothèses.

Introduction

"It would indeed be remarkable if Nature fortified herself against further advances in knowledge behind the analytical difficulties of the many-body problem."

Max Born, 1960

Many-body quantum physics deals with systems containing large numbers of particles and with the correlations among them. In many cases, the interactions on the microscopic level involve fantastic modifications of the behavior of the macroscopic system. Therefore, many-body physics is at the origin of a vast number of theoretical problems in condensed matter physics, as for example superconductivity, Bose-Einstein condensation or Luttinger liquids.

A new playground for the study of quantum correlations was opened in the eighties when the improvement of experimental techniques enabled the confinement of electrons in small regions of typical length of a few nanometers (a few tens of atoms), called quantum dots. This opened the field for descriptions at the interface between microscopic and macroscopic physics. The new discipline, called mesoscopic physics, studies objects containing large numbers of particles, but that are nevertheless sensitive to quantum fluctuations. It is of great interest in the prospect of applications in the electronics industry, which aims at a constant miniaturization of the size of the transistors.

In this work, I study the Kondo effect [46] that results from a many-body exchange interaction of itinerant electrons with a localized spin state. It was first studied in bulk systems after the measurement of a strong increase of the resistivity at low temperature in dilute magnetic alloys in the 1930s. The explanation for that experiment was given by J. Kondo about 30 years later and lies in coherent scattering processes in which the internal spin state of the impurity and of the scattered electron are exchanged, giving rise to logarithmically divergent contributions for the resistivity, and hence providing a satisfactory explanation to the above-cited experimental results. For a spin-1/2 magnetic moment, A.H. Wilson demonstrated that the localized impurity and the delocalized conduction electrons are bound together in a spin singlet Ground State [105].

The interest for the Kondo effect has undergone a strong revival these last ten years after its observation in small quantum dots tunnel-coupled to two-dimensional reservoirs of conduction electrons (also called leads) [32, 20, 94]. When the quantum

dot contains an odd number of electrons, it carries a spin that interacts with the spin of the conduction electrons in a very similar way to the case of dilute magnetic alloys. At low temperature, the many-particle spin-flip processes involved in the Kondo effect allow for the conduction electrons to tunnel freely from a reservoir to the other. As a consequence, system is completely transparent at zero temperature and the linear conductance of the system reaches the conductance quantum $2e^2/h$ (i.e. the maximum value for a single conductance channel). Thanks to the excellent tunability of their parameters (dot energy levels, charging energy, tunnel coupling, ...) quantum dots have broadened the horizon for the study of the Kondo effect, raising new questions and opening new areas for research.

On the theoretical level, the Kondo effect in quantum dots is often described by a model due to P.W. Anderson [7] in which the magnetic moment comes as a consequence of a localized Coulomb repulsion on the dot. When the chemical potentials of the leads are equal, the system is at equilibrium and most of its properties are now well understood as the Anderson model was solved by a panel of powerful techniques [36]. However most of them fail out of equilibrium, involving a huge interest for new methods to tackle the problem of the Kondo effect in that case, and more generally to study non-equilibrium effects in strongly-correlated electron systems.

An important theoretical feature of the non-equilibrium Kondo effect is the decoherence of the spin singlet Ground State associated to the Kondo effect [41], which evolves to a Steady State in the presence of electronic current through the device [24]. Within this framework, the theoretical description of the Kondo effect is far more cumbersome and no exact result has been obtained so far, leaving the door open for additional investigation. In this thesis the system is driven out of equilibrium by applying a bias voltage between the two leads connecting the dot. An equations-of-motion method is developed out of equilibrium in order to discuss some theoretical aspects of decoherence and its consequences on the physical behavior of the system. I also discuss other sources of decoherence for the the spin-flip processes such as the temperature and the magnetic field.

This manuscript is organized as follows: Chapter 1 introduces the main features of the Kondo effect, both on the theoretical and experimental point of views. I start with a short history of its discovery and its early explanations, and discuss the new fundamental problems it raised. I give the main consequences of the Kondo effect for the transport through quantum dots, and the experimental signatures that are associated with. Finally, I discuss the challenges for its future study.

Chapter 2 describes the equations-of-motion formalism that I used for solving the Anderson model. I review several approximation schemes proposed in the literature and discuss their successes and weaknesses. I propose and motivate an extension of those approximations in order to deal with non-equilibrium setups. I give the result for the Green's function and send the reader to Appendix B for more details about its derivation.

Chapter 3 presents the main features of the Kondo effect at equilibrium, in the framework of the different approximations developed in Chap. 2. I discuss the im-

provement brought by our approach in comparison with the decouplings at lower order, and compare with the experimental results. At the end of the chapter, I discuss the temperature-induced decoherence rate for the spin-flip excitations, and show the influence on the density of states in the dot.

Chapter 4 is dedicated to non-equilibrium transport through the quantum dot in the absence of magnetic field. I discuss the splitting of the Kondo resonance in the density of states inside the dot in the presence of a bias voltage, and the smearing of the corresponding peaks by the decay rates of the excitations. From the smearing of the divergent terms, a criterion is derived for the crossover from the strong- to the weak-coupling regime, where the perturbative corrections are small, and I discuss the applicability of the equations-of-motion method out of equilibrium. Eventually, I show the numerical results for the differential conductance, which develops a peaked structure at low bias, and compare it with the results obtained by other methods.

Chapter 5 is devoted to the influence of a magnetic field on the non-equilibrium transport through a quantum dot. The zero-bias peak in the differential conductance is split by an energy close to the double of the Zeeman splitting, as observed experimentally. The differential conductance is shown to be sensitive to the decoherence of the Kondo spin singlet Ground State, which has consequences on the distance between the peaks. An explanation is proposed for the crossover between a regime where this distance is smaller than twice the Zeeman splitting to another where it is larger, and is related to the decoherence effects. Finally, I propose an experimental setup that could detect a possible additional contribution to the decoherence rate.

All along this thesis, I have tried to present the developments as pedagogically as possible, hoping it could be useful to another Ph.D. student or any researcher who would like to continue this work and investigate other aspects of the non-equilibrium Anderson model using the equations-of-motion technique. This results in some technical sections - especially in Sec. 2 and App. B - essential for a deep understanding of the method, its applicability and limitations. The reader more interested in new physical results is directly sent to Chaps. 3, 4 and 5.

Chapter 1

General aspects on the Kondo effect and electronic transport through quantum dots

The improvement in the experimental fabrication processes over the last few years, together with the cryogenic techniques, brought to the surface the discovery of a wide range of new phenomena. For instance, by reaching sufficiently low temperatures to kill the thermal fluctuations, one has been able to reach quantum regimes where the transport properties are essentially determined by many-particle phenomena like superconductivity or the Kondo effect.

In this thesis, we describe the low-temperature transport through devices whose three dimensions are smaller than the coherence length. These objects, called quantum dots, are often referred to as artificial atoms (molecules) as the spacial confinement induces a discrete energy spectrum which can be tuned by acting on external parameters.

We give a general introduction on the electronic transport through quantum dots and the Kondo effect. In particular, we describe its signatures in the conductance and the theoretical challenges out of equilibrium. For more details on other aspects of the Kondo effect, see for instance [61, 82].

1.1 History of the Kondo effect in dilute magnetic alloys

For temperatures lower than the Debye temperature, the resistivity of a metal is essentially determined by electron-phonon scattering and decreases with T as $\rho(T) \propto T^5$. At even lower temperatures, it eventually saturates to a minimum resistivity which was found to be related to the scattering by the defects of the crystal lattice. However, in 1934, a different behavior was pointed out in an experiment on gold samples cooled down below 10K, in which a dramatic increase of the resistivity was observed at low temperature [22].

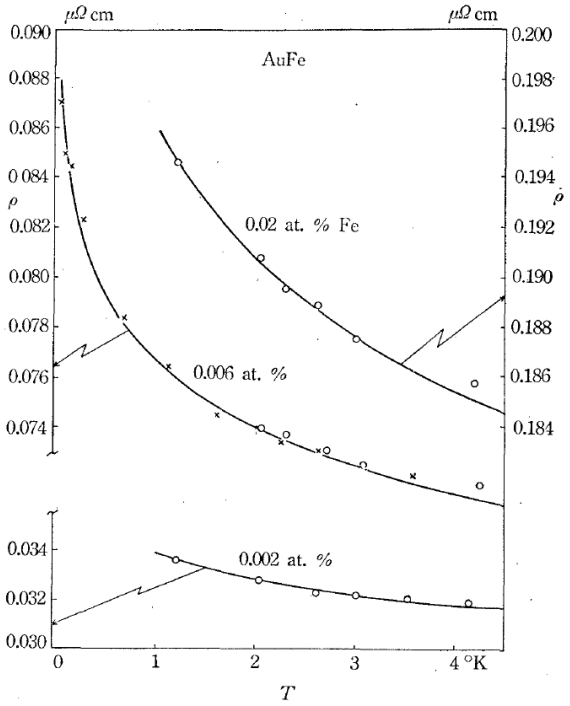

Figure 1.1: Comparison of the theoretical results obtained by Kondo and the experimental results for the temperature dependence of the resistivity in dilute magnetic alloys [46].

This remained a mystery until 1964, when an experiment showing the evidence of a relationship between this behavior and the presence of dilute magnetic impurities [90] motivated the Japanese theorist Jun Kondo to consider a model involving an antiferromagnetic exchange interaction J between the magnetic impurities and the sea of conduction electrons [46]. Using perturbation theory in J, he observed that the next-to-leading order terms involve logarithmic corrections responsible for the increase of the resistivity at low temperature

$$\rho(T) = aT^5 + c_{imp}\rho_0 - c_{imp}\rho_1 \ln(k_B T/D), \tag{1.1}$$

where the first term is the phonon contribution, the second one is the temperature-independent contribution from impurity scattering, and the final one accounts for spin-flip scattering off the local moment, which is responsible for the low-temperature increase of the resistivity. The comparison with experiments is given in Fig 1.1, and shows a very good agreement for different concentrations of impurities.

On the theoretical level, an earlier important model was developed for the description of localized impurities in a conduction electron bath, namely the *Anderson model* [7]. This model involves a short-range Coulomb interaction U between electrons on the localized site. Interestingly, it has been shown that the Kondo model can be derived from the Anderson model by mapping out the states with zero and double oc-

cupancy [96], which means that the local interaction U is responsible for the formation of local moments.

Although the pioneering work by Kondo had brought an accurate explanation for the experiments, it soon raised new questions as the logarithmic corrections diverge at zero temperature. After resummation on the infinite series of log-divergent terms [1], the divergence in the resistivity is shifted to an energy scale T_K, called *Kondo temperature*. Therefore, the results are valid only for $T \gg T_K$, and new conceptual techniques are required to study the regime $T \ll T_K$. This limitation, often referred to as the *Kondo problem*, called for a development of a non-perturbative method, and was solved by Wilson in 1975 by means of a new (logarithmic) renormalization group approach [105]. Within this new technique, the system is described by a strong coupling fixed point resulting in a spin singlet the Ground State between the magnetic impurity and the surrounding sea of conduction electrons. The effective interactions among the quasi-particles resulting from the polarization of the singlet are responsible for the power-law dependence of the resistivity in T^2/T_K^2 observed at low temperature.

In parallel, some low-energy effective Hamiltonians were derived in the 70s by Nozières [76] and Yamada [108], in terms of a Landau Fermi liquid theory that derived the $T \ll T_K$ results. Finally, exact solutions were found in the 80s for the thermodynamic properties of spin $S = 1/2$ case by means of Bethe ansatz techniques, both for the Kondo model [8] and the Anderson model [103].

This is however not the end of the end of the story. Indeed, an exact analytical solution is still missing for calculating the dynamical response of the system, which is needed to compare with some experimental techniques such as photo-emission or neutron scattering, or to study more exotic forms of Kondo effect.

1.2 Kondo effect in mesoscopic physics

In the last decade, there has been a strong experimental revival of the Kondo effect through the development of quantum dots, as it had been suggested theoretically long time before [10]. Quantum dots made possible the investigation of the Kondo effect on a much wider range of parameters, bringing with them many new challenging questions for the theorists.

1.2.1 Physical picture of a quantum dot

A quantum dot is a device in which a few electrons are confined in a region whose three dimensions are smaller than the coherence length of the electrons in the material. Experimentally, there are several ways to build a quantum dot, each of them offering different advantages: lateral and vertical semiconductor dots, and carbon nanotube quantum dots [61, 32, 91, 83]. In parallel, several experiments have been done where the quantum dot is replaced by a molecule (e.g. C_{60}), opening new perspectives to the existing issues [80, 84, 85]. In this thesis, we will mostly focus on the description of

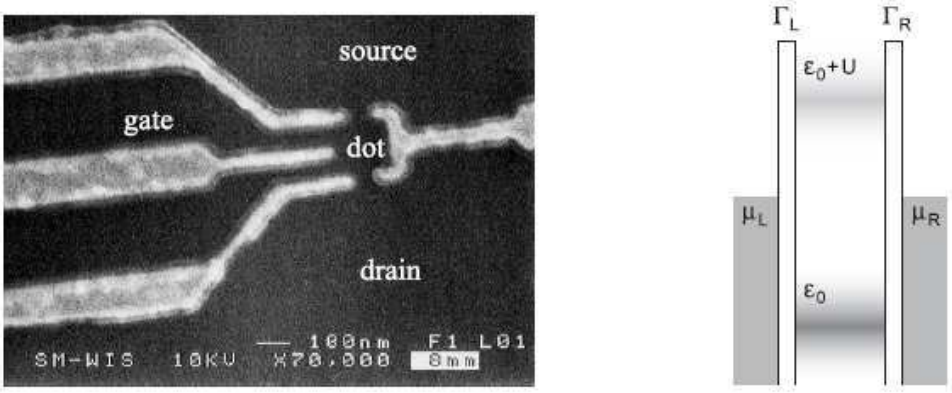

Figure 1.2: The left image shows a lateral quantum dot obtained by Scanning Electron Microscopy (SEM) [61]. The dot consists of a little region of an 2D electron gas, where the electrons are confined electrostatically by applying potentials on the gates. The transport happens between the extended 2D electron gases (source and drain) by tunneling electrons through the dot. The right image represents the energy levels in the system, with the discrete energy levels inside the dot connected to 2D Fermi seas through tunneling barriers.

lateral quantum dots, even if most of our results can be extended to the other setups.

To manufacture a lateral quantum dot, a two dimensional electron gas (2DEG) is formed by confining electrons at the interface of a semiconductor heterostructure (e.g. $GaAs/AlGaAs$). Several metallic gates are deposited on the top of the 2DEG, as shown on Fig 1.2. By applying a voltage on those gates, a small droplet of confined electrons can be defined, constituting the lateral quantum dot. Depending on the voltages applied on the different gates, one can cover a wide range of parameter regions. For instance, the central gate on Fig 1.2 can be used to control the electron occupancy in the dot. This size is of the order of a few tens of nanometers, much smaller than the electron coherence length, implying that only discrete quantum energy levels can be occupied by the electrons on the dot. The side gates control the tunnel-coupling with the extended sections of the 2DEG (called leads). In order to study the electronic transport through the system, the device can be driven out of equilibrium by applying a bias voltage V between the two leads (also called source and drain).

As we will see, much interesting physics comes from the fact that such a quantum dot has a very small capacitance, and therefore adding or removing an electron costs a large energy $2e^2/C$. As a consequence, the total occupation number of electrons inside the dot will be a well defined integer number N (the dot is in the state $|N\rangle$), except for the transition regions from $|N\rangle$ to $|N \pm 1\rangle$.

On the theoretical level, the Hamiltonian of the system can be decomposed in three parts

$$\mathcal{H} = \mathcal{H}_{dot} + \mathcal{H}_{leads} + \mathcal{H}_{tun}, \tag{1.2}$$

where $\mathcal{H}_{dot}$ describes the dot where the interactions take place, $\mathcal{H}_{leads}$ is the Hamilto-

nian for the non-interacting leads, and $\mathcal{H}_{tun}$ stands for the tunneling through the two junctions.

The isolated quantum dot can be modeled by

$$\mathcal{H}_{dot} = \sum_{i\sigma} \varepsilon_{i\sigma} \hat{n}_{i\sigma} + \frac{U}{2} \sum_{i\sigma} \sum_{i'\sigma' \neq i\sigma} \hat{n}_{i\sigma} \hat{n}_{i'\sigma'}, \tag{1.3}$$

with $\hat{n}_{i\sigma} = f^{\dagger}_{i\sigma} f_{i\sigma}$, where $f_{i\sigma}$ is the annihilation operator of an electron of spin σ on the i^{th} energy level in the quantum dot (with energy $\varepsilon_{i\sigma}$). The charging energy $2e^2/C$ for adding an electron on the dot is modeled as a Coulomb repulsion U between electrons.

In experiments, the dot is connected to extended 2DEG playing the role of the leads, which are described by non-interacting Fermi liquids

$$\mathcal{H}_{leads} = \sum_{\alpha k\sigma} \varepsilon_k \hat{n}_{\alpha k\sigma}, \tag{1.4}$$

where $\hat{n}_{\alpha k\sigma} = c^{\dagger}_{\alpha k\sigma} c_{\alpha k\sigma}$ and $c^{\dagger}_{\alpha k\sigma}(c_{\alpha k\sigma})$ is the creation (annihilation) operator of an electron of momentum k and spin σ in the $\alpha(= L,\ R)$ lead (with energy ε_k). The momentum distributions for electrons inside the two leads are given by Fermi-Dirac functions $f_\alpha(\varepsilon_k) = f(\varepsilon_k - \mu_\alpha)$, where μ_α is the chemical potential in the lead α.

Finally, the dot and the leads are connected through tunnel barriers

$$\mathcal{H}_{tun} = \sum_{\alpha k i\sigma} \left(t_{\alpha i\sigma} c^{\dagger}_{\alpha k\sigma} f_{i\sigma} + H.c. \right), \tag{1.5}$$

where $t_{\alpha i\sigma}$ is the tunneling matrix element between the state $|k\alpha\sigma\rangle$ in the lead α, and the state $|i\sigma\rangle$ in the dot. For simplicity, we assume $t_{\alpha i\sigma}$ to be real[1] and k-independent.

This model was originally introduced by Anderson to describe localized magnetic impurities in metals [7], and obtained a revival of interest with its application to quantum dot devices.

1.2.2 Current through a quantum dot

Let us consider a quantum dot connected to two leads (left and right). When a bias voltage is applied to the leads ($eV = \mu_L - \mu_R$), the system is driven out of equilibrium and a current is induced through the quantum dot. The current I within the Anderson model is expressed by the generalized Landauer formula [68, 21] accounting for the interactions among electrons

$$I = \frac{2e}{\hbar} \sum_{\sigma} \int_{-W}^{W} d\varepsilon \frac{\Gamma_{L\sigma}(\varepsilon)\Gamma_{R\sigma}(\varepsilon)}{\Gamma_{L\sigma}(\varepsilon) + \Gamma_{R\sigma}(\varepsilon)} \left[f_L(\varepsilon, V) - f_R(\varepsilon, V) \right] \rho_\sigma(\varepsilon, V), \tag{1.6}$$

where

[1] A complex phase would not change anything to the quantities discussed in this thesis since they involve only $|t_{\alpha i\sigma}|^2$

- W is the half-bandwidth of the conduction electron band in the leads,
- $\Gamma_{\alpha\sigma}(\varepsilon)$ is the tunneling rate of the spin σ dot electron at energy ε into the lead α, defined as $\Gamma_{\alpha\sigma}(\varepsilon) = \pi \sum_k t^2_{\alpha\sigma} \delta(\varepsilon - \varepsilon_{\alpha k}) = \pi t^2_{\alpha\sigma} \nu_\alpha(\varepsilon)$ with $\nu_\alpha(\varepsilon)$ the unrenormalized density of states at energy ε in the lead α,
- $f_\alpha(\varepsilon) = \{\exp[(\varepsilon - \mu_\alpha)/k_B T] + 1\}^{-1}$ is the Fermi-Dirac distribution function in the lead α,
- $\rho_\sigma(\varepsilon, V)$, the local density of states for spin σ in the dot, can be expressed in terms of the retarded electron Green's function in the dot $\mathcal{G}^r_\sigma(\varepsilon)$ according to $\rho_\sigma(\varepsilon) = -1/\pi \mathrm{Im}\mathcal{G}^r_\sigma(\varepsilon)$, where the dependence on V is implicit.

As pointed out in Ref. [68], Eq. (1.6) is valid provided that the tunneling couplings for both leads $\Gamma_{L\sigma}(\varepsilon)$ and $\Gamma_{R\sigma}(\varepsilon)$ differ only by a constant multiplicative factor. In the following, we take a constant density of states in the leads $\nu = 1/2W$, and therefore $\Gamma_{\alpha\sigma} = \pi t^2_{\alpha\sigma} \nu$ is also constant.

The differential conductance dI/dV can be derived from Eq. (1.6)

$$\begin{aligned} \frac{dI}{dV} &= \frac{2e}{\hbar} \sum_\sigma \frac{\Gamma_{L\sigma}\Gamma_{R\sigma}}{\Gamma_{L\sigma} + \Gamma_{R\sigma}} \int_{-W}^{W} d\varepsilon \left[\frac{df_L(\varepsilon, V)}{dV} - \frac{df_R(\varepsilon, V)}{dV} \right] \rho_\sigma(\varepsilon, V) \\ &\quad + \frac{2e}{\hbar} \sum_\sigma \frac{\Gamma_{L\sigma}\Gamma_{R\sigma}}{\Gamma_{L\sigma} + \Gamma_{R\sigma}} \int_{-W}^{W} d\varepsilon \left[f_L(\varepsilon, V) - f_R(\varepsilon, V) \right] \frac{d\rho_\sigma(\varepsilon, V)}{dV}. \end{aligned} \tag{1.7}$$

At equilibrium $V = 0$ and zero temperature, this simplifies to

$$G = \lim_{V \to 0} \frac{dI}{dV} = \frac{2e}{\hbar} \sum_\sigma \frac{\Gamma_{L\sigma}\Gamma_{R\sigma}}{\Gamma_{L\sigma} + \Gamma_{R\sigma}} \rho_\sigma(\varepsilon_F), \tag{1.8}$$

The linear conductance is related to the density of states in the dot at the Fermi level of the leads. Throughout this thesis, we choose the Fermi energy ε_F as origin of the energy axis ($\sum_\alpha \mu_\alpha = 0$).

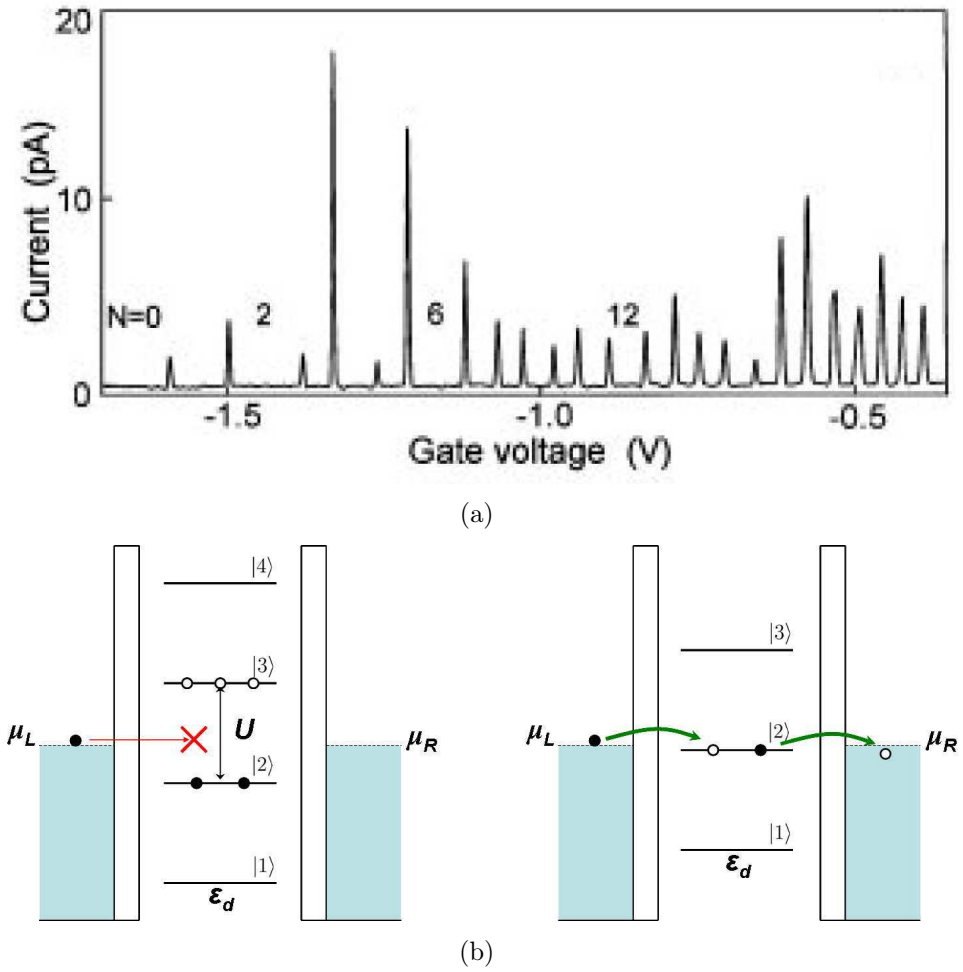

Figure 1.3: (a) Linear (zero-bias) conductance as a function of the gate voltage in the Coulomb blockade regime [97]. (b) Cartoon explaining the single-particle tunneling processes through a dot with degenerate energy levels ε_d and a Coulomb repulsion between electrons U. The transport is possible only when the effective dot energy level is aligned with the chemical potential of the leads (right). This is responsible for the conductance peaks in (a). In the other regimes (left), the dot occupation number is fixed and the transport through the quantum dot is blocked.

1.2.3 Single-particle transport and Coulomb blockade

When the coupling between the dot and the leads is weak, the system is in the sequential tunneling regime; the time between successive tunneling events is the largest scale in the problem, and there is therefore no coherence between them.

At high temperature ($T \gg U$), the transport through the quantum dot depends only on the series of two tunnel barriers between the dot and the left/right leads. The

conductance G of the system is

$$\frac{1}{G_\infty} = \frac{1}{G_L} + \frac{1}{G_R}, \tag{1.9}$$

where the left/right conductances depend on the strength of the tunnel barrier and the number of channels in the dot

$$G_\alpha = \frac{4e^2}{\hbar}\frac{\Gamma_\alpha}{\delta E}, \tag{1.10}$$

with $\alpha = L/R$, $\Gamma_\alpha = \sum_i \pi\nu t_{\alpha i}^2$ the escape rate of electrons to the lead α (ν being the density of states in the leads, assumed energy independent), and $1/\delta E$ the density of states in the dot.

When the temperature is lower than the charging energy ($\Gamma_\alpha \ll T \ll U$), the system behaves differently, as shown on Fig. 1.3(a). The total occupation number in the dot N is now fixed by the Coulomb repulsion and the electronic transport is blocked. This phenomenon is called the *Coulomb blockade regime*. The transport is only favored in the transition regions where the energy of the state $|N\rangle$ is aligned with the chemical potential of the leads, as illustrated on Fig. 1.3(b). On the left figure, a lead electron cannot enter the dot because the Coulomb repulsion would bring its energy much higher than the chemical potential of the leads, and the transport from one lead to the other is blocked. On the contrary, on the right figure, it is very easy for an electron to tunnel in or out of the dot without any energy cost. As a consequence, the linear conductance through the dot shows a succession of peaks associated with the degeneracy regions (Coulomb peaks), separated by regions of low conductance.

As the temperature is decreased, the Fermi momentum distribution function in the leads gets sharper, and the effect gets more pronounced: the height of the Coulomb peak grows while the Coulomb blockade is still more efficient. For more information on the transport through quantum dots put in the Coulomb blockade regime, see for instance [50].

1.2.4 Many-particle transport and the Kondo effect

When the temperature T becomes lower than the tunneling rate Γ between the dot and the leads, higher-order virtual tunneling processes though high-energy states become relevant and eventually dominate the transport. The coherence between electrons may involve a strong modification of the features described in Sec. 1.2.3. However, as long as we consider spinless levels, the conductance profile remains qualitatively the same, reaching small values in the Coulomb blockade region.

The situation gets dramatically different when we take the spin into account. Considering that the Coulomb repulsion on the dot U is smaller than the level spacing δE, the levels are filled one after the other because of the Pauli exclusion principle. In that case, an odd electron occupancy in the dot implies that it carries a net spin $1/2$. This situation is analogous to the case of the scattering by magnetic impurities described in

Section 1.1, and we can expect logarithmic divergent contributions for the conductance at low-temperature typical of the Kondo effect.

On the theoretical level, the Anderson Hamiltonian can be mapped on a low-energy Kondo Hamiltonian in the Coulomb blockade region for odd occupancy. This is done by applying the so-called Schrieffer-Wolff transformation [96] that projects out the high-energy empty and doubly occupied dot states of the Anderson model. For a single-level quantum dot in the absence of magnetic field, the effective Hamiltonian obtained after transformation reads

$$\mathcal{H}_{Kondo} = \sum_{k\sigma} \varepsilon_k c^\dagger_{k\sigma} c_{k\sigma} + J \sum_{kk'} \vec{S}_d . \vec{S}_{kk'}, \tag{1.11}$$

with

$$J = -2\left|t\right|^2 \left[\frac{1}{\varepsilon_d} - \frac{1}{\varepsilon_d + U}\right] > 0, \tag{1.12}$$

$$\vec{S}_{kk'} = \frac{\hbar}{2} \sum_{\alpha\alpha'} \sum_{\sigma\sigma'} \vec{\tau}_{\sigma\sigma'} c^\dagger_{\alpha' k' \sigma'} c_{\alpha k \sigma}, \tag{1.13}$$

where $\vec{\tau}_{\sigma\sigma'}$ are the matrix elements of the Pauli matrices τ^α ($\alpha = x, y, z$). The derivation is given in Appendix A. The second term in Eq. (1.11) involves an exchange interaction between the dot spin $\vec{S}_d$ and the spin density of the conduction electrons at the site of the impurity $\sum_{kk'} \vec{S}_{kk'}$. This exchange interaction is anti-ferromagnetic as $J > 0$.

In analogy with the study of bulk systems described in section 1.1, we can define a Kondo temperature

$$T_K = \tilde{W} \exp\left(-\frac{1}{\nu J}\right), \tag{1.14}$$

where $\tilde{W}$ is the effective bandwidth for the low-energy excitations. This Kondo scale can be interpreted as the binding energy of the spin singlet Ground State. At equilibrium, the temperature dependence of the linear conductance shows the following asymptotic behavior [82]

$$G(T) = \begin{cases} G_0 \left[1 - \left(\frac{\pi T}{T_K}\right)^2\right] & T \ll T_K \\ G_0 \, \frac{3\pi^2/16}{\ln^2\left(T/T_K\right)} & T \gg T_K \end{cases}, \tag{1.15}$$

with

$$G_0 = \frac{2e^2}{h} \frac{4\Gamma_L \Gamma_R}{\left(\Gamma_L + \Gamma_R\right)^2}. \tag{1.16}$$

While the Kondo effect in bulk systems induces an additional scattering process which increases the resistivity, it strongly enhances the transport in quantum dots by providing

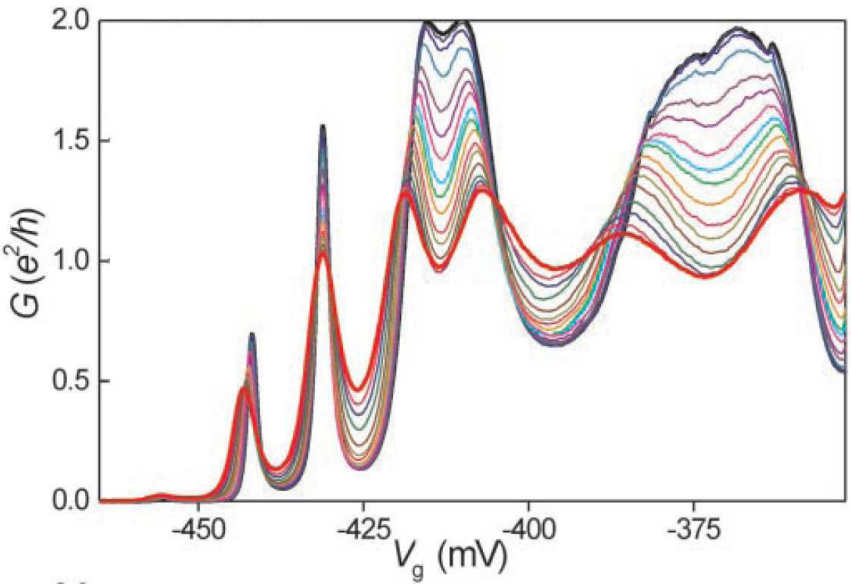

Figure 1.4: Linear conductance as a function of the gate voltage for different temperatures [100]. At high temperature ($T \gg T_K$, red curve), the conductance is blocked when the dot occupation number is fixed, while it shows peaks in the degeneracy regions. At lower temperature ($T \ll T_K$, black curve), the conductance gets enhanced in the odd occupancy regions because of the emergence of the Kondo effect.

a new transmission channel between the two leads. From Eq. (1.15), we can infer the main aspects to be checked when looking for Kondo effect in an experiment: the conductance should show a crossover from a Fermi liquid regime characterized by a quadratic temperature dependence for any physical quantity, to a weak-coupling regime showing a logarithmic decrease with temperature. The maximum conductance G_0 is obtained for zero temperature, and reaches the universal quantum of conductance $2e^2/h$ (called unitary limit) in the case of a symmetric coupling to the leads ($\Gamma_L = \Gamma_R$). In addition, universality is a hallmark of the Kondo effect, meaning that the same curve should be obtained after rescaling over the Kondo temperature T/T_K.

The first experiments showing evidence for Kondo effect in quantum dots were realized about ten years ago [32, 20, 94, 100]. Fig. 1.4 shows the crossover from the Coulomb blockade regime to the Kondo regime measured by lowering the temperature. At high temperature, we recover a succession of Coulomb peaks and valleys in which the conductance is blocked as in Fig. 1.3(a). When the temperature is lowered, the conductance is enhanced in one valley on the two. It can be interpreted by associating an odd number of electrons to these valleys, which implies that they carry a non-zero spin responsible for the enhanced conductance by the Kondo effect at low temperature. The conductance eventually reaches the unitary quantum limit $2e^2/h$ at zero temperature. In contrast, the regions of even occupancy, where no Kondo effect is possible, show a conductance that decreases with temperature because of the reinforcement of the

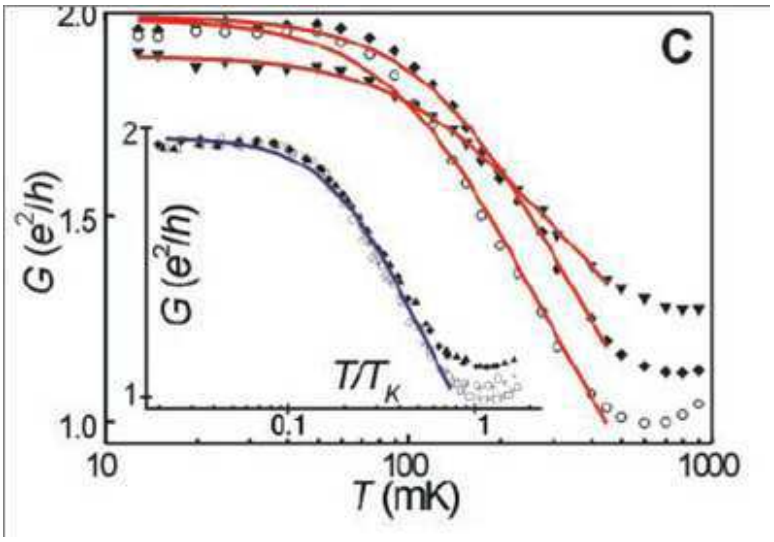

Figure 1.5: Linear conductance as a function of the temperature [100] for different gate voltages. The three curves lie on the top of each other after normalizing the temperature by the Kondo temperature and the conductance by its value at zero temperature (inset). This one-parameter scaling is observed over a wide range of parameters.

Coulomb blockade.

Another vantage in quantum dots for studying the Kondo effect lies in the tunability of the different parameters, allowing for the examination of the universality by studying the dependence on an external parameter (e.g. temperature, bias voltage, magnetic field) of several observables (e.g. conductance, noise) in different regimes (e.g. by changing the gate voltage). Indeed, theory predicts that all physical quantities should develop a universal behavior as a function of the external parameters (temperature, magnetic field, bias voltage) after normalizing them on the Kondo temperature T_K. This was observed in several experiments and for different devices as quantum dots [100] or molecules [100, 80].

In Fig. 1.5, we show the data obtained by van der Wiel et al. for the linear conductance as a function of the temperature. Three curves are obtained for different values of the gate voltage, corresponding to different values of the Kondo temperature T_K. After normalizing the temperature over the corresponding values for T_K, the three curves are found to sit on top of each other, providing a clear signature of the universality characteristic of the Kondo effect.

Another characteristic of the Kondo effect in quantum dots can be found in the bias-voltage dependence of the differential conductance dI/dV, that shows a narrow peak at low bias voltage V (Fig. 1.6). As noticed previously, the height of the peak reaches the unitary limit $2e^2/h$ at zero bias and zero temperature. When either the temperature or the bias voltage is increased, the spin-flip scattering processes become incoherent, destroying the coherent Kondo effect, and the conductance decreases. The

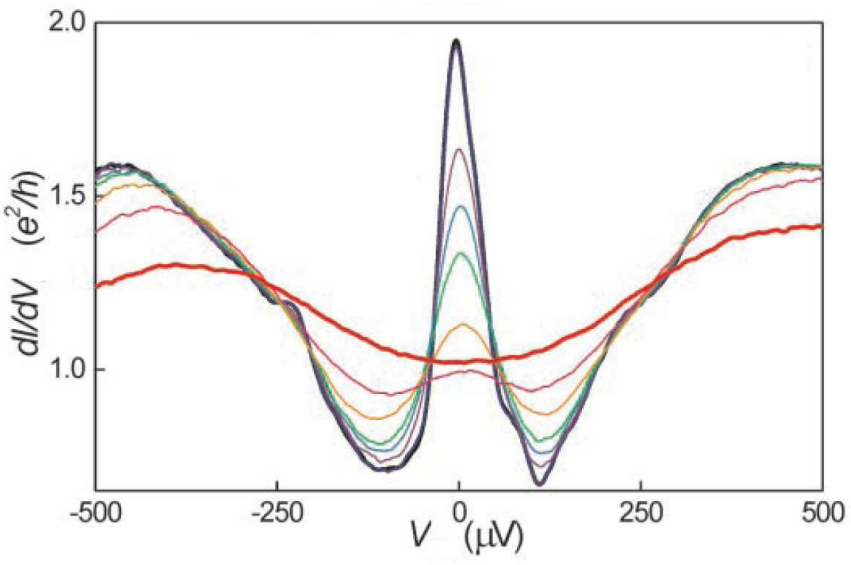

Figure 1.6: Differential conductance dI/dV as a function of the bias voltage V [100]. The narrow peak at low bias is due to the Kondo effect, while the high-voltage peaks are related to single-particle transport.

increase of the differential conductance at very high voltage occurs when the chemical potential of one lead is aligned with a dot level. In that case, the electrons can tunnel easily into or out of the dot through single-particle processes. On the theoretical point of view, the non-equilibrium transport for the Anderson model in the presence of a bias voltage has not been solved exactly so far. Therefore, the explanation of Fig. 1.6 is an important challenge, which we address in Chap. 4.

1.3 Perspectives

Due to its fairly ancient history in metals containing magnetic impurities, the theory of the Kondo effect is already well established and can interpret many experimental results with high accuracy. Because some aspects of the behavior of quantum dots are conceptually quite similar, there is no wonder that a fast agreement between theory and experiments has been reached on many points. Namely, exact solutions exist for the equilibrium $SU(2)$ case ($\mu_L = \mu_R$).

However, the framework of quantum dots has also brought to the surface a wide set of new problems [61, 5]. For instance, what happens when the dot is attached to ferromagnetic or superconducting leads? In the first case, the dynamics of Kondo spin-flip exchange turn out to be affected by the spin imbalance in the ferromagnetic reservoirs. When both leads have the same magnetic orientation [66], this has consequences on the density of states in the dot similar to the effect induced by a magnetic field (see Chap. 5). For anti-parallel magnetic lead alignment, the Kondo effect is equivalent

to the non-magnetic case at equilibrium, while the non-equilibrium behavior exhibits some differences. Despite the rich consequences predicted by theory, few experimental realizations have come out because of the difficulty of reliably creating magnetic semiconductor structures. The Kondo effect in presence of superconducting [28, 17] or Luttinger-liquid [42] leads is quite challenging as well because of the zero density of states at the Fermi level in the leads. The behavior of the system therefore depends on the interplay of many effects and on the relative values of the Kondo temperature and the superconducting gap (or Luttinger parameters).

Even more exotic features can be investigated in more complex systems such as double quantum dots [104, 14] or carbon nanotubes [83]. In those systems, a non-spin Kondo effect can take place through the two-fold degeneracy respectively in the two dots and in the orbital moment. This opens the door to systems where the dot exhibits a higher symmetry than $SU(2)$ [39, 72] leading to fundamental modification in its physical properties. All those questions have already generated an important literature, and are still open to debate. In this thesis, we address the transport through a quantum dot out of equilibrium (when the left and right leads are put to different chemical potentials). In that case, an electronic current flows through the system, and most equilibrium theories fail because of the decoherence of the resonant spin-flip scattering process.

Chapter 2

Equations-of-motion formalism

We want to characterize the electronic transport through the system. As we have shown in Eq. (1.6) that the current depends on the density of states in the dot, we need a method that gives the expression of the Green's function in the dot. To this end, we derive of the equations-of-motion (EOM) of the dot Green's function for the Anderson model. The recursive application of the Heisenberg equations-of-motion [109] generates an infinite hierarchy of equations, which relate the different Green's functions of the system. This hierarchy has to be truncated by a suitable approximation scheme in order to form a closed set of equations. The choice of the truncation scheme is crucial in order to treat carefully the correlation effects both from the Coulomb interaction and from the dot-lead tunneling.

The equations-of-motion technique was applied to the original Anderson model at equilibrium long time ago [25, 26, 11, 98, 63, 81, 52, 53] in the context of the dilute magnetic alloys. When applying the standard approximation based on a truncation of the equations of motion at second order in the hybridization term t_σ, it yields results which agree with perturbation theory calculations for temperatures above the Kondo temperature, T_K. This truncation scheme is usually referred to as the Lacroix approximation [52]. Even though the scheme has serious drawbacks at this level of approximation (underestimation of the Kondo temperature T_K, absence of Kondo effect just at the particle-hole symmetric point), it is acknowledged to provide a valuable basis for the description of the Kondo effect both at high and low temperatures. The applicability of the Lacroix approximation is nicely reported in a recent paper by V. Kashcheyevs *et al* [43].

There have been recent attempts to use an approximation which truncates the equations of motion at higher order in t_σ [71, 59, 38]. Their authors claimed to improve quantitatively at equilibrium the Kondo temperature and the density of states around the Fermi energy and have been able to investigate some nonequilibrium issues. However, there is need to clarify the decoherence effects in the framework of the equations-of-motion method. In this chapter we present the main approximation schemes and propose an extension to the often-used Lacroix approximation. We discuss the motivations and improvements of our method. The different approximation schemes will be

compared in Chapter 3.

2.1 Equation-of-motion for the Green's functions

Consider the retarded Green's function involving fermionic operators $\hat{A}$ and $\hat{B}$ in the Heisenberg representation

$$\mathcal{G}^r_{AB}(t,t') = -i\langle\{\hat{A}(t),\hat{B}(t')\}\rangle\Theta(t-t'). \tag{2.1}$$

In the frequency space, it writes

$$\langle\langle\hat{A},\hat{B}\rangle\rangle = -i\lim_{\delta\to 0^+}\int_0^\infty d\tau\; e^{i(\omega+i\delta)\tau}\;\langle\{\hat{A}(\tau),\hat{B}(0)\}\rangle, \tag{2.2}$$

where we used the Zubarev notation $\mathcal{G}^r_{AB}(\omega) = \langle\langle\hat{A},\hat{B}\rangle\rangle$ [109]. The infinitesimal positive number δ is needed to have a well-defined expression. Using the Heisenberg equations-of-motion $d\hat{A}(t)/dt = i/\hbar\left[\mathcal{H},\hat{A}\right]$ gives

$$\begin{aligned}\langle\langle\hat{A},\hat{B}\rangle\rangle &= -i\lim_{\delta\to 0^+}\frac{1}{i(\omega+i\delta)}\left[e^{i(\omega+i\delta)\tau}\langle\{\hat{A}(\tau),\hat{B}(0)\}\rangle\right]_0^\infty \\ &\quad -i\lim_{\delta\to 0^+}\left\{-\frac{i}{\hbar}\lim_{\delta\to 0^+}\int_0^\infty d\tau\; e^{i(\omega+i\delta)\tau}\;\langle\{\left[\mathcal{H},\hat{A}\right],\hat{B}\}\rangle\right\} \\ &= \lim_{\delta\to 0^+}\frac{-1}{(\omega+i\delta)}\left\{-\langle\{\hat{A},\hat{B}\}\rangle - \frac{i}{\hbar}\lim_{\delta\to 0^+}\int_0^\infty d\tau\; e^{i(\omega+i\delta)\tau}\;\langle\{\left[\mathcal{H},\hat{A}\right],\hat{B}\}\rangle\right\}.\end{aligned} \tag{2.3}$$

where we integrated Eq. (2.2) by parts. The small constant δ is important in order for the first term to be well defined. In the rest of the thesis, the imaginary part $i\delta$ going alongside ω will be implicit. Reorganizing the terms and using the definition (2.2)

$$\omega\langle\langle\hat{A},\hat{B}\rangle\rangle = \langle\{\hat{A},\hat{B}\}\rangle + \langle\langle[\hat{A},\mathcal{H}],\hat{B}\rangle\rangle. \tag{2.4}$$

The philosophy of the EOM is to develop the hierarchy of equations by using Eq. (2.4) recursively for the new Green's functions $\langle\langle[\hat{A},\mathcal{H}],\hat{B}\rangle\rangle$ that appear on the right-hand-side. Very often, this hierarchy generates an infinite number of equations and has to be truncated by an appropriate decoupling method. In this chapter, we show how this can be applied to the single-level Anderson model.

2.2 Equations-of-motion for the Anderson model

We model the quantum dot connected to N_α leads by the single-level (spin-1/2) Anderson impurity Hamiltonian introduced in Chapter 1

$$\mathcal{H} = \sum_{\alpha k\sigma}\varepsilon_k\hat{n}_{\alpha k\sigma} + \sum_\sigma\left(\varepsilon_d + \frac{\Delta}{2}\sigma\right)\hat{n}_\sigma + U\hat{n}_\sigma\hat{n}_{\bar{\sigma}} + \sum_{\alpha k\sigma}\left(t_{\alpha\sigma}c^\dagger_{\alpha k\sigma}f_\sigma + H.c.\right). \tag{2.5}$$

We consider the N_α leads to have the same constant density of states $\nu = 1/2W$, where W is the bandwidth for the conduction electrons. A magnetic field can split the single-particle energy of the dot ε_σ by a Zeeman energy $\Delta = g\mu_B B$ (we write $\varepsilon_\sigma = \varepsilon_d + \Delta\sigma/2$, with $\sigma = \pm 1$), where μ_B is the Bohr magneton and g is an effective gyromagnetic factor that depends on the screening of the magnetic field inside the material.

From Eq. (2.5), it is possible to perform a unitary transformation on the lead operators $c_{\alpha k\sigma}$ such that the dot will be coupled to a single effective lead. For that lead, the result of the transformation is

$$\tilde{c}_{k\sigma} = \frac{1}{\tilde{t}_\sigma} \sum_\alpha t_{\alpha\sigma} c_{\alpha k\sigma}, \tag{2.6a}$$

$$\tilde{t}_\sigma = \sqrt{\sum_\alpha t_{\alpha\sigma}^2}. \tag{2.6b}$$

The remaining $N_\alpha - 1$ uncoupled $\tilde{c}$ operators obtained from the unitary transformation can be built by means of the Gram-Schmidt orthonormalization procedure. However, finding them is unimportant as they do not couple to the dot. The remaining Hamiltonian (2.5) can be written

$$\mathcal{H} = \sum_{k\sigma} \varepsilon_k \tilde{c}_{k\sigma}^\dagger \tilde{c}_{k\sigma} + \sum_\sigma \varepsilon_\sigma \hat{n}_\sigma + U \hat{n}_\sigma \hat{n}_{\bar{\sigma}} + \sum_{k\sigma} \left(\tilde{t}_\sigma \tilde{c}_{k\sigma}^\dagger f_\sigma + H.c. \right). \tag{2.7}$$

We should remember about the transformation of Eqs. (2.6) when dealing with statistical parameters. Indeed, the distribution in the effective lead $\tilde{f}(\varepsilon_k)$ is given by the linear combination of the N_α initial leads

$$\tilde{f}(\varepsilon_k) = \langle \tilde{c}_{k\sigma}^\dagger \tilde{c}_{k\sigma} \rangle = \frac{1}{\tilde{t}_\sigma^2} \sum_\alpha t_{\alpha\sigma}^2 f_\alpha(\varepsilon_k). \tag{2.8}$$

In the following, we derive the equations of motion directly from Eq. (2.7), omitting the tilde on the c operators.

The equation (1.6) highlights the interest in computing the dot Green's function to determine the transport though the system. We derive a hierarchy of equations for the dot Green's function $\mathcal{G}_\sigma^r(\omega) \equiv \langle\langle f_\sigma, f_\sigma^\dagger \rangle\rangle$. As the EOM given by Eq. (2.4) acts only on the the left operator in the Green's function, we adopt a simpler notation by changing

$$\langle\langle \hat{A}, f_\sigma^\dagger \rangle\rangle \longrightarrow \langle\langle \hat{A} \rangle\rangle. \tag{2.9}$$

Using Eq. (2.4), the first equations-of-motion is

$$(\omega - \varepsilon_\sigma) \langle\langle f_\sigma \rangle\rangle = 1 + U \langle\langle n_{\bar{\sigma}} f_\sigma \rangle\rangle + t_\sigma \sum_k \langle\langle c_{k\sigma} \rangle\rangle. \tag{2.10}$$

Two new Green's functions appear on the right-hand side. Let us first write the EOM for the single-particle Green's function[1] $\langle\langle c_{k\sigma}\rangle\rangle$

$$(\omega - \varepsilon_k)\,\langle\langle c_{k\sigma}\rangle\rangle = t_\sigma \langle\langle f_\sigma\rangle\rangle. \tag{2.11}$$

Combining the equations (2.10) and (2.11) gives for the dot Green's function

$$\left(\omega - \varepsilon_\sigma - \Sigma^0_\sigma(\omega)\right)\,\langle\langle f_\sigma\rangle\rangle = 1 + U\langle\langle n_{\bar\sigma} f_\sigma\rangle\rangle, \tag{2.12}$$

where we introduced the non-interacting self-energy

$$\Sigma^0_\sigma(\omega) = t_\sigma^2 \sum_k \frac{1}{\omega - \varepsilon_k} = -i\Gamma_\sigma, \tag{2.13}$$

with $\Gamma_\sigma = \pi\nu t_\sigma^2 = \pi t_\sigma^2/2W$. The second equality in Eq. (2.13) stands if the half-bandwidth W is much larger than all the other energy scales, so that the band-edge effect does not affect the local density of states in the dot $\rho_\sigma(\omega)$. In this case, the properties of the system at low temperature do not depend on the exact value of W since only states around the Fermi level contribute, justifying the consideration of the wide-band limit $W \to \infty$ [11][2].

From Eq. (2.12), we notice that finding the dot Green's function $\langle\langle f_\sigma\rangle\rangle$ requires the expansion of the EOM for the two-particle Green's function $\langle\langle n_{\bar\sigma} f_\sigma\rangle\rangle$. This can be done through several approximation schemes that we discuss in this chapter.

2.3 Exact limits

Before treating the approximation schemes, it is illuminating to discuss two limiting cases for which the equations-of-motion provide exact results.

2.3.1 Non-interacting limit ($U = 0$)

When there is no Coulomb repulsion between the electrons on the dot ($U = 0$), the Eq. (2.12) simply becomes

$$\langle\langle f_\sigma\rangle\rangle = \frac{1}{\omega - \varepsilon_\sigma + i\Gamma_\sigma}. \tag{2.14}$$

The density of states in the dot $\rho_\sigma(\omega) = -\mathrm{Im}\langle\langle f_\sigma\rangle\rangle/\pi$ is a lorentzian centered at the dot energy level ε_σ.

$$\rho_\sigma(\omega) = \frac{1}{\pi}\frac{\Gamma_\sigma}{(\omega - \varepsilon_\sigma)^2 + \Gamma_\sigma^2}. \tag{2.15}$$

[1] We define the *n-particle Green's function* by a Green's function implying n creation operators and n destruction operators (including the implicit $f_\sigma^\dagger$ at time $t = 0$ in Eq. (2.9)). Note that in general a two-particle Green's functions means $\langle\langle ab, c^\dagger d^\dagger\rangle\rangle$ with two operators on both sides. In this manuscript, we extend the definition to functions as $\langle\langle c^\dagger ab, d^\dagger\rangle\rangle$ to which they are related by a phase factor.

[2] This is in agreement with experiments in quantum dots, in which U is typically 3 orders of magnitude smaller than W.

The finite width Γ_σ of the lorentzian corresponds to the escape rate of electrons from/into the dot due to the hybridization with the leads.

2.3.2 Atomic limit ($\Gamma = 0$)

When the dot is isolated from the leads ($t_\sigma = 0$), we obtain a closed system of equations for the Green's functions

$$(\omega - \varepsilon_\sigma)\,\langle\langle f_\sigma \rangle\rangle = 1 + U\langle\langle n_{\bar\sigma} f_\sigma \rangle\rangle, \tag{2.16}$$

$$(\omega - \varepsilon_\sigma - U)\,\langle\langle n_{\bar\sigma} f_\sigma \rangle\rangle = \langle n_{\bar\sigma}\rangle. \tag{2.17}$$

This leads to

$$\langle\langle f_\sigma \rangle\rangle = \frac{1 - \langle n_{\bar\sigma}\rangle}{\omega - \varepsilon_\sigma} + \frac{\langle n_{\bar\sigma}\rangle}{\omega - \varepsilon_\sigma - U}, \tag{2.18}$$

and, taking the imaginary part,

$$\rho_\sigma(\omega) = [1 - \langle n_{\bar\sigma}\rangle]\,\delta(\omega - \varepsilon_\sigma) + \langle n_{\bar\sigma}\rangle \delta(\omega - \varepsilon_\sigma - U). \tag{2.19}$$

The density of states shows two Dirac peaks located at the bare dot energy-levels ε_σ and $\varepsilon_\sigma + U$. They respectively correspond to the energy needed to add an electron in the state $|\sigma\rangle$ when the state $|\bar\sigma\rangle$ is unoccupied (resp. occupied), and the weight of the peaks are $1 - \langle n_{\bar\sigma}\rangle$ (resp. $\langle n_{\bar\sigma}\rangle$).

2.4 Hartree approximation (truncation at zeroth order in t)

For the general case ($U \neq 0, \Gamma \neq 0$), the easiest approximation possible is to truncate the hierarchy of equations at the mean-field level by decoupling directly the 2-particle Green's function

$$\langle\langle n_{\bar\sigma} f_\sigma \rangle\rangle \approx \langle n_{\bar\sigma}\rangle \langle\langle f_\sigma \rangle\rangle. \tag{2.20}$$

Using Eq. (2.12), the dot Green's function writes

$$\langle\langle f_\sigma \rangle\rangle = \frac{1}{\omega - \varepsilon_\sigma - U\langle n_{\bar\sigma}\rangle + i\Gamma_\sigma}. \tag{2.21}$$

The density of states is similar to the non-interacting case, except that the lorentzian peak is shifted toward higher energy by $U\langle n_{\bar\sigma}\rangle$ due to the Coulomb repulsion with electrons in the state $|\bar\sigma\rangle$. The approximation is obviously correct in the non-interacting limit $U \to 0$. The Eq. (2.21) has to be complemented by the equation for the occupation

number in the dot $\langle n_{\bar{\sigma}} \rangle$. From the fluctuation-dissipation theorem [89], it writes at zero temperature

$$\langle n_\sigma \rangle = \frac{1}{\pi} \int_{-W}^{0} d\omega \frac{\Gamma_\sigma}{\left(\omega - \varepsilon_\sigma - U\langle n_{\bar{\sigma}} \rangle\right)^2 + \Gamma_\sigma^2} = -\frac{1}{\pi} \arctan\left(\frac{\varepsilon_\sigma - U\langle n_{\bar{\sigma}} \rangle}{\Gamma_\sigma}\right) + \frac{1}{2}. \tag{2.22}$$

The Green's function and the occupation number are found by solving Eqs. (2.21) and (2.22) self-consistently. Anderson showed that such a treatment gives rise to a phase diagram with axes Γ/U and ε_d/U that exhibits a phase at small U with a single non-magnetic solution $\langle n_\uparrow \rangle = \langle n_\downarrow \rangle$ and a phase at large U with three mathematical solutions: the non-magnetic one $\langle n_\uparrow \rangle = \langle n_\downarrow \rangle$ and two magnetic ones $\langle n_\uparrow \rangle = 1 - \langle n_\downarrow \rangle$ with $\langle n_\uparrow - n_\downarrow \rangle \approx \pm 1$ [7]. In the second case, it turns out that only the magnetic solutions are stable, highlighting the formation of a local magnetic moment. The formation of such a magnetic moment is an indication that the Anderson model can be mapped on a Kondo model[3].

For $\langle n_\uparrow - n_\downarrow \rangle \approx +1$, the spin-up (resp. spin-down) density of states shows a peak at ε_d (resp. $\varepsilon_d + U$). The result should be averaged with the second solution at $\langle n_\uparrow - n_\downarrow \rangle \approx -1$ in order to restore the spin rotation symmetry. By doing so, the self-consistent Hartree solution recovers the atomic limit as will be shown in Chap. 3.

2.5 First-order approximation (truncation at first order in t)

In order to go beyond the Hartree approximation, we can expand the equations-of-motion for the Green's function $\langle\langle n_{\bar{\sigma}} f_\sigma \rangle\rangle$

$$\left(\omega - \varepsilon_\sigma - U\right) \langle\langle n_{\bar{\sigma}} f_\sigma \rangle\rangle = \langle n_{\bar{\sigma}} \rangle + \sum_k \left[t_\sigma \langle\langle n_{\bar{\sigma}} c_{k\sigma} \rangle\rangle + t_{\bar{\sigma}} \langle\langle f_{\bar{\sigma}}^\dagger c_{k\bar{\sigma}} f_\sigma \rangle\rangle - t_{\bar{\sigma}} \langle\langle c_{k\bar{\sigma}}^\dagger f_{\bar{\sigma}} f_\sigma \rangle\rangle \right]. \tag{2.23}$$

Three new Green's functions have appeared on the right-hand-side. A physical interpretation of those functions is obtained by applying the EOM on the implicit operator $f_\sigma^\dagger$ at time t', which tunnels to $c_{k\sigma}^\dagger$. $\langle\langle n_{\bar{\sigma}} c_{k\sigma}, c_{k\sigma}^\dagger \rangle\rangle$ is related to the potential scattering of a conduction electron on the impurity; $\langle\langle f_{\bar{\sigma}}^\dagger c_{k\bar{\sigma}} f_\sigma, c_{k\sigma}^\dagger \rangle\rangle$ stands for the co-tunneling scattering of a conduction electron with spin-flip and $\langle\langle c_{k\bar{\sigma}}^\dagger f_{\bar{\sigma}} f_\sigma, c_{k\sigma}^\dagger \rangle\rangle$ describes a process in which two conduction electrons leave the dot [37].

Turning back to Eq. (2.23), decoupling at this stage gives

$$\begin{aligned}
\langle\langle n_{\bar{\sigma}} c_{k\sigma} \rangle\rangle &\approx \langle n_{\bar{\sigma}} \rangle \, \langle\langle c_{k\sigma} \rangle\rangle, \\
\langle\langle f_{\bar{\sigma}}^\dagger c_{k\bar{\sigma}} f_\sigma \rangle\rangle &\approx \langle f_{\bar{\sigma}}^\dagger c_{k\bar{\sigma}} \rangle \, \langle\langle f_\sigma \rangle\rangle, \\
\langle\langle c_{k\bar{\sigma}}^\dagger f_{\bar{\sigma}} f_\sigma \rangle\rangle &\approx \langle c_{k\bar{\sigma}}^\dagger f_{\bar{\sigma}} \rangle \, \langle\langle f_\sigma \rangle\rangle.
\end{aligned}$$

[3]Of course, no Kondo physics can be obtained at the mean-field level as it results from strong correlations induced by higher-order virtual processes.

Introducing inside Eq. (2.23), we get

$$(\omega - \varepsilon_\sigma - U)\,\langle\langle n_{\bar\sigma} f_\sigma\rangle\rangle = \langle n_{\bar\sigma}\rangle - i\Gamma_\sigma\langle n_{\bar\sigma}\rangle\langle\langle f_\sigma\rangle\rangle - i\langle\hat{I}_{\bar\sigma}\rangle\langle\langle f_\sigma\rangle\rangle, \tag{2.24}$$

where we used Eq. (2.11) and defined the total spin-current operator

$$\hat{I}_\sigma = i\sum_k t_\sigma\left[f_\sigma^\dagger c_{k\sigma} - c_{k\sigma}^\dagger f_\sigma\right]. \tag{2.25}$$

If there is no current source inside the dot, the total average current entering the dot is always zero[4] ($\langle\hat{I}_{\bar\sigma}\rangle = 0$). Combining with Eq. (2.12), and after some straightforward algebra, the dot Green's function reads

$$\langle\langle f_\sigma\rangle\rangle = \frac{\omega - \varepsilon_\sigma - U\,(1 - \langle n_{\bar\sigma}\rangle)}{(\omega - \varepsilon_\sigma + i\Gamma_\sigma)\,(\omega - \varepsilon_\sigma - U) + i\Gamma_\sigma U\langle n_{\bar\sigma}\rangle}. \tag{2.26}$$

Using the identity $A + B\langle n_{\bar\sigma}\rangle = A(1 - \langle n_{\bar\sigma}\rangle) + (A + B)\langle n_{\bar\sigma}\rangle$, we can rewrite it under the form

$$\langle\langle f_\sigma\rangle\rangle = \frac{1 - \langle n_{\bar\sigma}\rangle}{\omega - \varepsilon_\sigma + i\Gamma_\sigma\left[1 + \frac{U\langle n_{\bar\sigma}\rangle}{(\omega - \varepsilon_\sigma - U)}\right]} + \frac{\langle n_{\bar\sigma}\rangle}{\omega - \varepsilon_\sigma - U + i\Gamma_\sigma\left[1 - \frac{U(1 - \langle n_{\bar\sigma}\rangle)}{\omega - \varepsilon_\sigma}\right]}. \tag{2.27}$$

Interestingly, this expression recovers directly both the non-interacting limit $U = 0$ and the atomic limit $\Gamma = 0$. In the general case, the dot density of states $\rho_\sigma(\omega)$ is given by two resonances centered around ε_σ and $\varepsilon_\sigma + U$. The height of the peaks is pinned at $1/\pi\Gamma_\sigma$ for any value of the dot energy level ε_σ or the Coulomb repulsion U, while their width of the resonances is renormalized in comparison with the Hartree case.

2.6 Lacroix approximation (truncation at second order in t)

The approximations dicussed in Sec. 2.4 and 2.5 are only able to describe single-particle physics. Some interesting many-body physics can be captured by going to the next order in the EOM, by expanding the three Green's functions appearing on the right-hand side of Eq (2.23)

$$\begin{aligned}
(\omega - \varepsilon_k)\,\langle\langle n_{\bar\sigma} c_{k\sigma}\rangle\rangle &= t_\sigma\langle\langle n_{\bar\sigma} f_\sigma\rangle\rangle \\
&\quad + \sum_{k_1} t_{\bar\sigma}\left[\langle\langle f_{\bar\sigma}^\dagger c_{k_1\bar\sigma} c_{k\sigma}\rangle\rangle - \langle\langle c_{k_1\bar\sigma}^\dagger f_{\bar\sigma} c_{k\sigma}\rangle\rangle\right], \quad \text{(2.28a)} \\
(\omega - \varepsilon_k - \Delta\sigma)\,\langle\langle f_{\bar\sigma}^\dagger c_{k\bar\sigma} f_\sigma\rangle\rangle &= \langle f_{\bar\sigma}^\dagger c_{k\bar\sigma}\rangle + t_{\bar\sigma}\langle\langle n_{\bar\sigma} f_\sigma\rangle\rangle \\
&\quad + \sum_{k_1}\left[t_\sigma\langle\langle f_{\bar\sigma}^\dagger c_{k\bar\sigma} c_{k_1\sigma}\rangle\rangle - t_{\bar\sigma}\langle\langle c_{k_1\bar\sigma}^\dagger c_{k\bar\sigma} f_\sigma\rangle\rangle\right], \quad \text{(2.28b)} \\
(\omega + \varepsilon_k - 2\varepsilon_d - U)\,\langle\langle c_{k\bar\sigma}^\dagger f_{\bar\sigma} f_\sigma\rangle\rangle &= \langle c_{k\bar\sigma}^\dagger f_{\bar\sigma}\rangle - t_{\bar\sigma}\langle\langle n_{\bar\sigma} f_\sigma\rangle\rangle \\
&\quad + \sum_{k_1}\left[t_{\bar\sigma}\langle\langle c_{k\bar\sigma}^\dagger c_{k_1\bar\sigma} f_\sigma\rangle\rangle + t_\sigma\langle\langle c_{k\bar\sigma}^\dagger f_{\bar\sigma} c_{k_1\sigma}\rangle\rangle\right]. \quad \text{(2.28c)}
\end{aligned}$$

[4] Remind that the c operator includes a sum over all the leads.

Again, we can decouple the new Green's functions appearing on the right-hand side

$$\begin{aligned}\langle\langle f^\dagger_{\bar\sigma} c_{k_1\bar\sigma} c_{k\sigma}\rangle\rangle &\approx \langle f^\dagger_{\bar\sigma} c_{k_1\bar\sigma}\rangle\, \langle\langle c_{k\sigma}\rangle\rangle,\\ \langle\langle c^\dagger_{k_1\bar\sigma} f_{\bar\sigma} c_{k\sigma}\rangle\rangle &\approx \langle c^\dagger_{k_1\bar\sigma} f_{\bar\sigma}\rangle\, \langle\langle c_{k\sigma}\rangle\rangle,\\ \langle\langle c^\dagger_{k_1\bar\sigma} c_{k\bar\sigma} f_{\sigma}\rangle\rangle &\approx \langle c^\dagger_{k_1\bar\sigma} c_{k\bar\sigma}\rangle\, \langle\langle f_{\sigma}\rangle\rangle.\end{aligned}$$

Decoupling at this stage is often referred to as the Lacroix approximation [52]. Using the equations (2.11) and (2.13), and reminding $\langle \hat{I}_{\bar\sigma}\rangle = 0$, the Eqs. (2.28) become

$$(\omega - \varepsilon_k)\,\langle\langle n_{\bar\sigma} c_{k\sigma}\rangle\rangle = t_\sigma \langle\langle n_{\bar\sigma} f_\sigma\rangle\rangle, \tag{2.29a}$$

$$\begin{aligned}(\omega - \varepsilon_k - \Delta\sigma)\,\langle\langle f^\dagger_{\bar\sigma} c_{k\bar\sigma} f_\sigma\rangle\rangle &= \langle f^\dagger_{\bar\sigma} c_{k\bar\sigma}\rangle + t_{\bar\sigma}\langle\langle n_{\bar\sigma} f_\sigma\rangle\rangle\\ &\quad -i\Gamma_\sigma \langle f^\dagger_{\bar\sigma} c_{k\bar\sigma}\rangle\, \langle\langle f_\sigma\rangle\rangle - t_{\bar\sigma}\sum_{k_1}\langle c^\dagger_{k_1\bar\sigma} c_{k\bar\sigma}\rangle\, \langle\langle f_\sigma\rangle\rangle,\end{aligned} \tag{2.29b}$$

$$\begin{aligned}(\omega + \varepsilon_k - 2\varepsilon_d - U)\,\langle\langle c^\dagger_{k\bar\sigma} f_{\bar\sigma} f_\sigma\rangle\rangle &= \langle c^\dagger_{k\bar\sigma} f_{\bar\sigma}\rangle - t_{\bar\sigma}\langle\langle n_{\bar\sigma} f_\sigma\rangle\rangle\\ &\quad +t_{\bar\sigma}\sum_{k_1}\langle c^\dagger_{k\bar\sigma} c_{k_1\bar\sigma}\rangle\, \langle\langle f_\sigma\rangle\rangle - i\Gamma_\sigma \langle c^\dagger_{k\bar\sigma} f_{\bar\sigma}\rangle\, \langle\langle f_\sigma\rangle\rangle.\end{aligned} \tag{2.29c}$$

Grouping the Equations (2.12), (2.23) and (2.29), we find the expression for the Green's function inside the dot

$$\begin{aligned}\langle\langle f_\sigma\rangle\rangle = &\left[u_{2\sigma}(\omega) - \langle n_{\bar\sigma}\rangle - \sum_k \frac{t_{\bar\sigma}\langle f^\dagger_{\bar\sigma} c_{k\bar\sigma}\rangle}{\omega - \varepsilon_k - \Delta\sigma} + \sum_k \frac{t_{\bar\sigma}\langle c^\dagger_{k\bar\sigma} f_{\bar\sigma}\rangle}{\omega + \varepsilon_k - 2\varepsilon_d - U}\right]\\ \times &\left[u_{1\sigma}(\omega)u_{2\sigma}(\omega) - \sum_{kk_1}\frac{t^2_{\bar\sigma}\langle c^\dagger_{k_1\bar\sigma} c_{k\bar\sigma}\rangle + i\Gamma_\sigma\langle f^\dagger_{\bar\sigma} c_{k\bar\sigma}\rangle\delta_{kk_1}}{\omega - \varepsilon_k - \Delta\sigma} - \sum_{kk_1}\frac{t^2_{\bar\sigma}\langle c^\dagger_{k\bar\sigma} c_{k_1\bar\sigma}\rangle - i\Gamma_\sigma\langle c^\dagger_{k\bar\sigma} f_{\bar\sigma}\rangle\delta_{kk_1}}{\omega + \varepsilon_k - 2\varepsilon_d - U}\right]^{-1},\end{aligned} \tag{2.30}$$

where

$$u_{1\sigma}(\omega) = \omega - \varepsilon_\sigma + i\Gamma_\sigma, \tag{2.31}$$

$$u_{2\sigma}(\omega) = -\frac{1}{U}\left[\omega - \varepsilon_\sigma - U + i\Gamma_\sigma + 2i\Gamma_{\bar\sigma}\right]. \tag{2.32}$$

The very new feature in comparison to lower-order approximations is that the Green's function contains terms which exhibit low-energy divergences around $\omega = \Delta\sigma$ and $\omega = 2\varepsilon_d + U$. As it can be seen from the Green's function in Eq. (2.29b), the divergence at $\omega = \Delta\sigma$ is related to many-particle spin-flip scattering processes, as involved in the Kondo effect. The divergence at $\omega = 2\varepsilon_d + U$ in Eq. (2.29c) corresponds to processes in which two electrons are removed/added at the same time in the dot. Such a process is highly unlikely and the corresponding peak turns out to be unphysical. It is projected out when using the Lacroix approximation in the $U \to \infty$ limit. For the general case of a finite interaction U, we need to go beyond the Lacroix approximation, as will be shown in Sec. 2.7.

2.6.1 Non self-consistent solution

In order to get some analytical results, we can take the lowest-order approximation for the the average values in Eq. (2.48) [70]

$$\begin{aligned}\langle f_{\bar{\sigma}}^{\dagger} c_{k\bar{\sigma}}\rangle = \langle c_{k\bar{\sigma}}^{\dagger} f_{\bar{\sigma}}\rangle &\approx 0,\\ \langle c_{k_1\bar{\sigma}}^{\dagger} c_{k\bar{\sigma}}\rangle = \langle c_{k\bar{\sigma}}^{\dagger} c_{k_1\bar{\sigma}}\rangle &\approx f(\varepsilon_k)\delta_{kk_1}.\end{aligned}$$

This approximation is accurate to describe the high-energy behavior where the corrections for the non-interacting average values are small. We can write the dot Green's function under the equivalent form

$$\begin{aligned}\langle\langle f_\sigma\rangle\rangle &= \frac{1-\langle n_{\bar{\sigma}}\rangle}{\omega-\varepsilon_\sigma+i\Gamma_\sigma+\dfrac{U}{\omega-\varepsilon_\sigma-U+i\Gamma_\sigma+2i\Gamma_{\bar{\sigma}}}t_{\bar{\sigma}}^2\displaystyle\sum_k\left[\frac{f(\varepsilon_k)}{\omega-\varepsilon_k-\Delta\sigma}+\frac{f(\varepsilon_k)}{\omega+\varepsilon_k-2\varepsilon_d-U}\right]}\\ &+ \frac{\langle n_{\bar{\sigma}}\rangle}{\omega-\varepsilon_\sigma-U+i\Gamma_\sigma-\dfrac{U}{\omega-\varepsilon_\sigma+i\Gamma_\sigma+2i\Gamma_{\bar{\sigma}}}t_{\bar{\sigma}}^2\displaystyle\sum_k\left[\frac{1-f(\varepsilon_k)}{\omega-\varepsilon_k-\Delta\sigma}+\frac{1-f(\varepsilon_k)}{\omega+\varepsilon_k-2\varepsilon_d-U}\right]}.\end{aligned} \tag{2.33}$$

We recognize the two resonances around ε_σ and $\varepsilon_\sigma+U$, as in the Hartree approximation. However, the renormalization of the parameters is different as the width of the peaks is now equal to $\Gamma_\sigma+\Gamma_{\bar{\sigma}}=\Gamma$. The position of those peaks is also renormalized according to the equation

$$\tilde{\varepsilon}_\sigma \approx \varepsilon_\sigma - \frac{\Gamma_{\bar{\sigma}}}{\pi}\ln\left|\frac{\tilde{\varepsilon}_\sigma-\Delta\sigma}{\tilde{\varepsilon}_\sigma-2\varepsilon_d-U}\right|, \tag{2.34}$$

which is obtained by solving for the real part of the first term in Eq. (2.33) around $\omega\approx\tilde{\varepsilon}_\sigma$. In the $U\to\infty$ limit, the dot level is shifted toward higher energies. In the mixed valence regime ($\mathrm{Min}\{\varepsilon_\sigma-\mu_\alpha,\mu_\alpha-\varepsilon_\sigma-U\}\approx\Gamma$), the renormalization of the bare energy-level is consistent with the prediction from the scaling theory [33, 36].

On the other side, the main interest of the Lacroix approximation is that the dot Green's function in Eq. (2.48) contains some low-energy divergences. At zero temperature, the real part of the denominator in the dot Green's function contains a term of the form

$$\frac{\Gamma_{\bar{\sigma}}}{\pi}\ln\left|\frac{\omega-2\varepsilon_d-U}{\omega-\Delta\sigma}\right|.$$

The logarithmic divergences around $\omega=\Delta\sigma$ and $\omega=2\varepsilon_d+U$ cancel each other out when $\Delta\sigma=2\varepsilon_d+U$. In the zero magnetic field case ($\Delta=0$), this corresponds to the particle-hole symmetric point $\varepsilon_d=-U/2$. As a consequence, no Kondo physics can be found at that point in the present approximation scheme. It is still the case when using a self-consistent scheme for the average values in Eq. (2.48), as discussed later on.

On the other hand, the approximations here above for the average values are accurate essentially far from the resonances $\omega = \Delta\sigma$ and $\omega = 2\varepsilon_d + U$. At resonance, the divergence in the denominator implies that the dot Green's function equals zero, and from Eq. (1.8) the linear conductance also vanishes at zero temperature, in opposition with the maximum conductance $G = 2e^2/h$ expected in the Kondo regime. We show in Sec. 2.6.4 that this pathology is cured in a self-consistent treatment.

2.6.2 Universality and Kondo temperature

Before addressing the issue of the self-consistency, it is enlightening to investigate further the low-energy properties under the approximations of Sec. 2.6.1. In the Kondo regime $\omega \ll \min(-\varepsilon_d, \varepsilon_d + U)$, and far from the particle-hole symmetric point $\omega \ll |2\varepsilon_d + U|$, the frequency dependence comes essentially from the resonance around $\omega = \Delta\sigma = 0$ (we still consider the absence of magnetic field). The non-self-consistent dot Green's function can then be written under the form

$$\langle\langle f_\sigma \rangle\rangle = \frac{u_{2\sigma}(0) - \langle n_{\bar\sigma}\rangle}{u_{1\sigma}(0)u_{2\sigma}(0) + \dfrac{\Gamma_{\bar\sigma}}{\pi}\ln\left|\dfrac{2\varepsilon_d + U}{\omega}\right| + i\Gamma_{\bar\sigma}\left[f(\omega) + f(2\varepsilon_d + U)\right]}. \quad (2.35)$$

For spin-independent coupling ($\Gamma_\sigma = \Gamma_{\bar\sigma} = \Gamma/2$) and $\Gamma \ll U$, this gives

$$\langle\langle f_\sigma \rangle\rangle \propto \frac{1}{1 - \ln\left|\dfrac{T_K}{\omega}\right| - i\dfrac{U\Gamma/2}{\varepsilon_\sigma\left(\varepsilon_\sigma + U\right)}\left[f(\omega) + f(2\varepsilon_d + U) + 1 + 4\dfrac{\varepsilon_d}{U}\right]}, \quad (2.36)$$

where we define

$$T_K = (2\varepsilon_d + U)\exp\left[\frac{2\pi\varepsilon_\sigma\left(\varepsilon_\sigma + U\right)}{U\Gamma}\right]. \quad (2.37)$$

The Eq. (2.36) shows that the Green's function depends only on the ratio ω/T_K for $|\omega| \gg T$. For zero temperature, we recover the universality characteristic of the Kondo effect. The energy scale T_K is identified with the Kondo temperature; its expression essentially differs from the exact result $(U\Gamma/4)^{1/2}\exp\left[\pi\varepsilon_0(\varepsilon_0 + U)/\Gamma U\right]$ [33] by a factor 2 in the exponential.

2.6.3 Self-consistency at equilibrium

The approximations made in Section 2.6.1 for the expectation values $\langle f_\sigma^\dagger c_{k\sigma}\rangle$, $\langle c_{k\sigma}^\dagger c_{k_1\sigma}\rangle$ and $\langle n_\sigma\rangle = \langle f_\sigma^\dagger f_\sigma\rangle$ appearing in the dot Green's function (2.48) were shown to be inaccurate at low-energy. In order to determine properly these quantities, we have to define a self-consistent scheme that connects them to the Green's functions. At equilibrium,

this can be done by means of the spectral theorem:

$$\langle n_\sigma \rangle = -\frac{1}{\pi}\int_{-W}^{W} d\varepsilon f(\varepsilon)\,\mathrm{Im}\mathcal{G}^r_\sigma(\varepsilon), \tag{2.38a}$$

$$\langle f^\dagger_\sigma c_{k\sigma}\rangle = -\frac{1}{\pi}\int_{-W}^{W} d\varepsilon f(\varepsilon)\,\mathrm{Im}\mathcal{G}^r_{k\sigma,\sigma}(\varepsilon), \tag{2.38b}$$

$$\langle c^\dagger_{k\sigma} c_{k_1\sigma}\rangle = -\frac{1}{\pi}\int_{-W}^{W} d\varepsilon f(\varepsilon)\,\mathrm{Im}\mathcal{G}^r_{k_1\sigma,k\sigma}(\varepsilon), \tag{2.38c}$$

where $\mathcal{G}^r_{k\sigma,\sigma}(\omega) = \langle\langle c_{k\sigma}, f^\dagger_\sigma\rangle\rangle$ and $\mathcal{G}^r_{k_1\sigma,k\sigma}(\omega) = \langle\langle c_{k_1\sigma}, c^\dagger_{k\sigma}\rangle\rangle$. The EOM for these two Green's functions are

$$\langle\langle c_{k\sigma}, f^\dagger_\sigma\rangle\rangle = \frac{t_\sigma}{\omega-\varepsilon_k}\langle\langle f_\sigma, f^\dagger_\sigma\rangle\rangle, \tag{2.39a}$$

$$\langle\langle c_{k_1\sigma}, c^\dagger_{k\sigma}\rangle\rangle = \frac{\delta_{kk_1}}{\omega-\varepsilon_k} + \frac{t^2_\sigma}{(\omega-\varepsilon_k)(\omega-\varepsilon_{k_1})}\langle\langle f_\sigma, f^\dagger_\sigma\rangle\rangle. \tag{2.39b}$$

Inserting Eqs (2.39) inside Eqs (2.38b-2.38c) leads to

$$\langle f^\dagger_\sigma c_{k\sigma}\rangle = -\frac{t_\sigma}{\pi}\lim_{\delta\to 0}\int_{-W}^{W} d\varepsilon f(\varepsilon)\,\mathrm{Im}\frac{\mathcal{G}^r_\sigma(\varepsilon)}{\varepsilon-\varepsilon_k+i\delta}, \tag{2.40a}$$

$$\langle c^\dagger_{k\sigma} c_{k_1\sigma}\rangle = f(\varepsilon_k)\delta_{kk_1} - \frac{t^2_\sigma}{\pi}\lim_{\delta\to 0}\int_{-W}^{W} d\varepsilon f(\varepsilon)\,\mathrm{Im}\frac{\mathcal{G}^r_\sigma(\varepsilon)}{(\varepsilon-\varepsilon_k+i\delta)(\varepsilon-\varepsilon_{k_1}+i\delta)}. \tag{2.40b}$$

Looking at the terms where these average values appear inside Eq. (2.30), we observe that they enter in a summation over ε_k and ε_{k_1}, with an additional pole in $\omega \pm \varepsilon_k + i\delta$. Let us look for instance at the term

$$\begin{aligned}
t_{\bar\sigma}\sum_k \frac{\langle f^\dagger_{\bar\sigma} c_{k\bar\sigma}\rangle}{\omega-\varepsilon_k-\Delta\sigma+i\delta} &= -\frac{t^2_{\bar\sigma}}{2W\pi}\int d\varepsilon_k \int d\varepsilon f(\varepsilon)\frac{1}{\omega-\varepsilon_k-\Delta\sigma+i\delta}\,\mathrm{Im}\frac{\mathcal{G}^r_{\bar\sigma}(\varepsilon)}{\varepsilon-\varepsilon_k+i\delta} \\
&= -\frac{\Gamma_{\bar\sigma}}{\pi}\int d\varepsilon_k \int d\varepsilon f(\varepsilon)\frac{1}{\omega-\varepsilon_k-\Delta\sigma+i\delta} \\
&\quad \times\frac{1}{2i}\left[\frac{\mathcal{G}^r_{\bar\sigma}(\varepsilon)}{\varepsilon-\varepsilon_k+i\delta} - \frac{\mathcal{G}^a_{\bar\sigma}(\varepsilon)}{\varepsilon-\varepsilon_k-i\delta}\right] \\
&= \frac{\Gamma_{\bar\sigma}}{2i\pi}\int d\varepsilon f(\varepsilon)\mathcal{G}^a_{\bar\sigma}(\varepsilon)\int d\varepsilon_k \frac{1}{\omega-\varepsilon_k-\Delta\sigma+i\delta}\,\frac{1}{\varepsilon-\varepsilon_k-i\delta} \\
&= \Gamma_{\bar\sigma}\int d\varepsilon \frac{f(\varepsilon)\mathcal{G}^a_{\bar\sigma}(\varepsilon)}{\omega-\varepsilon-\Delta\sigma+i\delta}
\end{aligned}$$

Only the terms with poles in the two quadrants give a non-zero contribution in the wide-band-limit. Proceeding similarly for the other terms, we end up with a closed system of equations. We will show in Sec. 4.1 how these expressions can be generalized out of equilibrium.

2.6.4 Unitary limit

The unitary limit $G = 2e^2/h$ for the zero-temperature conductance in the Kondo regime implies, according to Eq. (1.8), that the dot density of states at the Fermi level of the leads is pinned at a value $\rho_\sigma(0) = 1/\pi\Gamma_\sigma = 2/\pi\Gamma$.

It is interesting to check whether this is true for the Lacroix approximation. Obviously, the answer is negative at the particle-hole symmetric point $\varepsilon_d = -U/2$, as we already mentioned that the Lacroix approximation fails to recover any Kondo physics at this very point.

Therefore, we consider the case $\varepsilon_d \neq -U/2$. We look for the value of the density of states at the precise point $\omega = 0$; at that point, the result from the Lacroix approximation is dominated by the diverging terms at $\omega = \Delta = 0$ in Eq. (2.30). Considering that the Green's function varies slowly around the Fermi level compared to the Fermi-Dirac distribution, we can take the approximation [27]

$$\sum_{\alpha=L,R} \frac{\Gamma_{\alpha\sigma}}{\pi} \int d\varepsilon \frac{f_\alpha(\varepsilon)\mathcal{G}^a_\sigma(\varepsilon)}{\omega - \varepsilon} \approx \sum_{\alpha=L,R} \frac{\Gamma_{\alpha\sigma}}{\pi} \mathcal{G}^a_\sigma(0) \int d\varepsilon \frac{f_\alpha(\varepsilon) - 1/2}{\omega - \varepsilon} = -\frac{\Gamma_\sigma}{\pi} \mathcal{G}^a_\sigma(0) \ln\left|\frac{\omega}{W}\right|,$$

valid for $\ln(W/\omega) \gg \pi$. Putting these two expressions into the dot Green's function (2.30) gives

$$\mathcal{G}^r_\sigma(0) \approx \lim_{\omega\to 0} \frac{\frac{\Gamma_\sigma}{\pi}\mathcal{G}^a_\sigma(0) \ln\left|\frac{\omega}{W}\right|}{\frac{\Gamma_\sigma}{\pi} \ln\left|\frac{\omega}{W}\right| [1 + i\Gamma\mathcal{G}^a_\sigma(0)]}. \tag{2.41}$$

The divergent correction appears both in the numerator and the denominator; as a consequence, the Green's function itself is *not* divergent. Inverting Eq. (2.41) directly implies

$$\mathrm{Im}\,[\mathcal{G}^r_\sigma(0)]^{-1} = \frac{\Gamma}{2}. \tag{2.42}$$

This relation implies number conservation and is sometimes referred to as the unitary condition [54, 43]. It is satisfied in the Lacroix approximation for $\varepsilon_d \neq -U/2$. However, the real part of the inverse Green's function at the Fermi energy, should be given by the Friedel sum rule

$$\mathrm{Re}\,[\mathcal{G}^r_\sigma(0)]^{-1} = -\Gamma_\sigma \cot(\pi\tilde{n}_\sigma), \tag{2.43}$$

with

$$\tilde{n}_\sigma = -\frac{1}{\pi}\mathrm{Im} \int d\omega f(\omega) \left[1 - \frac{\partial\Sigma^r_\sigma(\omega)}{\partial\omega}\right] \mathcal{G}^r_\sigma(\omega).$$

The relation (2.43) is *not* satisfied in the Lacroix approximation, and the low-energy Fermi liquid relationships are therefore violated [43].

2.7 Beyond the Lacroix approximation (decoupling at order $O(t^4)$)

As we saw in Sec. 2.6, the Lacroix approximation is able to capture several aspects of the Kondo physics on the qualitative level. However, it also suffers some drawbacks that require a more sophisticated treatment. Let us summarize the main features of the self-consistent Lacroix decoupling

1. the renormalization of the high-energy parameters ε_σ and Γ_σ is correct,
2. the important spin-flip scattering processes associated to the Kondo effect lies inside the two-particle Green's function $\langle\langle f^\dagger_{\bar\sigma} c_{k\bar\sigma} f_\sigma\rangle\rangle$,
3. there is a spurious negative peak at $\omega = 2\varepsilon_d + U$, related to the pole of $\langle\langle c^\dagger_{k\bar\sigma} f_{\bar\sigma} f_\sigma\rangle\rangle$. It cancels out with the Kondo resonance at the particle-hole symmetric point, where $T_K = 0$,
4. the Kondo temperature differs from the exact result by a factor 2 in the exponential,
5. the low-energy density of states shows a universal behavior after rescaling ω/T_K,
6. the unitary condition $\mathrm{Im}\,[\mathcal{G}^r_\sigma(0)]^{-1} = \Gamma/2$ is satisfied due to a correct balance between the coefficients of the logarithmic terms in the numerator and denominator,
7. all the Fermi liquid relationships at low energy are not recovered. In particular, the density of states is not a function of ω^2/T_K^2 for $\omega \ll T_K$,
8. the divergent terms remain in the presence of a bias voltage or a magnetic field, while they are expected to be smeared out by decoherence effects.

Many of those points were investigated recently [27, 43]. We question whether a derivation of the EOM at higher order can improve some drawbacks of the Lacroix approximation. In this thesis, we develop a systematic method that captures contributions beyond the derivation at second-order in t. We show in the following chapters that our result solves the drawbacks 3 and 8 of the Lacroix approximation, and improves the point 4. The Holy Grail would be to recover the Fermi-liquid relations at low energy, which would probably drive the EOM technique high onto the front stage for Kondo-related problems [40]. The reader interested in digging in that direction should be aware of the work by Nagaoka [73] who applied of the EOM to the Kondo Hamiltonian and recovered a very accurate low-energy behavior[5]. Following the track of his approach while starting from the Anderson model might bring some clue to the problem. We do not address this issue in this thesis, as we focus on the high-energy behavior, for instance when the system is driven out of equilibrium by applying a bias

[5] See also [107]

voltage $V > T_K$. The parameter region $V = T = \Delta = 0$ will be looked at only to benchmark our approximation by comparing it to other ones. Therefore, the Fermi liquid regime is not our main concern and we propose an extension of the EOM whose roots are the Lacroix approximation.

Going beyond the Lacroix approximation has had several attempts (e.g. [25, 71, 59]), but few of them were able to extend it in a controllable way. The essence of the difficulty is the following: Lacroix had the good idea to stop the hierarchy of EOM by decoupling the two-particle Green's functions when only one dot operator remains at time t. If we wish to expand the hierarchy beyond this point, we have to deal with three-particle Green's functions, implying tricky correlations, and an exploding number of equations and combinations of energy parameters. Many of those terms turn out to be negligible, and keeping track of all of them is essentially irrelevant. Therefore, we show and discuss what terms we expect to give a sensible contribution to the Kondo effect. However, when decoupling Green's functions generated at different orders, there is a danger for double counting. A simple example can be found if we try to perform both the decoupling at the mean-field level (Sec. 2.4) and at first order (Sec. 2.5). This is forbidden because it corresponds to decoupling the *same* quantity twice, at different orders of the expansions of the EOM. We develop a new formalism that keeps track of the decouplings and avoids this kind of double couting.

2.7.1 Decoupling procedure

Let us first remind how the EOM work for the Anderson model. Each time we compute the anti-commutation of a Green's function with the Hamiltonian, the operators are changed according to

$$\begin{aligned} f_\sigma &\rightarrow t_\sigma c_\sigma + U n_{\bar\sigma} f_\sigma, \\ c_\sigma &\rightarrow t_\sigma f_\sigma. \end{aligned}$$

However, due to the finite Hilbert space on the dot, a Green's function of higher particle number appears only if includes a single dot operator f_σ ($f_\sigma^\dagger$). Hence, in order to generate a new Green's function with two additional dot operators generated by the Coulomb interaction U, two of the dot operators f from the group $n_{\bar\sigma} f_\sigma$ have to tunnel into lead operators c. This allows us to organize the hierarchy of EOM into different generations in U. A Green's function of generation[6] n will contain $2n+1$ operators at time t ($\langle\langle f_\sigma \rangle\rangle$ is the zeroth generation).

In order to stop the infinite hierarchy of EOM, we have to truncate it. The exact

[6]The Green's functions appearing at the n$^{\text{th}}$ generation are what we called n-particle Green's functions.

truncation follows the procedure due to Kubo [51] for fermionic operators $a, b, c, \cdots$

$$\langle\langle b^\dagger cd\rangle\rangle = \langle b^\dagger c\rangle\langle\langle d\rangle\rangle - \langle b^\dagger d\rangle\langle\langle c\rangle\rangle + \langle\langle b^\dagger cd\rangle\rangle_c, \tag{2.44}$$

$$\begin{aligned}\langle\langle a^\dagger b^\dagger cde\rangle\rangle = & -\langle a^\dagger c\rangle\langle\langle b^\dagger de\rangle\rangle + \langle a^\dagger d\rangle\langle\langle b^\dagger ce\rangle\rangle - \langle a^\dagger e\rangle\langle\langle b^\dagger cd\rangle\rangle \\ & +\langle b^\dagger c\rangle\langle\langle a^\dagger de\rangle\rangle - \langle b^\dagger d\rangle\langle\langle a^\dagger ce\rangle\rangle + \langle b^\dagger e\rangle\langle\langle a^\dagger cd\rangle\rangle \\ & +\langle a^\dagger b^\dagger cd\rangle\langle\langle e\rangle\rangle - \langle a^\dagger b^\dagger ce\rangle\langle\langle d\rangle\rangle + \langle a^\dagger b^\dagger de\rangle\langle\langle c\rangle\rangle \\ & +2\langle a^\dagger c\rangle\langle b^\dagger d\rangle\langle\langle e\rangle\rangle - 2\langle a^\dagger d\rangle\langle b^\dagger c\rangle\langle\langle e\rangle\rangle - 2\langle a^\dagger e\rangle\langle b^\dagger d\rangle\langle\langle c\rangle\rangle \\ & +2\langle a^\dagger d\rangle\langle b^\dagger e\rangle\langle\langle c\rangle\rangle - 2\langle a^\dagger c\rangle\langle b^\dagger e\rangle\langle\langle d\rangle\rangle \\ & +2\langle a^\dagger e\rangle\langle b^\dagger c\rangle\langle\langle d\rangle\rangle + \langle\langle a^\dagger b^\dagger cde\rangle\rangle_c, \end{aligned} \tag{2.45}$$

where $\langle\langle\cdots\rangle\rangle_c$ represents the correlated part which cannot be decoupled. This is completely general[7]. Let us stress that this decoupling takes the non-interacting Ground State average values *and* Green's functions. Computing carelessly the average values in a self-consistent scheme can lead to a double-counting problem. Indeed, in that case, the EOM hierarchy develops both in the decoupled expectation value and in the remaining Green's function. In order to avoid this, we have to keep track of the terms directly generated by the self-consistent calculation of the average values decoupled at a lower generation, not to decouple them another time. Introducing the decoupling of Eq. (2.44) inside Eq. (2.45) leads to

$$\begin{aligned}\langle\langle b^\dagger cd\rangle\rangle &= \langle b^\dagger c\rangle\langle\langle d\rangle\rangle - \langle b^\dagger d\rangle\langle\langle c\rangle\rangle + \langle\langle \dot{:}b^\dagger cd\dot{:}\rangle\rangle_c, \\ \langle\langle a^\dagger\dot{:}b^\dagger cd\dot{:}e\rangle\rangle &= -\langle a^\dagger c\rangle\langle\langle \dot{:}b^\dagger d\dot{:}e\rangle\rangle + \langle a^\dagger d\rangle\langle\langle \dot{:}b^\dagger c\dot{:}e\rangle\rangle + \langle b^\dagger e\rangle\langle\langle a^\dagger\dot{:}cd\dot{:}\rangle\rangle \\ & \quad -\langle a^\dagger\dot{:}b^\dagger c\dot{:}e\rangle\langle\langle d\rangle\rangle + \langle a^\dagger\dot{:}b^\dagger d\dot{:}e\rangle\langle\langle c\rangle\rangle \\ & \quad +2\langle a^\dagger d\rangle\langle b^\dagger e\rangle\langle\langle c\rangle\rangle - 2\langle a^\dagger c\rangle\langle b^\dagger e\rangle\langle\langle d\rangle\rangle + \langle\langle a^\dagger b^\dagger cde\rangle\rangle_c, \end{aligned}$$

where we put vertical dots to remind the operators that have already been decoupled in a previous generation. We stress that this is the *same* decoupling, but with average values and Green's functions computed self-consistently.

We build a new approximation on the top of the Lacroix scheme by introducing the higher-order contributions that are physically relevant. One of the biggest limitations of the Lacroix approximation lies in its unphysical anti-resonance in the dot density of states at $\omega = 2\varepsilon_d + U$. If we track the derivation of the corresponding term, it appears in Eq. (2.28) in the denominator of the Green's function $\langle\langle c^\dagger_{k\bar\sigma} f_{\bar\sigma} f_\sigma\rangle\rangle$. This gives us the motivation to look for the processes which give a self-energy to $\langle\langle c^\dagger_{k\bar\sigma} f_{\bar\sigma} f_\sigma\rangle\rangle$, with the hope that a finite imaginary part would smear the divergence out. Of course, we should do the same for the other two-particle Green's functions of the same order in Eq. (2.28), namely $\langle\langle n_{\bar\sigma} c_{k\sigma}\rangle\rangle$ and $\langle\langle f^\dagger_{\bar\sigma} c_{k\bar\sigma} f_\sigma\rangle\rangle$, and consider coupling terms between those three Green's functions.

[7] For the Anderson model, a spin-conservation condition has to be considered in the decoupling (i.e. we cannot decouple $\langle a^\dagger_\sigma c_{\bar\sigma}\rangle$).

We can write this in the following system of equations

$$\begin{aligned}
\big[\omega_{:k} - \Sigma_{1\sigma}(\omega_{:k})\big]\langle\langle n_{\bar\sigma} c_{k\sigma}\rangle\rangle &= t_\sigma \langle\langle n_{\bar\sigma} f_\sigma\rangle\rangle + \sum_{k_1} t_{12,\sigma}(\omega,k,k_1)\langle\langle f^\dagger_{\bar\sigma} c_{k'\bar\sigma} f_\sigma\rangle\rangle \\
&\quad + \sum_{k_1} t_{13,\sigma}(\omega,k,k_1)\langle\langle c^\dagger_{k'\bar\sigma} f_{\bar\sigma} f_\sigma\rangle\rangle, \qquad (2.46a)\\
\big[\omega_{\bar\sigma:k\sigma} - \Sigma_{2\sigma}(\omega_{:k})\big]\langle\langle f^\dagger_{\bar\sigma} c_{k\bar\sigma} f_\sigma\rangle\rangle &= \langle f^\dagger_{\bar\sigma} c_{k\bar\sigma}\rangle + t_{\bar\sigma}\langle\langle n_{\bar\sigma} f_\sigma\rangle\rangle \\
&\quad + \sum_{k_1}\Big[-t_{\bar\sigma}\langle c^\dagger_{k_1\bar\sigma} c_{k\bar\sigma}\rangle - i\Gamma_\sigma \langle f^\dagger_{\bar\sigma} c_{k\bar\sigma}\rangle\Big]\langle\langle f_\sigma\rangle\rangle \\
&\quad + \sum_{k_1} t_{23,\sigma}(\omega,k,k_1)\langle\langle c^\dagger_{k_1\bar\sigma} f_{\bar\sigma} f_\sigma\rangle\rangle, \qquad (2.46b)\\
\big[\omega_{k:\sigma\bar\sigma} - U - \Sigma_{3\sigma}(\omega_{k:})\big]\langle\langle c^\dagger_{k\bar\sigma} f_{\bar\sigma} f_\sigma\rangle\rangle &= \langle c^\dagger_{k\bar\sigma} f_{\bar\sigma}\rangle - t_{\bar\sigma}\langle\langle n_{\bar\sigma} f_\sigma\rangle\rangle \\
&\quad + \sum_{k_1}\Big[t_{\bar\sigma}\langle c^\dagger_{k\bar\sigma} c_{k_1\bar\sigma}\rangle - i\Gamma_\sigma \langle c^\dagger_{k\bar\sigma} f_{\bar\sigma}\rangle\Big]\langle\langle f_\sigma\rangle\rangle \\
&\quad + \sum_{k_1} t_{32,\sigma}(\omega,k,k_1)\langle\langle f^\dagger_{\bar\sigma} c_{k_1\bar\sigma} f_\sigma\rangle\rangle. \qquad (2.46c)
\end{aligned}$$

The Lacroix approximations is recovered by setting the functions $\Sigma_{i\sigma}$ and $t_{ij,\sigma}$ to zero. Those functions are calculated at second order in t in Appendix B; a schematic representation of the new approximation is given in Fig. 2.1. This leads to a Green's function $\langle\langle f_\sigma\rangle\rangle$ that is exact at fourth order in t. In order to simplify the expressions in Eqs. 2.46, we use a shorthand notation

$$\omega_{\alpha\beta\cdots:ab\cdots} \equiv \omega + \varepsilon_\alpha + \varepsilon_\beta + \cdots - \varepsilon_a - \varepsilon_b - \cdots, \qquad (2.47)$$

with $\{\alpha\beta\cdots, ab\cdots\}$ being any set of parameters within k and σ[8]. In order to summarize the ideas, a schematic representation of our approximation scheme is given in Fig. 2.1, where it is compared to the Lacroix approximation scheme.

The dot Green's function can be written

$$\langle\langle f_\sigma\rangle\rangle = \frac{u_{2\sigma}(\omega) - \langle n_{\bar\sigma}\rangle - \Pi_\sigma(\omega)}{u_{1\sigma}(\omega)u_{2\sigma}(\omega) + \Xi_\sigma(\omega)}, \qquad (2.48)$$

where the functions $\Pi_\sigma(\omega)$ and $\Xi_\sigma(\omega)$ are defined by

$$\begin{aligned}
\Pi_\sigma(\omega) &= \sum_k \frac{t_{2\sigma}(\omega_{:k})\langle f^\dagger_{\bar\sigma} c_{k\bar\sigma}\rangle}{\omega_{:k} - \Delta\sigma - \Sigma_{2\sigma}(\omega_{:k})} + \sum_k \frac{t_{3\sigma}(\omega_{k:})\langle c^\dagger_{k\bar\sigma} f_{\bar\sigma}\rangle}{\omega_{k:} - 2\varepsilon_d - U - \Sigma_{3\sigma}(\omega_{k:})}, \qquad (2.49a)\\
\Xi_\sigma(\omega) &= -t_{\bar\sigma}\sum_{kk_1}\left[\frac{t_{2\sigma}(\omega_{:k})\langle c^\dagger_{k_1\bar\sigma} c_{k\bar\sigma}\rangle}{\omega_{:k} - \Delta\sigma - \Sigma_{2\sigma}(\omega_{:k})} - \frac{t_{3\sigma}(\omega_{:k})\langle c^\dagger_{k\bar\sigma} c_{k_1\bar\sigma}\rangle}{\omega_{k:} - 2\varepsilon_d - U - \Sigma_{3\sigma}(\omega_{k:})}\right] - i\Gamma_\sigma\Pi_\sigma(\omega). \qquad (2.49b)
\end{aligned}$$

[8] We have for instance: $\omega_{:k} \equiv \omega - \varepsilon_k$, $\omega_{k:} \equiv \omega + \varepsilon_k$, $\omega_{\bar\sigma:k\sigma} \equiv \omega + \varepsilon_{\bar\sigma} - \varepsilon_k - \varepsilon_\sigma$, and $\omega_{k:\sigma\bar\sigma} \equiv \omega + \varepsilon_k - \varepsilon_\sigma - \varepsilon_{\bar\sigma}$.

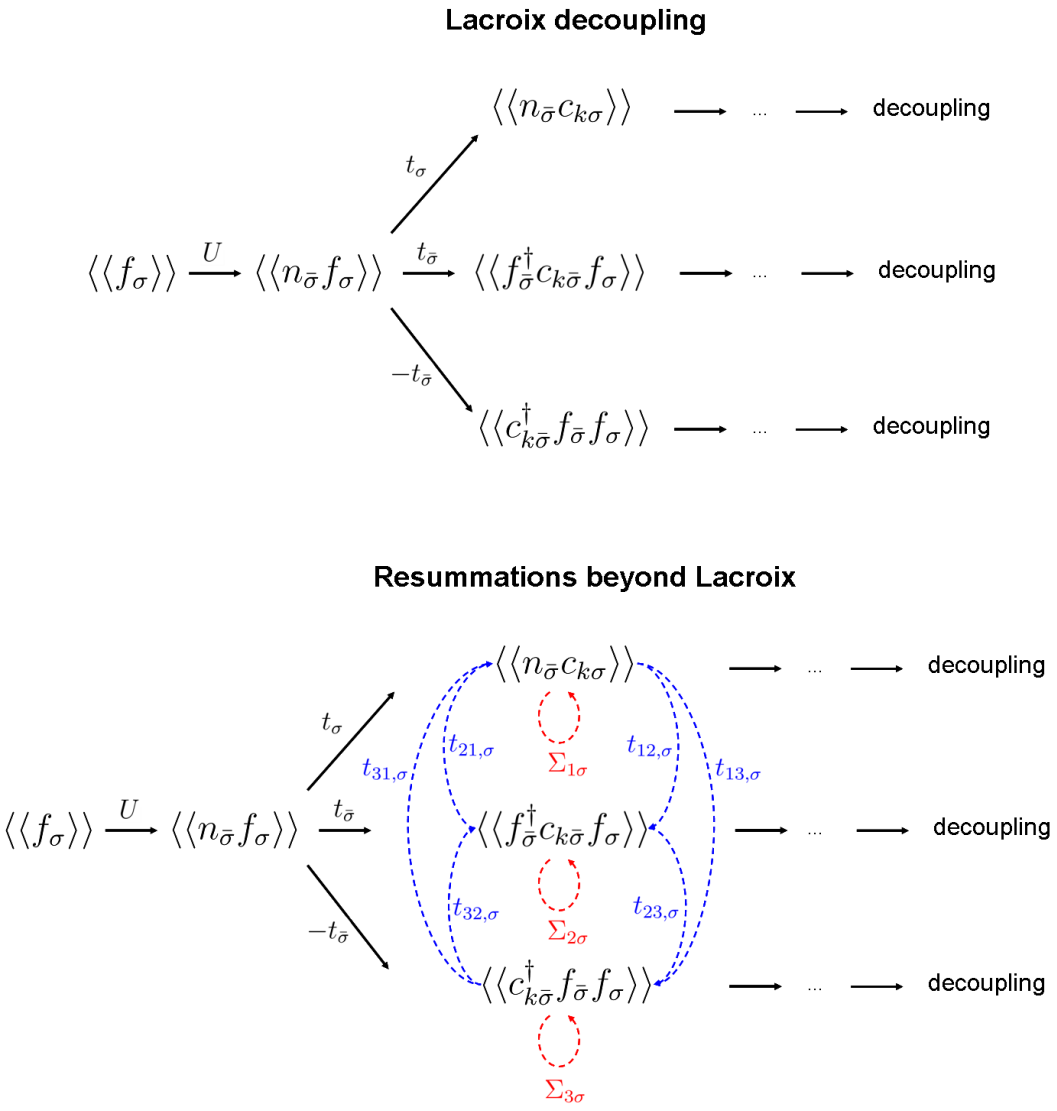

Figure 2.1: Schematic representation of the hierarchy of Green's functions and the resummations done within the Lacoix and the fourth order (in t) approximation schemes. The coefficients t_{21} and t_{31} are zero at second order in t, which explains why they are absent in Eqs. 2.46. The system of equations obtained at fourth order can be diagonalized, and we obtain effective coefficients $t_{i\sigma}$ from the Green's function $\langle\langle n_{\bar\sigma} f_\sigma\rangle\rangle$ to $\langle\langle n_{\bar\sigma} c_{k\sigma}\rangle\rangle$, $\langle\langle f^\dagger_{\bar\sigma} c_{k\bar\sigma} f_\sigma\rangle\rangle$ and $\langle\langle c^\dagger_{k\bar\sigma} f_{\bar\sigma} f_\sigma\rangle\rangle$.

The coefficients $t_{2\sigma}$ and $t_{3\sigma}$ are related to $t_{ij,\sigma}$ by Eqs. (B.10). Again, the Lacroix approximation corresponds to the lowest order in t for the coefficients: $\Sigma_{i\sigma}^{(0)} = 0$, $t_{1\sigma}^{(0)} = t_\sigma$, $t_{2\sigma}^{(0)} = t_{\bar\sigma}$ and $t_{3\sigma}^{(0)} = -t_{\bar\sigma}$. The renormalization of the coefficients $t_{i\sigma}$ changes the value of the Kondo temperature, which we discuss in Sec. 3.1.3, but has little influence on the qualitative point of view. Therefore, let us focus on the effect of the value of the self-energies $\Sigma_{i\sigma}$ at higher order in t in order to check whether they would introduce a finite cutoff to the poles in Eqs. (2.46). As demonstrated in Appendix B, we obtain at second order in t are

$$\Sigma_1^{(2)}(\omega_{:k}) = -2i\Gamma_{\bar\sigma}, \tag{2.50a}$$

$$\Sigma_{2\sigma}^{(2)}(\omega_{:k}) = -i\Gamma + \sum_{k_1}\left[-t_{\bar\sigma}^2 D_\sigma(\omega_{k_1:k}) + t_\sigma^2 D_{\bar\sigma}^*(-\omega_{k_1:k})\right] f(\varepsilon_{k_1}), \tag{2.50b}$$

$$\Sigma_{3\sigma}^{(2)}(\omega_{k:}) = -i\Gamma - \sum_{k_1}\left[t_\sigma^2 D_{\bar\sigma}(\omega_{k:k_1\bar\sigma}) + t_{\bar\sigma}^2 D_\sigma(\omega_{k:k_1\sigma})\right] f(\varepsilon_{k_1}), \tag{2.50c}$$

where the function $D_\sigma(\omega)$ is defined by

$$D_\sigma(\omega) = -U\frac{1}{\omega-\varepsilon_\sigma}\frac{1}{\omega-\varepsilon_\sigma-U}. \tag{2.51}$$

It is enlightening to relate D_σ to the Kondo exchange coupling $J = 2|t|^2 D_\sigma(0)$ for zero magnetic field, which enables easy comparison with results obtained from the Kondo model. As explained in Appendix B, D_σ can be replaced by a dressed expression by resumming higher-order terms:

$$\tilde D_\sigma(\omega) = \frac{1}{u_{1\sigma}(\omega)u_{2\sigma}(\omega) + \Xi_\sigma(\omega)}. \tag{2.52}$$

It is particularly interesting to study the value of the imaginary part of the self-energies at the pole of the corresponding Green's functions in Eq. (2.28) (e.g. at $\omega_{:k} = \Delta\sigma$ for $\langle\langle f_{\bar\sigma}^\dagger c_{k\bar\sigma} f_\sigma\rangle\rangle$). This quantity defines the decay rate of the excited state (e.g. $f_\sigma^\dagger c_{k\bar\sigma}^\dagger f_{\bar\sigma}|GS\rangle$, where the ground state is denoted by $|GS\rangle$). At zero temperature and for spin-independent tunneling, those decay rates are

$$\gamma_{1\sigma}^{(2)} = -\mathrm{Im}\Sigma_{1\sigma}^{(2)}(0) = \Gamma, \tag{2.53a}$$

$$\gamma_{2\sigma}^{(2)} = -\mathrm{Im}\Sigma_{2\sigma}^{(2)}(\Delta\sigma) = \frac{\Gamma}{2}\sum_\sigma\left[1 - f(\varepsilon_\sigma) + f(\varepsilon_\sigma+U)\right], \tag{2.53b}$$

$$\gamma_{3\sigma}^{(2)} = -\mathrm{Im}\Sigma_{3\sigma}^{(2)}(2\varepsilon_d+U) = \frac{\Gamma}{2}\sum_\sigma\left[1 + f(\varepsilon_\sigma) - f(\varepsilon_\sigma+U)\right]. \tag{2.53c}$$

In the Kondo regime ($\varepsilon_\sigma/\Gamma \ll 0 \ll (\varepsilon_\sigma+U)/\Gamma$), we get $\gamma_{2\sigma}^{(2)} = 0$ and $\gamma_{3\sigma}^{(2)} = 2\Gamma$. Therefore, only the divergence of $\langle\langle f_{\bar\sigma}^\dagger c_{k\bar\sigma} f_\sigma\rangle\rangle$ survives in Eq. (2.46), giving rise to large corrections around $\omega = \Delta\sigma$ associated with spin-flip transitions, while the spurious

	MF	HF	Lacroix	our method
$U \to 0$ limit	OK	OK	OK	OK
atomic limit	$\approx$ OK	OK	OK	OK
high-energy spectrum	$\approx$ OK	$\approx$ OK	OK	OK
low-energy spectrum	-	-	$\approx$ OK	$\approx$ OK
T-dependent spectrum	no	no	yes	yes
Coulomb blockade	$\approx$ OK	OK	OK	OK
Unitary limit for G	-	-	OK	OK
			for $\varepsilon_d \neq -U/2$	
decoherence effects	no	no	no	yes

Table 2.1: Comparison of the different approximation schemes within the EOM

divergence at $\omega = 2\varepsilon_d + U$ obtained in the Lacroix approximation is completely washed out.

The main features captured within the different approximation schemes for the EOM are briefly reviewed in Tab. 2.1. This is illustrated in more detail in Chapter 3, where we compare the numerical results.

2.8 Particle-hole symmetry

Besides the improvement brought by our approximation scheme, as listed in Tab. 2.1, the Green's function (2.48) slightly violates the particle-hole symmetry. This can for instance be checked by noticing that the dot density of the states at the particle-hole symmetric point $2\varepsilon_d + U$ is not exactly an even function. In this section, we show how this symmetry can be restored in the general case.

Let us consider the charge conjugation operator $\mathcal{C}$ which transforms an creation- into a destruction operator, or in other terms an electron into a hole: $f_\sigma \to \mathcal{C}(f_\sigma) = f_\sigma^\dagger,\ c_{k\sigma} \to \mathcal{C}(c_{k\sigma}) = c_{k\sigma}^\dagger$. This gives us an identity that relates the electron- to the hole Green's function

$$\mathcal{C}\left[\mathcal{G}_\sigma^r(\omega)\right] \equiv \langle\langle \mathcal{C}(f_\sigma), \mathcal{C}(f_\sigma^\dagger)\rangle\rangle_\omega = -\mathcal{G}_\sigma(-\omega). \tag{2.54}$$

In addition, the Anderson Hamiltonian for holes $\mathcal{C}\left[\mathcal{H}\right] = \mathcal{H}_h$ is, to within an additive constant,

$$\begin{aligned} \mathcal{H}_h &= \sum_{\alpha\sigma k} (-\varepsilon_k)\mathcal{C}(c_{\alpha k\sigma})\mathcal{C}(c_{\alpha k\sigma}^\dagger) + \sum_\sigma \left(-\varepsilon_\sigma - U\right)\mathcal{C}(n_\sigma) + U\mathcal{C}(n_\uparrow)\mathcal{C}(n_\downarrow) \\ &\quad - \sum_{\alpha\sigma k}\left(t_{\alpha\sigma}\mathcal{C}(f_\sigma)\mathcal{C}(c_{\alpha k\sigma}^\dagger) + h.c.\right), \end{aligned} \tag{2.55}$$

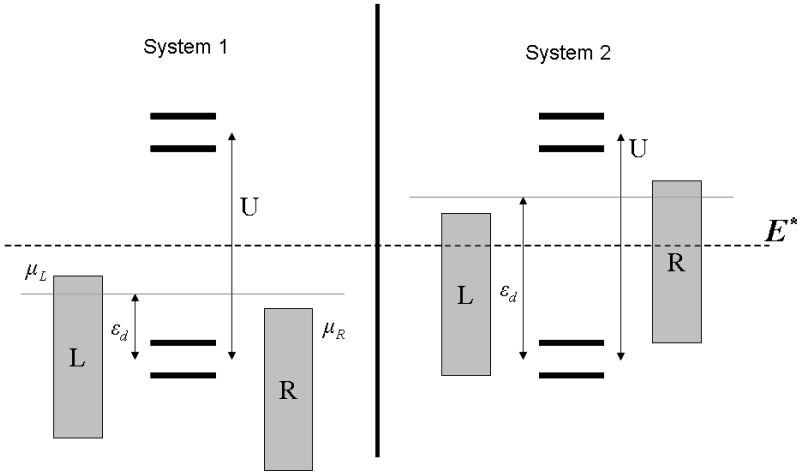

Figure 2.2: Schematic representation of two dual systems in the electron picture. The dotted line represents the particle-hole symmetric point E^*. Each system is equal to the mirror symmetry of its dual counterpart around E^* in energy space . The electrons in System 1 must behave exactly the same as the holes in System 2, and reversely.

where we keep the parameters of the original Hamiltonian for electrons. It maintains the structure of an Anderson Hamiltonian, but with new parameters given by

$$\mathcal{C}(\varepsilon_\sigma) = -\varepsilon_\sigma - U, \quad \mathcal{C}(U) = U, \quad \mathcal{C}(t_\sigma) = -t_\sigma, \quad \mathcal{C}(\varepsilon_k) = -\varepsilon_k. \tag{2.56}$$

To the hole Hamiltonian $\mathcal{H}_h$ (2.55) corresponds an electron Hamiltonian $\mathcal{H}_e^{\text{Syst2}}$ of another system, whose parameters share with $\mathcal{H}_h$:

$$\mathcal{H}_e^{\text{Syst2}} = \sum_{\alpha\sigma k} \varepsilon_k c^\dagger_{\alpha k\sigma} c_{\alpha k\sigma} + \sum_\sigma \left(-\varepsilon_\sigma - U\right) n_\sigma + U n_\uparrow n_\downarrow - \sum_{\alpha\sigma k} \left(t_{\alpha\sigma} f^\dagger_\sigma c_{\alpha k\sigma} + h.c.\right), \tag{2.57}$$

with a Fermi distribution $f(\varepsilon_k + \mu_\alpha)$ in the leads. We call dual systems two systems showing the symmetry $\mathcal{H}_h^{\text{Syst1}} = \mathcal{H}_e^{\text{Syst2}}$, as illustrated in Fig. 2.2. For instance, we can have the following parameters

	System 1	System 2
$\mathcal{H}_e$	$\varepsilon_d = -2$; $U = 6$	$\varepsilon_d = -4$; $U = 6$
$\mathcal{H}_h$	$\mathcal{C}(\varepsilon_d) = -4$; $\mathcal{C}(U) = 6$	$\mathcal{C}(\varepsilon_d) = -2$; $\mathcal{C}(U) = 6$

An electron in the first system behaves exactly as a hole in the second (dual) system and reversely.

This symmetry is slightly broken by our approximation scheme in the single-occupancy Coulomb blockade regime. The reason is due to the fact that at order t_σ^4 we do not

treat the particle and hole contributions on an equal footing. The decay rates extracted from the self-energies $\Sigma_{2\sigma}$ and $\Sigma_{3\sigma}$ have different values in the frequency range $\varepsilon_\sigma \leq \omega \leq \varepsilon_\sigma + U$. This leads to slightly asymmetric renormalization of the position and the broadening of the resonant peaks at ε_σ and $\varepsilon_\sigma + U$, which affects the occupation number. For instance, at the particle-hole symmetric point ($\varepsilon_\sigma = -U/2$, $\mu_L = -\mu_R$), the dot occupation number $\langle n_\sigma \rangle$ is expected to be exactly $1/2$ at equilibrium or in the symmetric bias setting, for which our numerical result shows a deviation by a few percents at worst. However, it has almost no effect on the low-frequency density of states structure.

In order to restore the symmetry, we compute the Green's function in the dual system. Because of the definition of the duality, we have the identity

$$\mathcal{G}_\sigma^{\text{Syst1}}(\omega) = \mathcal{C}\left[(\mathcal{G}_\sigma^{\text{Syst2}}(\omega)\right], \tag{2.58}$$

where Systems 1 and 2 are dual of each other. Using Eq. (2.54) on System 2, we can express this equality in terms of electron Green's functions only:

$$\mathcal{G}_\sigma^{\text{Syst1}}(\omega) = -\left[\mathcal{G}_\sigma^{\text{Syst2}}(-\omega)\right]^*.$$

As mentioned earlier, this equality is slightly violated at high frequencies by our approximation scheme. We therefore symmetrize the two by setting

$$\mathcal{G}_\sigma^r(\omega) = \frac{1}{2}\left\{\mathcal{G}_\sigma^{\text{Syst1}}(\omega) - \left[\mathcal{G}_\sigma^{\text{Syst2}}(-\omega)\right]^*\right\}. \tag{2.59}$$

Chapter 3

Equilibrium properties of the Anderson model

The transport observables of the single-level Anderson model at equilibrium have been solved exactly by means of Bethe Ansatz techniques [103, 9]. In addition, many energy-dependent quantities can be solved by numerical methods such as the numerical renormalization group [105, 16]. Several other techniques were developed for the study of a specific range of parameters, such as the Fermi-liquid theory [76], conformal field theory [2], density matrix renormalization group [102], slave boson [13] and equation-of-motion approaches [52]).

Therefore, it is insightful to look at the results obtained with the EOM in order to check the agreement with exact methods in order to build its extensions out of equilibrium on a solid basis. We compare the various approximations schemes presented in Chapter 2, and discuss the improvements brought by our method. We also discuss the effect of a finite temperature on the density of states in the dot and on the differential conductance, and we introduce the concept of decoherence. Throughout this chapter, we consider a zero magnetic field $\Delta = 0$.

3.1 Results at zero temperature

At zero temperature, divergent logarithmic corrections appear in the perturbative expansion in the exchange coupling J of any physical quantity and the system sits in the strong coupling regime. Therefore, the higher-order corrections are large and the bare perturbation theory cannot be applied. As the EOM are essentially a perturbative method too, we expect its results to be badly controlled. However, thanks to a resummation of some divergent series at all orders, the divergent terms eventually cancel each other out in the Green's function, and we get a finite density of states $\rho_\sigma(\omega)$ even at zero temperature[1]. Therefore, we expect that our equations-of-motion can describe qualitatively several features of the Kondo effect even at zero temperature, where the

[1]However, the derivative $d\rho_\sigma(\omega)/d\omega$ is divergent at the Fermi level.

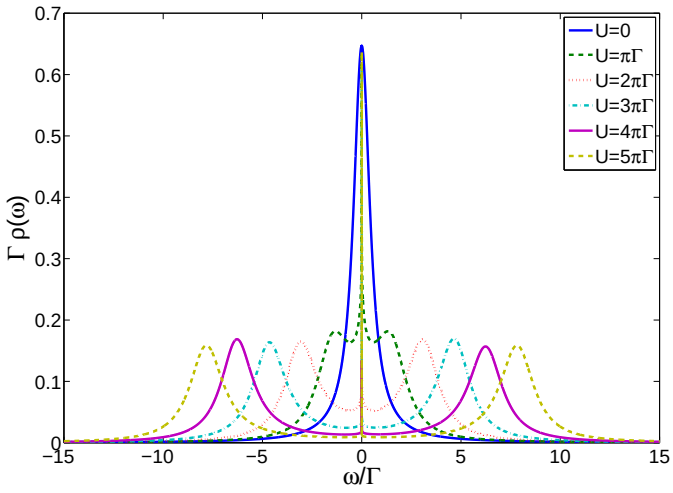

Figure 3.1: Equilibrium density of states in the particle-hole symmetric case at $T = 0$ for different values of the parameter U (the chemical potential of the leads μ_{eq} is taken equal to 0). The density of states for large U shows a three-peak structure with two broad side peaks and a narrow Kondo resonance peak centered at the Fermi level.

comparison with exact methods is easier[2]. In this section, we compare the approximation schemes presented in Chapter 2, and discuss the improvements brought by our method.

3.1.1 Density of states in the dot

The density of states in the dot is an interesting quantity in the Kondo effect, as it provides a clear signature of the many-body singlet state around the Fermi level of the leads. In addition, it is required to study the transport through the dot, and more precisely the compute the current from Eq. (1.6). The figure 3.1 represents the density of states in the dot $\rho_\sigma(\omega) = -1/\pi \mathrm{Im}\mathcal{G}^r_\sigma(\omega)$ at equilibrium for different values of the parameter U using our equations-of-motion approach. The Fermi level of the leads μ_{eq} is taken equal to zero. We willingly choose to consider the particle-hole symmetric case ($\varepsilon_d = -U/2$) since we know that it is a delicate case in the sense that the EOM approaches developed so far have failed to describe it correctly. As soon as U becomes larger than $\pi\Gamma$, a local moment develops inside the dot [7], and the density of states shows a three-peak structure with two broad peaks at high energy and a narrow Kondo resonance peak.

Let us first focus on the broad peaks. They are related to single-particle processes in which an electron is added in the dot state $|\sigma\rangle$, either when the other dot state $|\bar{\sigma}\rangle$ is unoccupied (left peak around ε_σ) or when another electron sits in the state $|\bar{\sigma}\rangle$,

[2]The reader interested in the validity of the Lacroix approximation at zero temperature should read [27] and [43].

costing an additional energy U because of the Coulomb repulsion (right peak around $\varepsilon_\sigma + U$). Including higher order processes does not modify this qualitative picture, but only involves a renormalization of the dot energies ε_σ and U. In order to quantify this renormalization, we can take the lowest order corrections to the pole in the denominator of the Green's function $\mathcal{G}_\sigma(\omega)$ in Eq. (2.48). Around $\omega \approx \varepsilon_\sigma$, we find

$$\mathcal{G}_\sigma(\omega \approx \varepsilon_\sigma) \approx \frac{1 - \frac{\langle n_{\bar\sigma}\rangle}{u_{2\sigma}(\omega)}}{\omega - \varepsilon_\sigma + i\Gamma_\sigma + \frac{\Xi_\sigma(\omega)}{u_{2\sigma}(\omega)}} \approx \frac{1 - \langle n_{\bar\sigma}\rangle}{\omega - \varepsilon^*_\sigma + i\Gamma^*_\sigma}, \tag{3.1}$$

with the recursive identity

$$\varepsilon^*_\sigma = \varepsilon_\sigma + t_{\bar\sigma} \sum_k f(\varepsilon_k)\, \mathrm{Re}\left[\frac{t_{2\sigma}(\omega_{:k}) \big[\omega_{\bar\sigma:k\sigma} - \Sigma_{2\sigma}(\omega_{:k})\big]^{-1} - t_{3\sigma}(\omega_{k:}) \big[\omega_{k:\sigma\bar\sigma} - U - \Sigma_{3\sigma}(\omega_{k:})\big]^{-1}}{u_{2\sigma}(\omega)} \right]_{\omega=\varepsilon^*_\sigma}. \tag{3.2}$$

The value of U^* can be deduced directly from particle-hole symmetry $\varepsilon^*_d + U^*/2 = \varepsilon_d + U/2$. In addition, the width of the peak gets also renormalized, and its value is given by

$$\Gamma^*_\sigma = \Gamma_\sigma - t_{\bar\sigma} \sum_k f(\varepsilon_k)\, \mathrm{Im}\left[\frac{t_{2\sigma}(\omega_{:k}) \big[\omega_{\bar\sigma:k\sigma} - \Sigma_{2\sigma}(\omega_{:k})\big]^{-1} - t_{3\sigma}(\omega_{k:}) \big[\omega_{k:\sigma\bar\sigma} - U - \Sigma_{3\sigma}(\omega_{k:})\big]^{-1}}{u_{2\sigma}(\omega)} \right]_{\omega=\varepsilon^*_\sigma}. \tag{3.3}$$

The renormalization of those peaks is close to the value obtained within the Lacroix approximation in Eq. (2.34); their position, intensity and amplitude agree quantitatively with the numerical renormalization group result [19]. As expected, the renormalization effects are small around the particle-hole symmetric case ($\varepsilon_\sigma = -U/2$). In the large $U/|\varepsilon_\sigma|$ limit, the renormalization effects are very important, as it is the case for quantum dots coupled to ferromagnetic leads [66, 99].

Let us now describe the central narrow peak in Fig. 3.1. It is the consequence of the low-energy divergent terms inside $\Pi_\sigma(\omega)$ and $\Xi_\sigma(\omega)$ in the dot Green's function (2.48). As we discussed in Sec. 2.7.1, the poles of those terms appear in the expansion of the EOM for higher-order Green's functions in Eqs. (2.46). The imaginary part of the corresponding self-energies evaluated at the pole of the Green's functions (e.g. at $\omega_{:k} = \varepsilon^*_\sigma - \varepsilon^*_{\bar\sigma}$ for $\langle\langle f^\dagger_{\bar\sigma} c_{k\bar\sigma} f_\sigma \rangle\rangle$) defines the decay rate of the excited state $f^\dagger_\sigma c^\dagger_{k\bar\sigma} f_{\bar\sigma} |GS\rangle$, where the ground state is denoted by $|GS\rangle$. Within second order in t_σ, and taking into account the renormalization of the dot level energies, the decay rates are given by Eqs. (2.53).

At the particle-hole symmetric point, a single decay rate (namely $\gamma_{2\sigma}$) is zero, while the other ones are finite and smear out the corresponding divergences. As a consequence, the only divergences that eventually survive are those located at $\omega = \Delta\sigma$. Therefore, in the absence of magnetic field ($\Delta = 0$), the Kondo resonance peak is pinned at the Fermi level of the leads. The relevant pole appears in the expansion of the EOM

for $\langle\langle f^\dagger_{\bar\sigma} c_{k\bar\sigma} f_\sigma, f^\dagger_\sigma\rangle\rangle$, which is related to the many-particle spin-flip scattering processes involved in the Kondo effect, as described in Chapter 1. Moreover, the density of states at the Fermi level is found to be $\rho_\sigma(\mu_{eq}) = 2/\pi\Gamma$, in agreement with the Fermi liquid property at zero temperature and hence respecting the unitarity condition. This can be shown by similar arguments as in Sec. 2.6.4, and the relationship

$$\mathcal{G}^r_\sigma(0) \approx \lim_{\omega\to 0} \frac{\mathcal{G}^a_\sigma(0)\ln\left|\frac{\omega}{W}\right|}{\ln\left|\frac{\omega}{W}\right|\left[1+i\Gamma\mathcal{G}^a_\sigma(0)\right]}$$

holds even at the particle-hole symmetric point $\varepsilon_d = -U/2$. The fact that our equations-of-motion scheme correctly describes the particle-hole symmetric case is one of the successes of the w nemethod. This can be understood by the fact that in the previous EOM approaches, for the Kondo regime, there is an exact cancellation of the divergent terms in the Lacroix Green's function (2.30) for $\Delta = 2\varepsilon_d + U = 0$

$$-\sum_k \frac{t_{\bar\sigma}\langle f^\dagger_{\bar\sigma} c_{k\bar\sigma}\rangle}{\omega-\varepsilon_k} + \sum_k \frac{t_{\bar\sigma}\langle c^\dagger_{k\bar\sigma} f_{\bar\sigma}\rangle}{\omega+\varepsilon_k} = t^2_{\bar\sigma}\sum_k\left[-\frac{f(\varepsilon_k)\mathcal{G}^r_\sigma(\varepsilon_k)}{\omega-\varepsilon_k} + \frac{f(\varepsilon_k)\mathcal{G}^a_\sigma(\varepsilon_k)}{\omega+\varepsilon_k}\right] = 0,$$

$$\sum_{kk_1}\frac{t^2_{\bar\sigma} f(\varepsilon_k)}{\omega-\varepsilon_k} + \sum_{kk_1}\frac{t^2_{\bar\sigma} f(\varepsilon_k)}{\omega+\varepsilon_k} = -2i\Gamma_{\bar\sigma}.$$

In order to prove the first identity, we used the relation $\mathcal{G}^a_\sigma(\varepsilon) = -\mathcal{G}^r_\sigma(-\varepsilon)$, valid at the particle-hole symmetric point. The cancellation of the two divergences is cured in our EOM approach since the denominator $\omega + \varepsilon_k$ acquires a finite decay rate $\gamma_{3\sigma} = 2\Gamma$, and the corresponding divergence is smeared out. Therefore, the cancellation does not occur any longer, and we are left with a single divergence from the pole at $\omega = \varepsilon$ at the origin of the formation of the Kondo resonance peak.

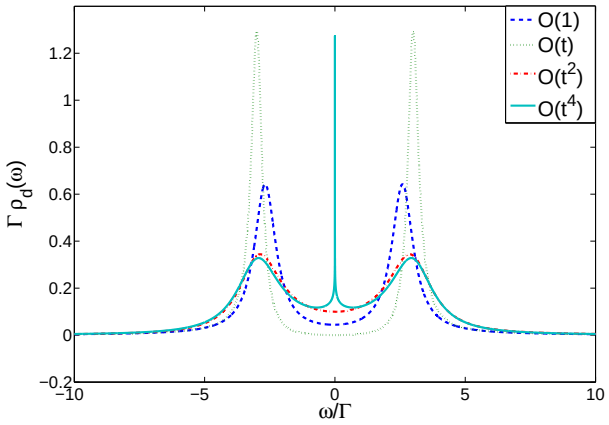

(a) Density-of-states in the dot for $U/\Gamma = 6$ and $\varepsilon_d/\Gamma = -3$

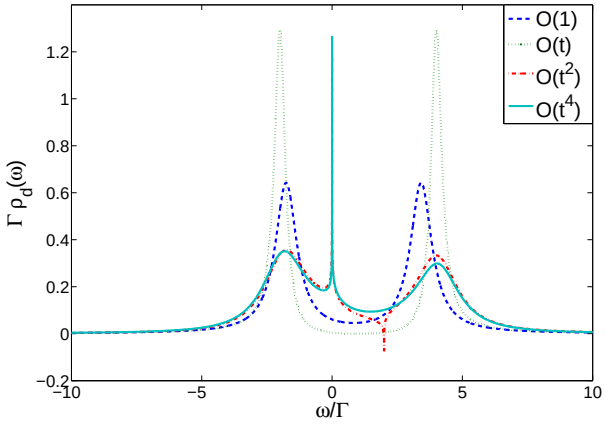

(b) Density-of-states in the dot for $U/\Gamma = 6$ and $\varepsilon_d/\Gamma = -2$

Figure 3.2: Total density of states in the dot $\rho_d(\omega) = \rho_\uparrow(\omega) + \rho_\downarrow(\omega)$, for the different decoupling schemes of the equations-of-motion. (a) At the particle-hole symmetric point $\varepsilon_d = -U/2$, the Lacroix approximation (at $O(t^2)$) fails to produce the Kondo resonance at the Fermi level. This pathology is cured by our approximation scheme (at $O(t^4)$). (b) Outside the particle-hole symmetric point $\varepsilon_d \neq -U/2$, the Lacroix approximation produces a Kondo resonance at the Fermi level which is in qualitative agreement with the peak at fourth order. However, the second order approximation also shows an unphysical anti-resonnance at $\omega = 2\varepsilon_d + U$, which is smeared out by our higher-order approximation scheme.

The comparison of our approach with lower-order approximation schemes is shown in Fig. 3.2. The approximations at zeroth and first order in t are unable to describe the many-particle Kondo effect and the related resonance at the Fermi level of the leads. They reproduce two single-particle peaks around ε_d and $\varepsilon_d + U$. For the self-consistent Hartree solution (at order 1), the two peaks are lorentzians of width Γ. Their position is renormalized in comparison with the bare dot energy parameters because of the effective mean field generated by the Coulomb repulsion inside the dot (see Sec. 2.4). Let us stress that the result in Fig. 3.2 is the average on the two stable solutions obtained from the self-consistent treatment. For a particular solution, one peak (say at ε_d) would correspond to the density of states in one of the spin states (say spin-up), while the other peak would be associated to the opposite spin.

The total density of states is quite similar at first order in t. The two peaks sit a the bare dot energy levels ε_d and $\varepsilon_d + U$ and their widths are renormalized, as expressed in Eq. (2.27).

At the particle-hole symmetric point $\varepsilon_d = -U/2$ (Fig. 3.2(a)), our approximation

	$\gamma_{1\sigma}^{(2)}$	$\gamma_{2\sigma}^{(2)}$	$\gamma_{3\sigma}^{(2)}$
Empty dot ($\varepsilon_\sigma - \mu_\alpha \gg \Gamma$)	Γ	Γ	Γ
Kondo regime ($\varepsilon_\sigma + U - \mu_\alpha,\ \mu_\alpha - \varepsilon_\sigma \gg \Gamma$)	Γ	0	2Γ
Doubly-occupied dot ($\mu_\alpha - \varepsilon_\sigma - U \gg \Gamma$)	Γ	Γ	Γ
Mixed valence regime (Min$\{\varepsilon_\sigma - \mu_\alpha, \mu_\alpha - \varepsilon_\sigma - U\} \approx \Gamma$)	Γ	Γ	Γ

Table 3.1: Decay rates $\gamma_i^{(2)}$ at the second order in t_σ and at zero temperature, as given in Eq. (2.53), for the different regimes of the Anderson model obtained by the EOM approach. Notice that, in the Kondo regime, $\gamma_2^{(2)} = 0$ yields low-energy logarithmic divergence of the self-energy of the dot Green's function, responsible for the Kondo effect.

scheme (at fourth order in t) is the only one able to recover the Kondo resonance at the Fermi level. At high energy, there is a good agreement between our method and the Lacroix approximation (second order in t): the two broad single-particle peaks are located at the renormalized dot levels ε_d^* and $\varepsilon_d^* + U^*$, and their width is equal to Γ.

For the other cases $\varepsilon_d \neq -U/2$ (Fig. 3.2(b)), both our approach and the Lacroix approximation are able to recover the Kondo resonance at the Fermi level of the leads. However, as we discussed in Sec. 2.6, the Lacroix approximation shows a spurious negative peak at $\omega = 2\varepsilon_d + U$. That feature corresponds to processes in which two electrons enter/leave the quantum dot at the same time, and we have shown that the related excited states acquire a finite decay rate $\gamma_{3\sigma} = 2\Gamma$ at higher order that smears out the resonance.

So far, we only discussed the Kondo regime where $\varepsilon_d/\Gamma < -1$ and $(\varepsilon_d + U)/\Gamma > 1$. In order to describe the transport through the quantum dot for any dot energy level ε_d and Coulomb interaction U, it is instructive to study the second-order decay rates in the different transport regimes. Let us consider the case of spin-independent tunneling ($\Gamma_\uparrow = \Gamma_\downarrow = \Gamma/2$) to make the discussion easier. The results are reported in Table 3.1 for the different regimes of the Anderson model at zero temperature.

From Eq. (2.53), we can note that, in the wide-band limit, the value of $\gamma_{1\sigma}^{(2)} = \Gamma$ does not depend on the occupancy in the dot. In contrast, the other transition rates vary depending on the regimes considered. Putting the dressed D functions into the expressions of the $\gamma_{i\sigma}$ leads to

$$\gamma_{2\sigma}^{(2)} \approx \frac{\Gamma}{2} \sum_\sigma \left[1 - f(\varepsilon_\sigma^*) + f(\varepsilon_\sigma^* + U^*)\right], \tag{3.4a}$$

$$\gamma_{3\sigma}^{(2)} \approx \frac{\Gamma}{2} \sum_\sigma \left[1 + f(\varepsilon_\sigma^*) - f(\varepsilon_\sigma^* + U^)\right]. \tag{3.4b}$$

We can distinguish three regimes:

a) In both the empty and doubly-occupied dot regimes, $\gamma_{2\sigma}^{(2)} = \gamma_{3\sigma}^{(2)} = \Gamma$. The

finite values of $\gamma_{2\sigma}^{(2)}$ and $\gamma_{3\sigma}^{(2)}$ provide a cut-off to the integrals involved in the calculation of the remaining terms, thereby preventing them from diverging at low energy. As a result, the electron density of states in the dot does not show any resonance peak but only two broad peaks located at the positions of the renormalized dot level energies. As all the diverging corrections are smeared out, the lowest order approximation schemes is quite accurate and higher-order corrections are negligible.

b) In the mixed valence regime (take for instance $\varepsilon_\sigma - \mu_\alpha \approx \Gamma$), the renormalization effects push the dot level energies above the chemical potential, hence the decay rates are identical to those found in the two regimes of a). Our numerical results for the density of states are in better agreement with the exact numerical renormalization group result than those found in the Lacroix approximation or the non-crossing approximation, for which a spurious peak may appear at the Fermi level, as it has been shown in Ref. [71].

c) The singly-occupied dot (Kondo) regime is the most interesting since one of the decay rates, namely $\gamma_{2\sigma}^{(2)}$, vanishes. This gives rise to a logarithmical divergence at low energy of the integral involved in the calculation of the first term of $\Xi_\sigma(\omega)$ and $\Pi_\sigma(\omega)$ in Eqs. (2.49). The presence of the above-mentioned logarithmical divergence is responsible for the formation of the Kondo resonance peak in the electron density of states in the dot.

3.1.2 Linear conductance

The electrons around the chemical potential of the leads can tunnel through the dot if there is an open channel at the Fermi level. At zero temperature, the linear conductance is therefore directly related to the value of the dot density of states at $\omega = \mu_L = \mu_R$, as discussed in Sec. 1.2.2. In particular, we discussed in the previous section the occurrence of a resonant peak in the dot density of states around the Fermi level in the Kondo regime, with a height equal to $\rho_\sigma(0) = 2/\pi\Gamma$. From Eq. (1.8), it implies a maximum conductance $G = 2e^2/h$ in the case of a symmetric coupling to the leads ($\Gamma_L = \Gamma_R$).

Outside the Kondo regime, we saw in Sec. 3.1.1 that the divergent terms at the Fermi level are smeared out. As a consequence, the density of states inside the dot is only a single-particle spectrum composed by two lorentzians of width Γ around the dot energy levels ε_d and $\varepsilon_d + U$, and the conductance is large only when one of those levels is close the the chemical potential in the leads. We compare the dependence of the linear conductance on the gate voltage ($V_g \propto -\varepsilon_d + \mathrm{cst}$) for the different approximation schemes of equations-of-motion in Fig. 3.3.

In our approximation scheme at fourth order in t, the linear conductance is enhanced in the Kondo regime to a maximum value of $2e^2/h$ (central region). The conductance starts decreasing when it approaches the mixed-valence regime (in a bandwidth

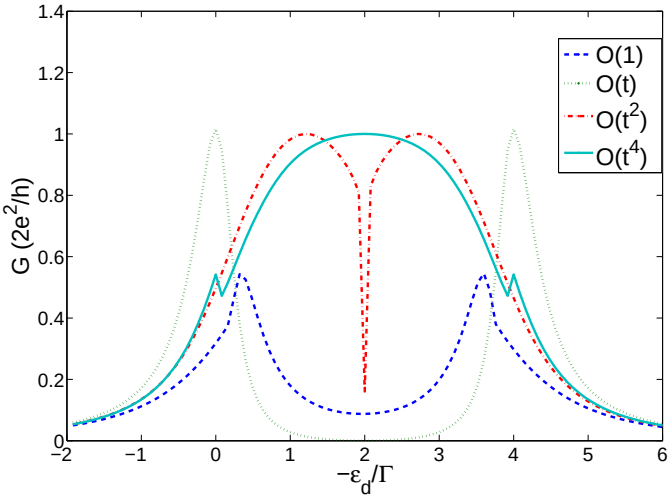

Figure 3.3: Linear conductance as a function of the gate voltage $V_g \propto -\varepsilon_d + \text{cst}$ at zero temperature and for $U = 4\Gamma$. We compare the different approximation schemes. The conductance obtained after truncation at zeroth and first order only reproduces the Coulomb blockade regime. At second order (Lacroix approximation), the conductance is increased in the single-occupancy region $-\varepsilon_d \in [\Gamma, U - \Gamma]$ because of the Kondo effect, except around the particle-hole symmetric point $\varepsilon_d = -U/2$, where the approximation fails. This problem is solved at fourth order (our study).

Γ around $\varepsilon_d = 0$ or $\varepsilon_d + U = 0$), where the charge fluctuations from the single-particle states become dominant. Finally, it goes to zero in the empty ($\varepsilon_d \gg 0$) or doubly occupied ($\varepsilon_d + U \ll 0$) regimes because of the Coulomb blockade. This picture is in perfect agreement with experimental results (see for instance Fig. 1.4).

A small discontinuity is observed around $\varepsilon_d = 0$ or $\varepsilon_d + U = 0$ due to the presence of step function in the bare expression of $\gamma_{2\sigma}$ in Eq. (2.53). This discontinuity can be smeared out by replacing the bare D function by a dressed one in the expression for $\Sigma_{2\sigma}$, see Eq. (B.4). However, if this is valid in the mixed-valence regime, it involves higher-order terms which cancel out in the Kondo regime with other fourth order contributions to $\Sigma_{2\sigma}$ as discussed in App. B, and we prefer showing the result with the bare expression everywhere.

None of the lower-order approximation schemes is able to reproduce the correct qualitative behavior of the conductance for any dot level ε_d. As expected from the discussion in Sec. 3.1.1, the Lacroix approximation (second order in t) fails to recover the unitary limit $G = 2e^2/h$ at the particle-hole symmetric point, while it is rather accurate for $\varepsilon_d \neq -U/2$. On the other hand, the truncations at zeroth and first order capture only the Coulomb blockade regime, but are unable to describe the Kondo physics.

3.1.3 Kondo temperature

At equilibrium and at zero temperature, the Kondo scale T_K can be roughly estimated from the real part of the pole of $\mathcal{G}^r_\sigma(\omega)$ in Eq. (2.48) located near the chemical potential [36]. Considering spin-independent couplings $\Gamma_\sigma = \Gamma_{\bar\sigma} = \Gamma/2$ in the wide-band limit, the real part of the denominator of the dot Green's function around the $\omega \approx 0$ is, at second order in t

$$u_{1\sigma}(0)u_{2\sigma}(0) + \frac{\Gamma_{\bar\sigma}}{\pi}\frac{t_{2\sigma}(0)}{t_{\bar\sigma}} \ln\left|\frac{\max(2\varepsilon_d + U, 2\Gamma)}{\omega}\right| = 0. \tag{3.5}$$

Solving for $\omega = T_K$ gives

$$T_K \simeq \max(2\varepsilon_d + U, 2\Gamma) \exp\left\{\frac{2\pi\varepsilon_d(\varepsilon_d + U)}{\Gamma U}\frac{t_{\bar\sigma}}{t_{2\sigma}(0)}\right\}, \tag{3.6}$$

T_K is independent of W, as expected since the high-energy scale is now regulated by U.

The result for T_K in Eq. (3.6) shows two improvements in comparison with the expression found within the Lacroix approximation $[2\varepsilon_d + U]\exp[2\pi\varepsilon_d(\varepsilon_d + U)/\Gamma U]$. First, the Lacroix result for T_K is improved by an exponential factor $t_{\bar\sigma}/t_{2\sigma}(0) < 1$, in better agreement with Haldane's prediction $(U\Gamma/4)^{1/2}\exp[\pi\varepsilon_d(\varepsilon_d + U)/\Gamma U]$ [33]. This is due to the renormalization of the coupling $t_{2\sigma}$ between $\langle\langle n_{\bar\sigma} f_\sigma\rangle\rangle$ and $\langle\langle f^\dagger_{\bar\sigma} c_{k\bar\sigma} f_\sigma\rangle\rangle$ at fourth order in t (see Fig. 2.1). Secondly, at the particle-hole symmetric point $(2\varepsilon_d + U = 0)$, the proposed approximation cures the aforementioned pathology of the Lacroix approximation for which T_K vanishes. The expression of T_K at that point is given by

$$T_K \simeq 2\Gamma \exp\left[\frac{\pi\varepsilon_d}{\Gamma}\frac{t_{\bar\sigma}}{t_{2\sigma}(0)}\right]. \tag{3.7}$$

The analytical expression given by Eq. (3.6) is only approximate since it neglects the self-consistent treatment. Therefore, we will rather calibrate it numerically when we show the curves. As it is done in experiments, it can be extracted from the temperature dependence of the zero-bias conductance

$$\left.\frac{dI}{dV}\right|_{T=T_K;V=0} = \frac{1}{2}G_0, \tag{3.8}$$

where $G_0 = 2e^2/h$ is the zero-bias conductance at zero temperature.

3.2 Finite temperature

At finite temperature, the system can no longer be described by its Ground State only, and the quantum description is more difficult. As a consequence, the system lies in a superposition of the spin-singlet Ground State and its excited states.

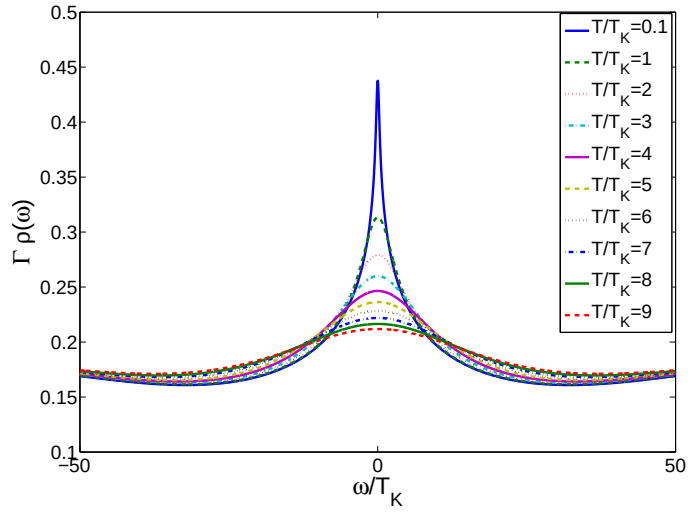

Figure 3.4: Kondo resonance in the dot density of states for different temperatures at the particle-hole symmetric point $\varepsilon_d = -U/2$ and for $U = \pi\Gamma$.

Therefore, the spin-flip scattering processes associated with the Kondo effect no longer involves energy conservation. As a consequence, we expect that the related excited state $f^\dagger_{\bar{\sigma}} c_{k\bar{\sigma}} f_\sigma \left|GS\right\rangle$ acquires a finite decay rate $\gamma_{2\sigma}$. As $\gamma^{(2)}_{2\sigma} = 0$ at second order in t, it motivates us to check whether a finite temperature-dependent contribution is obtained at fourth order in t. The calculation is done in Appendix B. We obtain a new contribution $\gamma^{(4)}_{2\sigma}$ in Eq. (B.17) which is expressed as an integral over an energy window $f(x)\left[1-f(x)\right]$. For $T \ll \left|\varepsilon_\sigma\right|, \varepsilon_\sigma + U$, the energy window for the conduction electrons can be approximated by a Dirac peak: $f(x)\left[1-f(x)\right] \to T\delta(x)$. The decoherence rate $\gamma^{(4)}_{2\sigma}$ is given by

$$\gamma^{(4)}_{2\sigma}(T) = T \sum_{\sigma'\sigma''} \frac{\Gamma_{\sigma'}\Gamma_{\sigma''}}{\pi} D^2_{\sigma''}(0) = T \frac{\Gamma^2 U^2}{\pi\varepsilon_d^2 \left(\varepsilon_d + U\right)^2} = \left(\nu J\right)^2 \pi T. \tag{3.9}$$

πT is the phase factor accounting for the electronic density of states near the Fermi surface and $\nu J = \Gamma D_\sigma(0)$ accounts for the spin-flip probability. This result can be compared to the Korringa width $\gamma_{2\sigma} = \hbar/\tau_2$ in nuclear magnetic resonance [49], where τ_2 is the average time for the spin fluctuations. It is not surprising because the equations-of-motion are a perturbative method valid for $T \gg T_K$; in that regime, the spin fluctuations are controlled by the scattering of the conduction electrons on the magnetic impurity. This result was already obtained by means of an EOM method applied to the Kondo model [107]. At low temperature $T \ll T_K$, τ_2 is related to the binding energy of the singlet state $\hbar/\tau_2 = T_K$ [77]. As the system lies in a spin-singlet Ground State, an external conduction electron sees a non-magnetic impurity. The latter regime is however out of scope of the equations-of-motion.

The occupation of excited states leads at finite temperature to a smearing of the

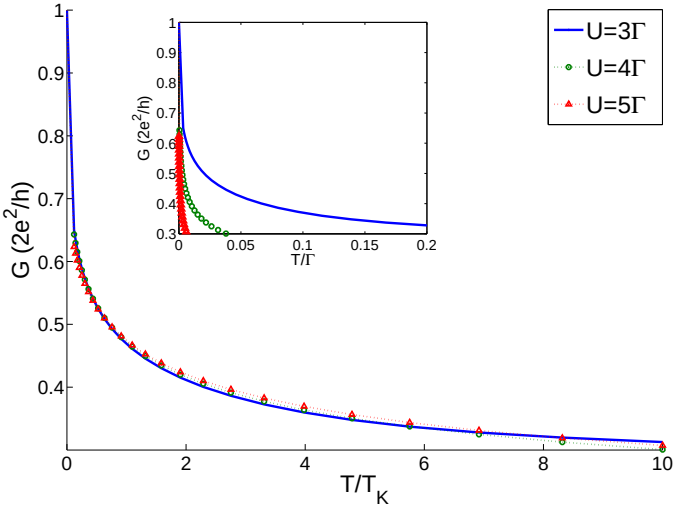

Figure 3.5: Temperature dependence of the linear conductance at the particle-hole symmetric point $\varepsilon_d = -U/2$ for different values of the Coulomb interaction U. We rescaled the temperature on T_K in order to show the universal behavior of $G(T/T_K)$. The unscaled curves $G(T)$ are shown in the inset.

Kondo peak in the dot density of states. On Fig. 3.4, we show the Kondo peak for different temperatures. As the temperature is increased, the height of the peak goes down while its width is increased. By definition of the Kondo temperature, the height of $\rho_\sigma(\omega)$ at $T = T_K$ is half of the value at zero temperature: $\rho_\sigma(\omega = T_K) = 1/\pi\Gamma$.

The temperature dependence of the conductance is shown on Fig. 3.5. A fast decay of the conductance is observed when the temperature is increased. Let us stress that the mechanism governing this decrease is essentially independent of the smearing of the Kondo resonance in the density of states. Instead, it is related to the fact that we integrate over an energy window of width T around the Fermi level to compute the current; the conductance is proportional to the weight of the density of states in that interval around the Fermi level (and, as a consequence, around the Kondo resonance). The main effect of the decoherence rate $\gamma_{2\sigma}$ is to smear the resonance in the density of states by a quantity proportional to the temperature T. As a consequence, the weight of the resonance is essentially redistributed in that window, and the result of the integration that gives the conductance is almost independent of the decoherence rate $\gamma_{2\sigma}$ of the excited state $f^\dagger_{\bar\sigma} c_{k\bar\sigma} f_\sigma |GS\rangle$. The linear conductance was calculated for different values of the Coulomb interaction U. When U/Γ is increased, the Kondo temperature T_K diminishes, which implies that the Kondo resonance in the density of states is narrower, as it was illustrated in Fig. 3.1. Therefore, its weight in the energy-window of width T is smaller and the decrease of the conductance with the temperature is faster (see inset of Fig. 3.5). When the temperature T is normalized on the Kondo temperature T_K, we recover the universal behavior for the conductance $G(T/T_K)$ (main figure of Fig. 3.5). This is a hallmark of the Kondo effect and was

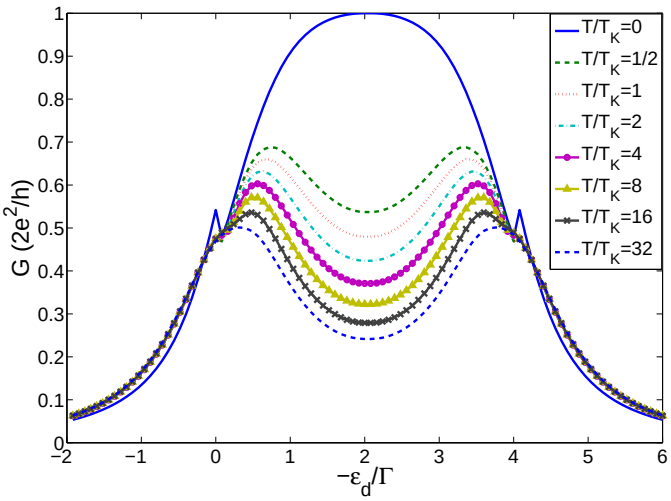

Figure 3.6: Linear conductance as a function of dot level energy ε_d, for $U/\Gamma = 4$ and at different temperatures. We choose for T_K the Kondo temperature at the particle-hole symmetric point. When the temperature is lowered, the conductance is enhanced in the singly-occupied regime $-\varepsilon_d/\Gamma \in [0, 4]$, and eventually reaches the maximum conductance $2e^2/h$ for a single channel at zero temperature.

observed experimentally in many devices (see for instance Fig. 1.5).

Figure 3.6 shows the linear conductance as a function of dot energy level ε_d at different temperatures for $U/\Gamma = 4$. At zero temperature, we recover the unitary limit $2e^2/h$ in the Kondo regime $\varepsilon_d \in [-U+\Gamma, -\Gamma]$, as discussed previously. When the temperature is raised, the linear conductance decreases in the Kondo regime, and eventually reaches a Coulomb blockade regime when $T \gg T_K$. The Kondo temperature depends on the position of the dot level and reaches a minimum at the particle-hole symmetric point (we choose that value of T_K for the scaling of the temperature). Therefore, the Kondo effect is destroyed faster at that point than closer to the single-particle peaks, which explains why the conductance is lower in the middle of the Kondo region. Finally, the external regions of zero and double occupancy are always in the Coulomb blockade regime as they carry a zero spin. Therefore, the conductance is independent of T_K in those regions and tends to be slightly raised by an increase of the temperature.

Chapter 4

Non-equilibrium transport

At equilibrium, the Anderson model can be solved exactly and a good agreement is found between theory and experiment. In opposite, several new questions arise when the system is put out of equilibrium by applying a bias voltage V between two leads, as no exact theoretical method could be extended from a Ground State basis to a Steady State basis. Theoretically, the Kondo effect out of equilibrium has been investigated by a variety of techniques developed most of the time within the Keldysh formalism: perturbation theory and perturbative renormalization group approach [41, 18, 79, 86, 87, 78], slave-boson formulation solved by using either mean-field [3] or non-crossing approximation [106], equation-of-motion approaches [71, 38]. Exact solutions at the Toulouse limit have been proposed [92]. Other ones have extended the Bethe ansatz out of equilibrium [48, 47], and in some cases have used the results to construct a Landauer-type picture of transport through the quantum dot. There have also been important efforts to develop numerical techniques such as time-dependent Numerical Renormalization Group [16, 6], time-dependent Density-Matrix Renormalization-Group [23] and imaginary-time theory solved by using Quantum Monte Carlo [35]. All those approaches have only a limited validity of their parameter regimes since they mostly describe the properties of the system in its Ground State, and not in the excited many-body states reached when the bias voltage drives a current through the dot.

The approximation scheme that we developed in Chapter 2 for the equations-of-motion can be extended directly out of equilibrium by keeping the lead indexes α alongside the wavenumber k in the derivations. The only difference lies inside the computation of the average values, which are to be determined within the Keldysh formalism. In this chapter, we show how this can be done, making the EOM a new candidate for the non-equilibrium description of the Anderson model. We present the results obtained for the density of states and the differential conductance. We also discuss the decoherence of the Kondo state induced by the bias voltage, and discuss when the system is driven to the weak-coupling regime.

4.1 Self-consistency out of equilibrium

The derivations of the average values in Sec. 2.6.3 are not valid out of equilibrium, and we demonstrate in this section how the calculation of the average values can be extended for a finite bias voltage. In the general case, the expectation values (as for instance $\langle f_\sigma^\dagger c_{\alpha k\sigma}\rangle$) can be expressed in terms of the related lesser Green's function

$$\langle f_\sigma^\dagger c_{\alpha k\sigma}\rangle \equiv -i\int \frac{d\omega}{2\pi}\mathcal{G}^<_{\alpha k\sigma,\sigma}(\omega), \tag{4.1}$$

where $\mathcal{G}^<_{\alpha k\sigma,\sigma}(\omega) = \langle\langle c_{\alpha k\sigma}, f_\sigma^\dagger\rangle\rangle^<$ is the Fourier transform of the lesser Green's function $\mathcal{G}^<_{\alpha k\sigma,\sigma}(t,t') = i\langle f_\sigma^\dagger(t')c_{\alpha k\sigma}(t)\rangle$ [62]. We reintroduce the lead index α, which was implicit in Sec. 2.2, because the different leads no longer carry the same chemical potential ($\mu_\alpha \neq 0$).

At equilibrium, the relationship $\mathcal{G}^<_{\alpha k\sigma,\sigma}(\omega) = -f(\omega-\mu_\alpha)[\mathcal{G}^r_{\alpha k\sigma,\sigma}(\omega)-\mathcal{G}^a_{\alpha k\sigma,\sigma}(\omega)]$ holds, relating the lesser Green's functions to the retarded and advanced ones, $\mathcal{G}^r_{\alpha k\sigma,\sigma}(\omega)$ and $\mathcal{G}^a_{\alpha k\sigma,\sigma}(\omega)$ respectively. The expectation value is then given by

$$\langle f_\sigma^\dagger c_{\alpha k\sigma}\rangle = -\frac{1}{\pi}\int d\omega\, f(\omega-\mu_\alpha)\,\mathrm{Im}\mathcal{G}^r_{\alpha k\sigma,\sigma}(\omega), \tag{4.2}$$

as it was shown in Sec. 2.6.3. This relationship is nothing else but the spectral theorem which expresses the expectation value in terms of a functional of the corresponding retarded Green's function.

However, the spectral theorem does not apply out of equilibrium [68] and it is therefore necessary to invoke the non-equilibrium Keldysh formalism. We show how to rewrite the expectation values in Eq. (2.48) in terms of integral functions. Making use of the Dyson equation and the Langreth theorem [55], we find

$$\begin{aligned}\langle f_\sigma^\dagger c_{\alpha k\sigma}\rangle \equiv& -i\int\frac{d\omega}{2\pi}\mathcal{G}^<_{\alpha k\sigma,\sigma}(\omega) = -it_\sigma\int\frac{d\omega}{2\pi}\left[g^r_{\alpha k\sigma}(\omega)\mathcal{G}^<_\sigma(\omega)+g^<_{\alpha k\sigma}(\omega)\mathcal{G}^a_\sigma(\omega)\right]\\ =&t_\sigma\left[f(\varepsilon_k-\mu_\alpha)\mathcal{G}^a_\sigma(\varepsilon_k)+\int\frac{d\omega}{2\pi i}\frac{\mathcal{G}^<_\sigma(\omega)}{\omega_{:k}+i\delta}\right], \qquad (4.3a)\\ \langle c^\dagger_{\alpha k\sigma} f_\sigma\rangle \equiv& -i\int\frac{d\omega}{2\pi}\mathcal{G}^<_{\sigma,\alpha k\sigma}(\omega) = -it_\sigma\int\frac{d\omega}{2\pi}\left[\mathcal{G}^r_\sigma(\omega)g^<_{\alpha k\sigma}(\omega)+\mathcal{G}^<_\sigma(\omega)g^a_{\alpha k\sigma}(\omega)\right]\\ =&t_\sigma\left[f(\varepsilon_k-\mu_\alpha)\mathcal{G}^r_\sigma(\varepsilon_k)+\int\frac{d\omega}{2\pi i}\frac{\mathcal{G}^<_\sigma(\omega)}{\omega_{:k}-i\delta}\right], \qquad (4.3b)\end{aligned}$$

$$\begin{aligned}\langle c^\dagger_{\alpha_1 k_1\sigma} c_{\alpha k\sigma}\rangle \equiv & -i\int\frac{d\omega}{2\pi}\mathcal{G}^<_{\alpha k\sigma,\alpha_1 k_1\sigma}(\omega)\\ =& -i\int\frac{d\omega}{2\pi}\Big\{\delta_{\alpha\alpha_1}\delta_{kk_1}g^<_{\alpha k\sigma}(\omega)+t_\sigma^2\left[g^r_{\alpha k\sigma}(\omega)\mathcal{G}^r_\sigma(\omega)g^<_{\alpha_1 k_1\sigma}(\omega)\right.\\ &\left.+g^r_{\alpha k\sigma}(\omega)\mathcal{G}^<_\sigma(\omega)g^a_{\alpha_1 k_1\sigma}(\omega)+g^<_{\alpha k\sigma}(\omega)\mathcal{G}^a_\sigma(\omega)g^a_{\alpha_1 k_1\sigma}(\omega)\right]\Big\}\\ =&\delta_{\alpha\alpha_1}\delta_{kk_1}f(\varepsilon_k-\mu_\alpha)+t_\sigma^2\frac{f(\varepsilon_k-\mu_\alpha)\mathcal{G}^a_\sigma(\varepsilon_k)-f(\varepsilon_{k_1}-\mu_{\alpha_1})\mathcal{G}^r_\sigma(\varepsilon_{k_1})}{\varepsilon_k-\varepsilon_{k_1}-i\delta}\\ &+t_\sigma^2\int\frac{d\omega}{2\pi i}\frac{\mathcal{G}^<_\sigma(\omega)}{(\omega_{:k}+i\delta)(\omega_{:k_1}-i\delta)},\end{aligned}\tag{4.3c}$$

where we used the unperturbed Green's functions for conduction electrons

$$\begin{aligned}g^{r/a}_{\alpha k\sigma}(\omega) &= \frac{1}{\omega_{:k}\pm i\delta},\\ g^<_{\alpha k\sigma}(\omega) &= 2\pi i f(\varepsilon_k-\mu_\alpha)\,\delta(\omega_{:k}).\end{aligned}$$

Using Eqs. (4.3c), we obtain after summation the two functions defined by $\Pi_\sigma(\omega)$ and $\Xi_\sigma(\omega)$ in Eqs. (2.49a-2.49b)

$$\begin{aligned}\Pi_\sigma(\omega) =& \sum_\alpha\frac{\Gamma_{\alpha\bar\sigma}}{\pi}\int d\varepsilon_k\frac{t_{2\sigma}(\omega_{:k})}{t_{\bar\sigma}}\frac{f(\varepsilon_k-\mu_\alpha)\mathcal{G}^a_\sigma(\varepsilon_k)}{\omega-\varepsilon_k-\Delta\sigma-\Sigma_{2\sigma}(\omega_{:k})}\\ &-\sum_\alpha\frac{\Gamma_{\alpha\bar\sigma}}{\pi}\int d\varepsilon_k\frac{t_{3\sigma}(\omega_{:k})}{-t_{\bar\sigma}}\frac{f(\varepsilon_k-\mu_\alpha)\mathcal{G}^r_\sigma(\varepsilon_k)}{\omega+\varepsilon_k-2\varepsilon_d-U-\Sigma_{3\sigma}(\omega_{k:})},\end{aligned}\tag{4.4a}$$

$$\begin{aligned}\Xi_\sigma(\omega) =& -\sum_\alpha\frac{\Gamma_{\alpha\bar\sigma}}{\pi}\int d\varepsilon_k\frac{t_{2\sigma}(\omega_{:k})}{t_{\bar\sigma}}\frac{f(\varepsilon_k-\mu_\alpha)}{\omega-\varepsilon_k-\Delta\sigma-\Sigma_{2\sigma}(\omega_{:k})}\\ &-\sum_\alpha\frac{\Gamma_{\alpha\bar\sigma}}{\pi}\int d\varepsilon_k\frac{t_{3\sigma}(\omega_{:k})}{-t_{\bar\sigma}}\frac{f(\varepsilon_k-\mu_\alpha)}{\omega+\varepsilon_k-2\varepsilon_d-U-\Sigma_{3\sigma}(\omega_{k:})}-i\Gamma\Pi_\sigma(\omega),\end{aligned}\tag{4.4b}$$

Notice that the imaginary part self-energies $\Sigma_{i\sigma}$ is always negative, so that the poles in the integrals are all in the same half of the complex plane. In deriving the Eqs. (4.4b), the terms associated with the lesser Green's function $\mathcal{G}^<_\sigma(\omega)$ vanish upon summing over k in the wide-band limit, since their denominators have two poles in the upper half complex plane. It implies that the non-equilibrium functions $\Pi_\sigma(\omega)$and $\Xi_\sigma(\omega)$ take the same form as in equilibrium in the wide-band limit, except that the Fermi-Dirac distributions in the left and right leads carry different chemical potentials. No knowledge of lesser Green's functions is needed. This constitutes a huge simplification in the computations.

As far as the occupation number in the dot $\langle n_\sigma\rangle = \langle f^\dagger_\sigma f_\sigma\rangle$ is concerned, the calculation is rather more complicated out of equilibrium since the simplification that takes place for the calculation of $\Pi_\sigma(\omega)$ and $\Xi_\sigma(\omega)$ does not occur, and we need to know the lesser Green's function $\mathcal{G}^<_\sigma(\omega)$ in order to derive $\langle n_\sigma\rangle$ by the use of

$$\langle n_\sigma\rangle \equiv -i\int\frac{d\omega}{2\pi}\mathcal{G}^<_\sigma(\omega).\tag{4.5}$$

To find $\mathcal{G}^<_\sigma(\omega)$, we use the Dyson equation written in the Keldysh formalism $\mathcal{G}^<_\sigma(\omega) = \mathcal{G}^r_\sigma(\omega)\Sigma^<_\sigma(\omega)\mathcal{G}^a_\sigma(\omega)$ and express the lesser self-energy $\Sigma^<_\sigma(\omega)$ via the Ng ansatz [74]

$$\Sigma^<_\sigma(\omega) = -2i \sum_{\alpha=L,R} \frac{\Gamma_{\alpha\sigma}}{\Gamma_\sigma} f(\omega - \mu_\alpha)\, \mathrm{Im}\Sigma^r_\sigma(\omega), \tag{4.6}$$

where $\Sigma^r_\sigma(\omega) \equiv \omega - \varepsilon_\sigma - [\mathcal{G}^r_\sigma(\omega)]^{-1}$ is the retarded self-energy. This ansatz is based on an extrapolation from both the non-interacting limit out of equilibrium and the interacting limit at equilibrium. Thanks to this ansatz, the calculation of $\langle n_\sigma \rangle$ can be performed from the knowledge of $\mathcal{G}^r_\sigma(\omega)$ only. We expect this assumption to be accurate as the occupation number is essentially influenced by the broad single-particle peaks around ε_σ and $\varepsilon_\sigma + U$ in the density-of-states, and not by some sharp resonances around the Fermi-level which develop in the Kondo regime. Let us also mention that many results can be obtained at the particle-hole symmetric point (also out of equilibrium), where the occupation number is identically 1/2.

Therefore, all the expectation values relevant to the calculations can be expressed in terms of $\mathcal{G}^r_\sigma(\omega)$, and the self-consistent scheme is straightforward. Eq. (2.48) ends up being a complex integral equation with respect to $\mathcal{G}^r_\sigma(\omega)$, exactly as in the equilibrium situation, except that the different chemical potentials of the two leads have to be entered explicitly.

4.2 Density of states

At equilibrium, we have shown that the Kondo effect is responsible for the emergence of divergent terms around the Fermi level of the leads in the Green's function inside the dot. Let us remind the EOM for the two-particle Green's function $\langle\langle f^\dagger_{\bar\sigma} c_{k\bar\sigma} f_\sigma \rangle\rangle$ that was shown produce the Kondo divergence in the density of states

$$(\omega_{:k} - \Sigma_{2\sigma}(\omega_{:k}))\, \langle\langle f^\dagger_{\bar\sigma} c_{\alpha k\bar\sigma} f_\sigma \rangle\rangle = \langle f^\dagger_{\bar\sigma} c_{k\bar\sigma} \rangle + t_{\bar\sigma} \sum_{\alpha' k'} \langle c^\dagger_{\alpha' k'\bar\sigma} c_{\alpha k\bar\sigma} \rangle \langle\langle f_\sigma \rangle\rangle + O(t^3),$$

where the lead index α was made explicit again in comparison with Eq. (2.46b). At lowest order, we have $\langle c^\dagger_{\alpha' k'\bar\sigma} c_{\alpha k\bar\sigma} \rangle = f(\varepsilon_k - \mu_\alpha)\delta_{kk'}\delta_{\alpha\alpha'}$, and the contribution to the corresponding term in $\Xi_\sigma(\omega)$ is

$$\sum_{\alpha k\sigma} t_{\alpha\bar\sigma} \frac{f(\varepsilon_k - \mu_\alpha)}{\omega_{:k} - \Sigma_{2\sigma}(\omega_{:k})}.$$

Therefore, the divergence is shifted to the two points $\omega = \mu_L$ and $\omega = \mu_R$, as could be seen from the Eqs. (4.4b).

In addition, we expect that the Kondo effect is progressively destroyed by the application of a bias voltage because related excited states acquire a finite decoherence rates induced by the voltage-driven current.

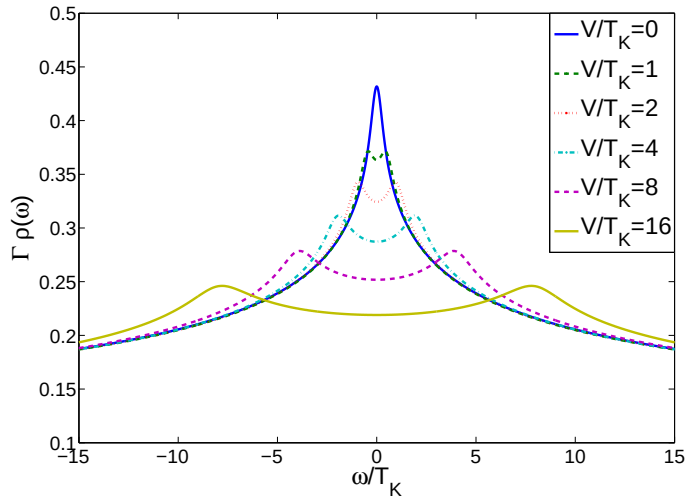

Figure 4.1: Non-equilibrium density of states in the particle-hole symmetric case at $U = 4\Gamma$ and $T = 10^{-1}T_K$, for different values of the bias voltage V. The chemical potentials of the two leads are taken equal to $\mu_{L/R} = \pm V/2$. The Kondo resonance peak splits into two side peaks located at $\omega = \pm V/2$, i.e. at the positions of the left- and right-lead chemical potentials. For convenience we choose to represent the two energy scales (energy ω and bias voltage V) as normalized by the factor T_K^{-1}.

Those excited states originate physically from the energy-conserving processes in which an conduction electron hops onto the dot while another electron with opposite spin hops out of the dot to one of the leads. When the two leads carry different chemical potentials, such a process can result in the transfer of a conduction electron above the Fermi level, destroying the coherence of the spin singlet wavefunction. Since the processes involve two electrons hopping in and out, the lowest-order contribution is fourth order in t. This motivated us to look for the higher order contribution to $\gamma_{2\sigma}$. Its expression for zero magnetic field is given by Eq. (B.17)

$$\gamma_{2\sigma}^{(4)} = \sum_{\alpha_1\alpha_2}\sum_{\sigma_1\sigma_2} \frac{\Gamma_{\alpha_1\sigma_1}\Gamma_{\alpha_2\sigma_2}}{\pi} \int_{-W}^{W} d\varepsilon_k f(\varepsilon_k - \mu_{\alpha_1}) \left[1 - f(\varepsilon_k - \mu_{\alpha_2})\right] \; D_{\sigma_2}^2(\varepsilon_k).$$

As for the current, the decohrence rate $\gamma_{2\sigma}$ is an integral function on an energy window $[\mu_L, \mu_R]$. At zero temperature and for spin-independent tunneling, we find at lowest order in t

$$\gamma_{2\sigma}(V) = \frac{\Gamma_L\Gamma_R}{\pi} D_\sigma^2(0)V + O(t^6) = \pi\frac{\Gamma_L\Gamma_R}{\Gamma^2}(\nu J)^2 V + O(J^3 V). \tag{4.7}$$

As a consequence, the divergences in the dot density of states are smeared out when current flows through the dot. The finite decoherence rate $\gamma_{2\sigma}$ broaden and diminish the Kondo resonance peaks in the density of states as the bias voltage increases, as shown

on Fig. 4.1. The figure reports our results for the non-equilibrium density of states, in the particle-hole symmetric case at $T = T_K/10$ and $U = 4\Gamma$ for different values of the bias voltage V. In contrast with the situation at equilibrium, the Kondo resonance peak splits into two lower peaks pinned at the chemical potentials of the two leads. The reason is that the transitions between the Ground State and the excited states of the dot are now mediated by the conduction electrons with energies lying close to the left- and right-lead chemical potentials.

4.3 Crossover from the strong-coupling to the weak-coupling regime

In Chapter 1, we discussed the breakdown of the perturbative treatment of the Anderson and Kondo models under a certain energy, because of the occurrence of low-energy diverging terms in the series. This limits the applicability of the equilibrium perturbation theory to temperatures larger than T_K, which is called the weak-coupling regime. In the strong-coupling regime, non-perturbative methods are required for solving the problem.

When a bias voltage is applied to the leads, it is interesting to investigate whether or not the decoherence induced by the voltage-driven current may drive the system from strong- to weak-coupling regime. We point out that this problem has been discussed in previous studies for the Kondo model using either a perturbative renormalization approach [18] or a slave-boson technique within non-crossing approximation [86]. As the equations-of-motion are a perturbative method as well, it is interesting to tackle this question for our approximation scheme. At lowest order in t and for $V \gg T_K$, the dot Green's function $\mathcal{G}^r_\sigma(\omega)$ in the Kondo regime has a denominator of the form

$$\mathcal{G}^r_\sigma(\omega) \propto \left[1 - \ln\left(\frac{(\omega - V/2 + i\gamma_{2\sigma})(\omega + V/2 + i\gamma_{2\sigma})}{T_K^2}\right)\right]^{-1}, \tag{4.8}$$

In order to avoid the Green's function $\mathcal{G}^r_\sigma(\omega)$ given by Eq. (4.8) to develop a pole on the real axis, the following condition must be fulfilled

$$F(\omega, V) \equiv \left[\omega^2 - V^2/4 - \gamma_{2\sigma}^2\right]^2 + \left[2\gamma_{2\sigma}\omega\right]^2 - e^2 T_K^4 \;>\; 0, \tag{4.9}$$

where e is Euler's number. We compute the two first derivatives of $F(\omega, V)$ in order to find the extrema

$$\begin{aligned} \frac{\partial F(\omega, V)}{\partial \omega} &= 4\omega\left[\omega^2 - V^2/4 + \gamma_{2\sigma}^2\right], \\ \frac{\partial^2 F(\omega, V)}{\partial \omega^2} &= 12\omega^2 - V^2 + 4\gamma_{2\sigma}^2 \end{aligned}$$

There are 3 extrema, located at $\omega = 0$ and $\omega = \pm\sqrt{V^2/4 - \gamma_{2\sigma}^2}$. We have a minimum at $\omega = 0$ at low bias ($|V| < 2\gamma_{2\sigma}$), and at $\omega = \pm\sqrt{V^2/4 - \gamma_{2\sigma}^2}$ at high bias ($|V| > 2\gamma_{2\sigma}$).

The condition (4.9) in those two cases becomes

$$\begin{aligned} F(0,V) > 0 \quad &\Leftrightarrow \quad \left|V^2/4 - \gamma_{2\sigma}^2\right| > eT_K^2, \\ F(\pm\sqrt{V^2/4 - \gamma_{2\sigma}^2}, V) > 0 \quad &\Leftrightarrow \quad \gamma_{2\sigma} V > eT_K^2. \end{aligned}$$

Combining those results, we find out that the dot Green's function develops a pole as soon as $\gamma_{2\sigma}$ is smaller than a characteristic energy scale defined by T^*

$$T^* = \begin{cases} \sqrt{eT_K^2 - V^2/4} & : \quad |V| < \sqrt{2e}\, T_K \\ eT_K^2/V & : \quad |V| > \sqrt{2e}\, T_K \end{cases} \tag{4.10}$$

From that expression, we define a criterion controlling the crossover between strong-coupling ($\gamma_{2\sigma} < T^*$) and weak-coupling ($\gamma_{2\sigma} > T^*$) regime, as proposed in Ref. [86]. In order to obtain the nontrivial decoherence rate $\gamma_{2\sigma}$ as a function of bias voltage V, we replace $D_\sigma(\varepsilon)$ appearing inside the bare exchange coupling $J_{\alpha\sigma,\beta\sigma'}$ in the decoherence rate by the dressed $\widetilde{D}_\sigma(\varepsilon)$, as defined in Eq. (2.52)[1]. In that way, we obtain a renormalized exchange coupling $\widetilde{J}_{\alpha\sigma,\beta\sigma'} \equiv 2t_{\alpha\sigma}t_{\beta\sigma'}\widetilde{D}_\sigma(\mu_\alpha)$. In the limit $V \gg T_K$, the scaling theory predicts $\widetilde{J}_{\alpha\sigma,\beta\sigma'} \propto 1/[2\,\ln(V/T_K)]$ and $\gamma_{2\sigma} \propto V/[2\,\ln(V/T_K)]^2$, which is always larger than T^*.

The results for the normalized decoherence rate $\gamma_{2\sigma}/T_K$ as a function of the bias voltage are reported in Fig. 4.2(a) for different values of U. Strikingly, the curves coincide after normalizing over T_K, underlining the universality of the evolution of $\gamma_{2\sigma}/T_K$ as a function of V/T_K. Combining the results for T^*/T_K and $\gamma_{2\sigma}/T_K$, we can derive the universal crossover bias voltage V_c/T_K from strong- to weak-coupling regime.

At finite temperature, the derivation for T^* is the same except for replacing $\gamma_{2\sigma} \to \sqrt{(\gamma_{2\sigma})^2 + \pi^2 T^2}$ in Eq. (4.8). The results are given in Fig. 4.2(b) in the $V - T$ plane, displaying the crossover from strong-coupling to weak-coupling regime. Although the physical mechanism at the origin of the crossover is different, both the bias voltage and the temperature drive the system to the weak-coupling regime (see Sec. 3.2).

This analysis has interesting consequences concerning the applicability of the equations-of-motion. Indeed, the perturbative corrections are small in the weak-coupling regime; therefore, we expect that our method gives reliable results in that case. As a consequence, it is a good candidate for studying non-equilibrium physics when the bias voltage drives the system in the weak-coupling regime. In the strong coupling regime, the EOM are more unstable but they nevertheless provide some qualitative results, as we illustrated in Chapter 3, because of the resummation of the divergent terms in the dot Green's function.

[1]However, the RG analysis indicates that the flow of $J_{LL(RR)}$ is different from that of J_{RL} for $\Lambda < V$, where Λ is the cutoff, see Refs. [18, 86]. We suspect that this substitution does not work in the low-energy regime where $\omega < V$.

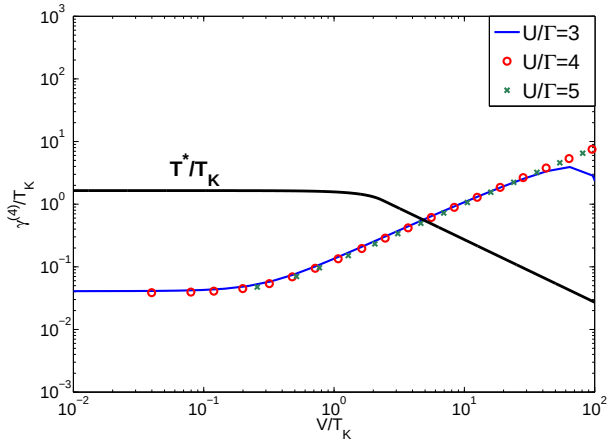

(a)

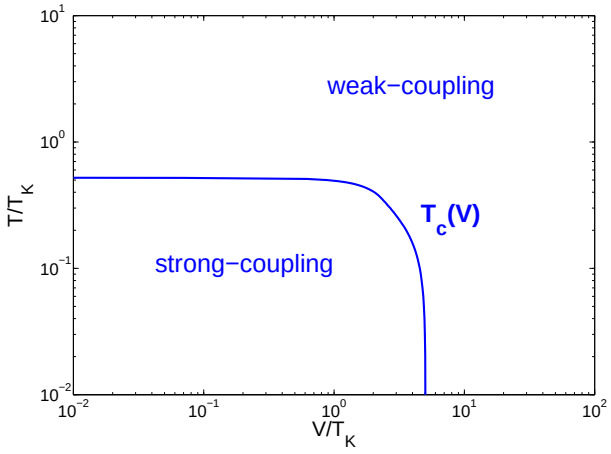

(b)

Figure 4.2: (a) Decoherence rate $\gamma_{2\sigma}$ and characteristic energy scale T^* versus the normalized bias voltage V/T_K at $T/T_K = 10^{-1}$ in the particle-hole symmetric case for several values of U/Γ. $\gamma_{2\sigma}/T_K$ is a universal function of V/T_K over a large range of bias voltage V. The comparison of both energy scales ($\gamma_{2\sigma}$ and T^*) determines whether the system is in the strong-coupling regime ($\gamma_{2\sigma} < T^*$) or weak-coupling regime ($\gamma_{2\sigma} > T^*$). (b) Stability phase diagram of the strong-coupling and weak-coupling regimes in the $V-T$ plane. The normalized crossover temperature $T_c(V)/T_K$ is a universal function of V/T_K.

4.4 Differential conductance

One of the main observables in non-equilibrium experiments on quantum dots is the differential conductance dI/dV. Using the equations-of-motion to find the density of states inside the dot and the expression of Eq. (1.6) the current, we obtain at zero temperature and for a symmetric bias $[\mu_L, \mu_R] = [V/2, -V/2]$

$$\frac{dI}{dV} = \frac{2e}{\hbar}\frac{\Gamma_L\Gamma_R}{\Gamma_L+\Gamma_R}\sum_\sigma\left[-\frac{1}{2}\rho_\sigma(V/2) - \frac{1}{2}\rho_\sigma(-V/2) + \int_{-V/2}^{V/2} d\varepsilon \frac{\partial\rho_\sigma(\varepsilon,V)}{\partial V}\right] \qquad (4.11)$$

As $\partial\rho_\sigma(\varepsilon,V)/\partial V \neq 0$, the conductance is no longer proportional to the probing of the density of states at the chemical potential of the leads, in opposition to the equilibrium case. In this Chapter, we show the results obtained by solving the equation numerically over a wide range of parameters. An analytical formula for the differential conductance in the weak-coupling regime will be derived in Chapter 5.

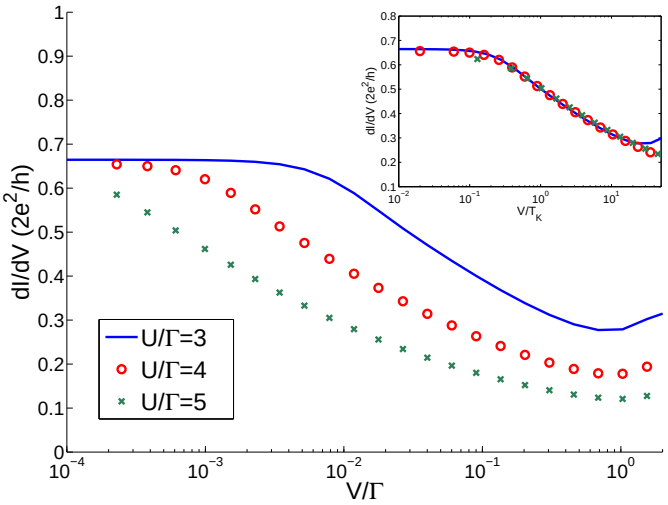

Figure 4.3: Differential conductance dI/dV as a function of the bias voltage V at $T/T_K = 0.1$ in the particle-hole symmetric case, and for different values of the Coulomb repulsion U. The conductance saturates a low bias at a value determined by the temperature, and decreases logarithmically when the bias voltage is increased. The inset shows that the differential conductance as a function of normalized bias voltage V/T_K scales to a single universal curve $dI/dV = f(V/T_K)$. At higher voltages, the universal behavior is destroyed by a broad peak resulting from charge fluctuations.

We present the bias voltage dependence of the differential conductance in Fig. 4.3 for different values of the Coulomb interaction U. The differential conductance exhibits a narrow[2] peak at low bias (often called zero-bias anomaly) saturating at at zero bias and zero temperature, reflecting the Kondo effect as in the experiment discussed in Fig 1.6. For our numerical study out of equilibrium, we are restricted to finite temperatures if we want the results to be independent of the accuracy of the discretization in energy (see App. C). We choose $T = T_K/10$, which explains why the maximum in the conductance is actually lower than the unitary limit. The differential conductance decreases logarithmically at intermediate voltages $V \in [T_K/10, 10T_K]$, before the bias voltage reaches the renormalized value of the dot level energy, where the conductance increases again because of single-electron charge transfers through the resonant level.

In the inset, the differential conductance is found to be a universal function of the normalized bias voltage V/T_K, independent of any other energy parameter. This one-parameter scaling is obtained over a large range of V, before universality is lost around $V > 10T_K$ because of the charge fluctuations. We stress that the Kondo temperature has been obtained from the *equilibrium* temperature dependence of the linear conductance (see Sec. 3.1.3), which is intrinsically independent of the non-equilibrium differential conductance represented in Fig. 4.3. Let us notice that the figure encom-

[2]mind the logarithmic horizontal axis

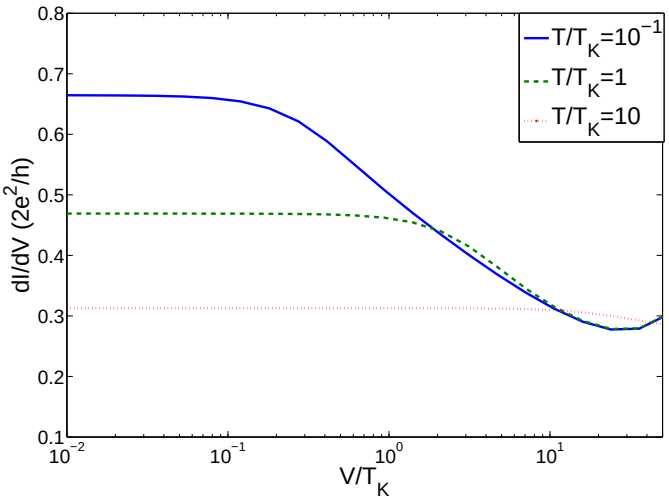

Figure 4.4: Differential conductance dI/dV as a function of the bias voltage V in the particle-hole symmetric case at $U/\Gamma = 3$, for different values of temperature. The differential conductance is reduced when either the temperature or the bias voltage increases.

passes universality *both* in the bias voltage and the temperature. This highlights the fact that, after rescaling *any* external low-energy parameters on T_K, all observables should develop a universal behavior in the Kondo regime.

The temperature dependence of the differential conductance is shown in Fig. 4.4. The narrow peak at low bias in the differential conductance is destroyed by increasing the temperature because the Fermi distributions inside the expression for the current (1.6) are smoothed, and are less sensitive to the resonances around $\omega = \mu_\alpha$ in the density of states inside the dot. As at equilibrium, the destruction of the Kondo features by the temperature in the differential conductance is not directly related to the half-width γ_{2sa} of the peak in the dot density of states. Indeed, the current is proportional to the area between the two maximums in the density of states and is therefore insensitive to a redistribution of the weight of the resonances inside the integration interval.

To further demonstrate that our extension of the equations-of-motion technique can work over a wide range of parameters, we report in Fig. 4.5 the differential conductance in a three-dimensional plot, as a function of the bias voltage V and gate voltage $V_g \propto -\varepsilon_d$. The figure shows the so-called Coulomb diamond, whose edges correspond to the alignment of the chemical potential of the leads with the single-particle energy levels ε_d and $\varepsilon_d + U$ inside the dot (with some additional renormalization effects in the mixed valence regime). The inside of the diamonds defines regions in the Coulomb blockade regime, where the total occupation number in the dot N ($N = \sum_\sigma n_\sigma$) is fixed. Sweeping the gate voltage $V_g \propto -\varepsilon_d$, we successively find the empty region $N = 0$, the single-occupancy region $N = 1$ and the doubly-occupied region $N = 2$. In the single-occupancy region (central region on Fig. 4.5), we observe a strong increase

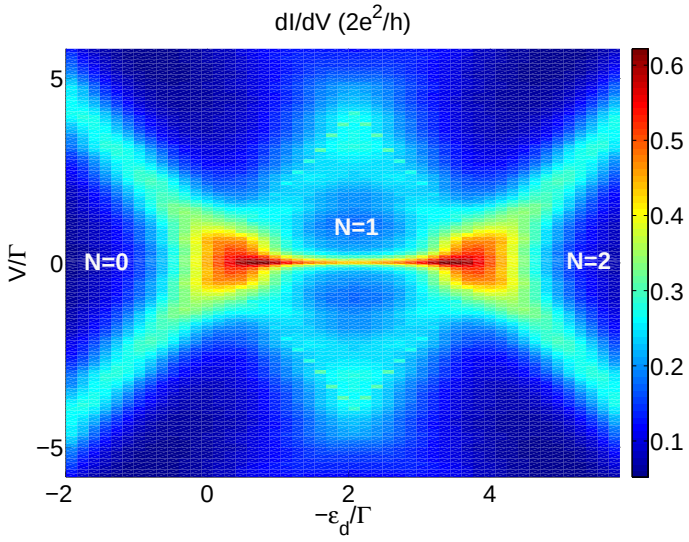

Figure 4.5: Color plot of the differential conductance dI/dV as a function of bias voltage V and dot-level energy ε_d for $U/\Gamma = 4$ and $T = 10^{-3}\Gamma$. The contour of the Coulomb peaks delimits the Coulomb blockade diamond, separating areas with well-defined dot occupation number N ranging from 0, 1 to 2 at low V, and areas of charge fluctuations at high V. In the $N = 1$ central valley, dI/dV shows a zero-bias peak related to the Kondo effect.

of the conductance at zero-bias, giving a signature of the Kondo effect. Making a cut along the $V = 0$ line, we recover the linear conductance discussed in Fig. 3.6, which was shown to be enhanced at low temperature in the Kondo regime. At zero temperature, the zero-bias conductance reaches the unitary limit $2e^2/h$, and decreases logarithmically when the temperature and/or the bias voltage is increased.

4.5 Comparison with other studies

We compare our results for the differential conductance with those obtained by other groups using numerical methods such as the time-dependent Numerical Renormalisation Group [6] and an imaginary-time theory solved by using Quantum Monte Carlo [35, 34]. We plot the results obtained for the bias voltage dependence of the differential conductance at zero temperature for comparison (Fig. 4.6). We find a qualitative agreement at low bias voltage, when the system is in the strong-coupling regime. In that regime, our method slightly underestimates dI/dV because it gives a smaller Kondo scale. The three curves join at higher bias voltages, where a quantitative agreement is found. A little local bump is observed for the EOM result at $V = U$, when the chemical potentials of the leads are aligned with the resonant levels of the dot ($\mu_L = \varepsilon_d + U$, $\mu_R = \varepsilon_d$). This is related to the fact that we used the bare $D_\sigma(\varepsilon)$ functions (2.51) in the non-Kondo regime, leading to divergence at $\mu_{L(R)} = \{\varepsilon_d, \varepsilon_d + U\}$, as discussed in Sec. 3.1. This bump can be smeared out by replacing the bare functions by the dressed ones $\tilde{D}_\sigma(\varepsilon)$.

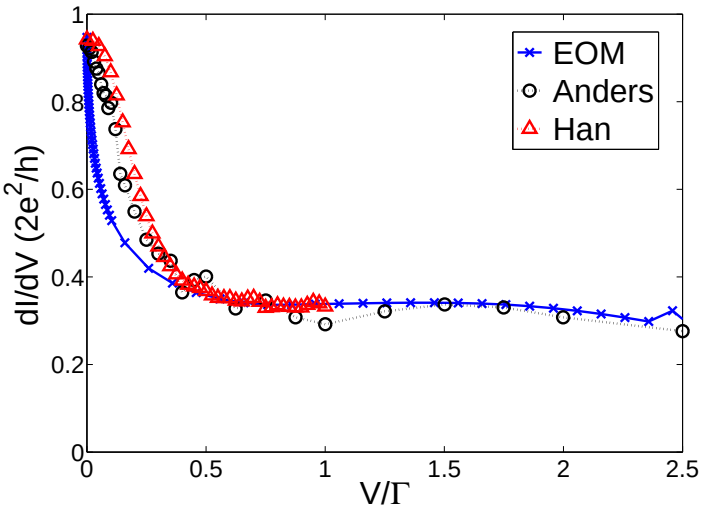

Figure 4.6: Comparison of the differential conductance dI/dV as a function of bias voltage V with the results obtained by Anders [6] and Han [34] for $-2\varepsilon_d/\Gamma = U/\Gamma = 2.5$ and $T/\Gamma = 0.008 \ll T_K/\Gamma$ (We are grateful to J.E. Han for providing us with his data points). Our curve is plotted for $T = 0$ in order to compare the three results in the strong-coupling regime. The differential conductance at small V is slightly different in the EOM approach because its value for T_K is smaller. At high bias voltage, the results of the three approaches agree perfectly.

4.6 Non-equilibrium occupation number in the dot

At equilibrium and for zero temperature, $\langle n_\sigma \rangle$ is mainly determined by the weight of the broad resonance peak far below the Fermi level. The narrow Kondo resonance near the Fermi energy has little weight in comparison. Thus, even if a equations-of-motion approach in a certain approximation scheme happens to describe only qualitatively Kondo physics, it is able to determine numerically an occupation number that agrees reasonably well with the Bethe ansatz or the numerical renormalization group.

When the system is driven out of equilibrium, the problem becomes more complicated as we should use lesser Green's functions instead of retarded ones to compute the expectation values. As discussed in Sec. 4.1, the only place where this cannot be circumvented is precisely for the dot occupation number $\langle n_\sigma \rangle$ appearing in the Green's function (2.48). A rigorous treatment would require to compute the lesser Green's function $\mathcal{G}^<_\sigma(\omega)$ and then obtain $\langle n_\sigma \rangle$ according to Eq. (4.5), which is beyond the scope of this work. So far, we considered the particle-hole symmetric case ($\varepsilon_d = -U/2$) and a symmetric bias voltage setting $[\mu_L, \mu_R] = [V/2, -V/2]$, in which case the occupation number is identically $\langle n_\sigma \rangle = 1/2$ by symmetry.

Now, let us take an asymmetric bias voltage $[\mu_L, \mu_R] = [0, -V]$, which is more in agreement with experiments. In that case, the occupation number $\langle n_\sigma \rangle$ is no longer fixed by symmetry arguments, and we use the Ng ansatz to compute the dot occupation number, as described in Sec. 4.1. The bias voltage dependence of the occupation number is shown on the solid blue curve in Fig. 4.7. As V increases, $\langle n_\sigma \rangle$ decreases rapidly

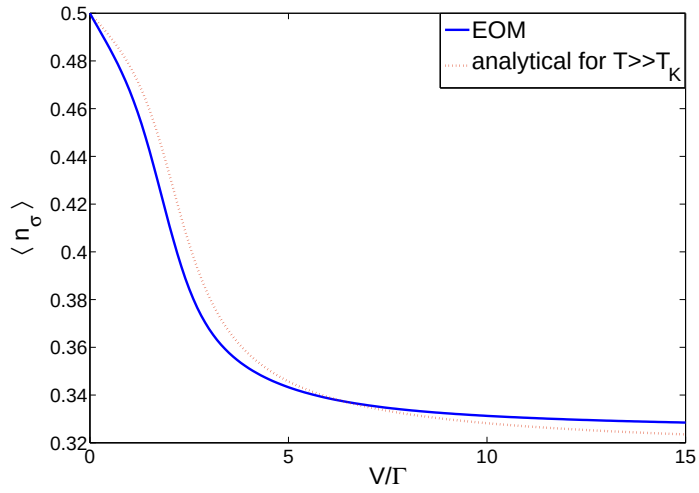

Figure 4.7: Electron occupation number in the dot $\langle n_\sigma \rangle$ versus the bias voltage V in the particle-hole symmetric case for $U/\Gamma = 4$ and $T/\Gamma = 8.5\ 10^{-4}$, and under an asymmetric bias voltage setting $\mu_L = 0$ and $\mu_R = -V$. The numerical result obtained from the EOM (solid blue curve) is compared to the approximate analytical expression Eq. (4.12) obtained from a single-particle picture (dotted red curve). We conclude that the Kondo effect has little influence on the occupation number in the dot.

till V passes the dot-level energy $U/2$ and comes to stabilize at large V. This can be qualitatively explained by the fact that at large V, the current through the dot no longer increases monotonously with the bias voltage and reaches a horizontal asymptote. This makes the occupation number insensitive to the bias voltage.

As the occupation number is mainly affected by the broad single-particle peaks in the density of states, it is interesting to derive the non-equilibrium occupation number within a simple high-energy model. For $T_K \ll T \ll \Gamma$, the single-particle density of states of the Anderson model has the form

$$\rho_\sigma(\omega) = \frac{1}{\pi}\left[(1 - \langle n_{\bar{\sigma}}\rangle)\,\frac{\Gamma}{(\omega - \varepsilon_\sigma)^2 + \Gamma^2} + \langle n_{\bar{\sigma}}\rangle \frac{\Gamma}{(\omega - \varepsilon_\sigma - U)^2 + \Gamma^2}\right],$$

while the dot occupation number is given by

$$\langle n_d\rangle = \frac{1}{2}\int_{-W}^{\mu_L} d\omega \rho_d(\omega) + \frac{1}{2}\int_{-W}^{\mu_R} d\omega \rho_d(\omega),$$

where $n_d = n_\uparrow + n_\downarrow$ and $\rho_d(\omega) = \rho_\uparrow(\omega) + \rho_\downarrow(\omega)$. In the absence of magnetic field, this leads to the self-consistent equation

$$\langle n_d\rangle = 1 - \frac{1}{\pi}\sum_\alpha \left[\left(1 - \frac{\langle n_d\rangle}{2}\right)\arctan\left(\frac{\varepsilon_d - \mu_\alpha}{\Gamma}\right) + \frac{\langle n_d\rangle}{2}\arctan\left(\frac{\varepsilon_d + U - \mu_\alpha}{\Gamma}\right)\right]. \tag{4.12}$$

This expression gives a result quite close to the result obtained numerically within the equations-of-motion approach and Ng's Ansatz, as shown in Fig. 4.7. The two results are quite close to each other, and we assume that the occupation number inside the dot is almost independent of the Kondo effect.

Chapter 5

Transport under a magnetic field

When a magnetic field is applied on an isolated quantum dot, the discrete energy levels inside the dot are split by the Zeeman energy Δ, which is proportional to the magnetic field. On the other hand, the effect on the conduction electrons can be absorbed in a renormalization of the bandwidth and has little influence on the Kondo effect since it leaves the Fermi level unchanged. Therefore, the single-level Anderson Hamiltonian for the total system of the dot connected to N_α leads becomes

$$\mathcal{H} = \sum_{\alpha\sigma k} \varepsilon_k c^\dagger_{\alpha k\sigma} c_{\alpha k\sigma} + \sum_\sigma (\varepsilon_d + \Delta\sigma/2)\, f^\dagger_\sigma f_\sigma + U n_\uparrow n_\downarrow + \sum_{\alpha\sigma k} (t_\alpha c^\dagger_{\alpha k\sigma} f_\sigma + H.c.),$$

in which the dot energy levels are set to $\varepsilon_d \pm \Delta/2$. As a consequence, flipping the spin of the dot costs an energy $\pm\Delta$, and we expect a shift of the Kondo resonance in the dot density of states.

An interesting experimental signature of the magnetic field in the Kondo regime can be found in the differential conductance dI/dV. By applying a finite bias to the system, it is provided the external energy for the spin-flip scattering processes to occur, and we can probe the Kondo-like resonances in the density of states. The zero-bias peak described in Chapter 4 is split into two side peaks located around $V \approx \pm\Delta$ [70]. Higher order calculations suggest that the splitting slightly deviates from 2Δ because of the screening of the magnetic field by the conduction electrons, and report a distance between peaks equal to $2\Delta_K < 2\Delta$ [30]. However, recent experiments show that the actual deviation rather evolves from a regime where $\Delta_K < \Delta$ at low magnetic field to a regime where $\Delta_K > \Delta$ at high magnetic field [57]. This crossover has not been explained by theory, and we draw the results obtained within the equations-of-motion framework. The method we developed in the previous chapters accommodates quite well to the study of this problem: first it is able to cover a wide range of parameters, and more particularly non-equilibrium configurations; secondly, as the system lies in the weak-coupling regime when the peak is split by the magnetic field, our results are expected to be qualitatively reliable.

We show that the splitting in the differential conductance Δ_K is connected to the decoherence rate $\gamma_{2\sigma}$, and propose an experimental setup in order to trace the presence

of additional contributions to $\gamma_{2\sigma}$.

5.1 Splitting of the Kondo resonance in the density of states

We have seen that the Ground State of the Anderson model in the absence of magnetic field is a many-particle spin singlet, and that the relevant excitations at low energy happen through spin-flip scattering processes. Within the equations-of-motion framework, this process gets described by the high-order Green's function $\langle\langle f^\dagger_{\bar\sigma} c_{k\bar\sigma} f_\sigma\rangle\rangle$ whose equation under magnetic field is given by

$$\begin{aligned}(\omega_{:k} - \Delta\sigma - \Sigma_{2\sigma}(\omega_{:k}))\,\langle\langle f^\dagger_{\bar\sigma} c_{k\bar\sigma} f_\sigma\rangle\rangle &= \langle f^\dagger_{\bar\sigma} c_{k\bar\sigma}\rangle + t_{\bar\sigma}\sum_{k_1}\langle c^\dagger_{k_1\bar\sigma} c_{k\bar\sigma}\rangle\langle\langle f_\sigma\rangle\rangle \\ &\quad -i\Gamma_\sigma\langle f^\dagger_{\bar\sigma} c_{k\bar\sigma}\rangle\langle\langle f_\sigma\rangle\rangle + O(t^3). \end{aligned} \tag{5.1}$$

In the Lacroix approximation, $\Sigma_{2\sigma} = 0$, and the divergence in the Green's function is shifted to $\omega = \Delta\sigma$, corresponding to the energy cost for the spin-flip scattering process. At equilibrium, the dot density of states exhibits a two-peak structure located at $\pm\Delta$; the distance between them is exactly equal to 2Δ, i.e. twice the splitting of a single-particle level [70]. While it captures the effect of the magnetic field on the Kondo effect qualitatively, the Lacroix approximation suffers two main drawbacks. First, it is unable to provide an explanation to the renormalization of the splitting predicted by other theories [58] and some experiments [45, 4, 57], that show deviations form 2Δ. Secondly, we expect the divergence to be smeared out by the decoherence of the spin singlet state because the many-particle spin-flip scattering process is no longer an elastic process. This motivates us to go beyond the Lacroix approximation in the same spirit of the previous chapters and study the effect of the higher-order self-energy $\Sigma_{2\sigma}$ of $\langle\langle f^\dagger_{\bar\sigma} c_{k\bar\sigma} f_\sigma\rangle\rangle$.

5.1.1 Renormalization of the splitting of the Kondo resonance

The real part of $\Sigma_{2\sigma}$ implies a shift from $\Delta\sigma$ to $\Delta^*\sigma$ in the pole of $\langle\langle f^\dagger_{\bar\sigma} c_{k\bar\sigma} f_\sigma\rangle\rangle$ (with respect to $\omega_{:k}$) in Eq. (5.1), where the renormalized value Δ^* is given by the recursive equation

$$\Delta\sigma + \ \mathrm{Re}\widehat{\Sigma}_{2\sigma}(\Delta^*\sigma) = \Delta^*\sigma.$$

At equilibrium and zero temperature, the renormalized splitting of the Kondo resonance Δ^* at lowest order in t writes

$$\begin{aligned}\Delta^* &= \Delta + \frac{\Gamma}{2\pi}\left\{\ln\left|\frac{\varepsilon_d + \Delta/2}{\varepsilon_d - \Delta/2}\right| - \ln\left|\frac{\varepsilon_d - \Delta/2 + U}{\varepsilon_d + \Delta/2 + U}\right|\right\} + O(\Gamma^2/U) \\ &= (1 - \nu J/2)\,\Delta + O(J^2). \end{aligned} \tag{5.2}$$

This result is in agreement with perturbation theory [30]. In the Kondo regime ($J > 0$), the renormalized value Δ^* is always smaller the the bare one. This phenomenon, also known as the Knight shift [44], is related to the overpopulation of spin-down conduction electrons with respect to spin-up ones in a magnetic field. As a consequence, the spin operator brought by the conduction electrons in the Kondo model has a non-zero expectation value $\langle \sum_{kk'} \vec{S}_{kk'}.\vec{1}_z \rangle = -\nu\Delta/2$ (where $\vec{1}_z$ is the direction of the magnetic field) that results in an additional effective magnetic field $-J\nu\Delta/2$ acting on the localized spin.

It is interesting to compare the renormalization of the Zeeman energy Δ with that of the dot energy levels. At lowest order, the latter is given by

$$\varepsilon_\sigma^* = \varepsilon_\sigma - \frac{\Gamma}{2\pi} \ln \left| \frac{\varepsilon_\sigma^* - \Delta\sigma}{\varepsilon_\sigma^* - 2\varepsilon_d - U} \right| + O(\Gamma^2/U),$$

and the distance between the renormalized levels is

$$\varepsilon_\uparrow^* - \varepsilon_\downarrow^* = \varepsilon_\uparrow - \varepsilon_\downarrow - \frac{\Gamma}{2\pi} \left\{ \ln \left| \frac{\varepsilon_d - \Delta/2}{\varepsilon_d + \Delta/2} \right| + \ln \left| \frac{\varepsilon_d + \Delta/2 + U}{\varepsilon_d - \Delta/2 + U} \right| \right\} + O(\Gamma^2/U) = \Delta^*.$$

Therefore, the renormalization of the high-energy dot levels ε_σ is in adequacy with the low-energy renormalization of the pole of $\langle\langle f_{\bar{\sigma}}^\dagger c_{k\bar{\sigma}} f_\sigma \rangle\rangle$.

5.1.2 Smearing of the Kondo resonance by a magnetic field

We expect that the coupling of the system to an external magnetic field implies a decoherence of the Kondo spin-singlet Ground State, resulting in a smearing of the related low-energy peak in the dot density of states. Within the EOM framework, this can be obtained through the imaginary part of $\Sigma_{2\sigma}$, similarly to the case of a bias voltage. At equilibrium and for zero temperature, the decoherence rate (B.17) is, at fourth order in t,

$$\begin{aligned}
\gamma_{2\sigma}|_{(\Delta, V=0)} &= \frac{\Gamma^2}{4\pi} \int_{-\Delta}^{0} d\varepsilon_k \; D_\downarrow^2(\varepsilon_k) \\
&= \frac{\Gamma^2}{4\pi} \left[\frac{U^2}{\varepsilon_d^2 \left(\varepsilon_d + U\right)^2} \Delta - 2 \frac{U^2}{\varepsilon_d^2 \left(\varepsilon_d + U\right)^2} \frac{2\varepsilon_d + U}{\varepsilon_d \left(\varepsilon_d + U\right)} \Delta^2 + O(\Delta^3) \right] + O(\Gamma^3) \\
&= \frac{\pi}{4} \left(\nu J\right)^2 \left[\Delta + \frac{8\pi\nu K}{\Gamma} \Delta^2 + O(\Delta^3) \right] + O(J^3),
\end{aligned} \tag{5.3}$$

where K is the potential scattering term introduced in Eq. (A.24). At the particle-hole symmetric point, $K = 0$ and the decoherence rate is proportional to the Zeeman energy. When K is finite, the quadratic contribution should nevertheless remain negligible because $\nu K \Delta/\Gamma \ll 1$.

On the other hand, we will also need the non-equilibrium decoherence rate for $V \approx \Delta$, corresponding to the bias voltage for which resonances in the dot density of

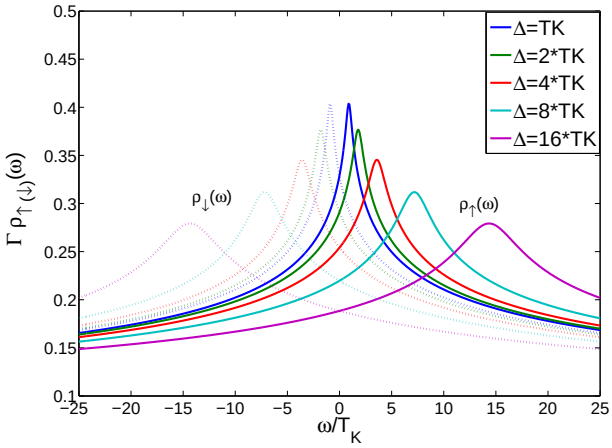

(a)

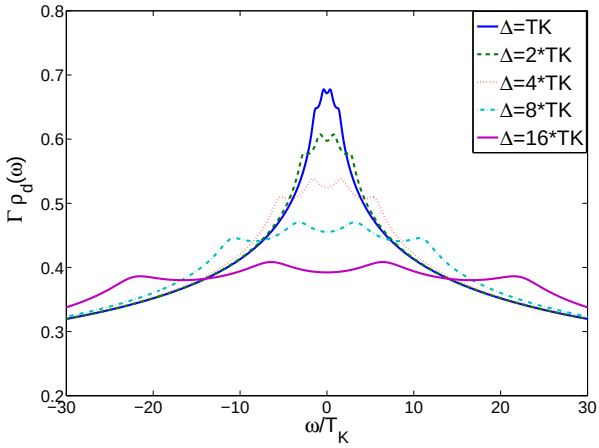

(b)

Figure 5.1: (a) Equilibrium density of states in the dot at zero temperature for $U = 4\Gamma$, for spin-up electrons (solid curves) and spin-down electrons (dotted curves), and for different values of the magnetic field. (b) Total density of states in the dot ($\rho_d(\omega) = \rho_\uparrow(\omega) + \rho_\downarrow(\omega)$) out of equilibrium for $U = 4\Gamma$. We chose a symmetric bias voltage $[\mu_L, \mu_R] = [V/2, -V/2]$ with $V = \Delta$.

states are aligned with the chemical potentials of the leads. It is given by

$$\begin{aligned}\gamma_{2\sigma}|_{(V=\Delta)} &= \frac{\Gamma^2}{4\pi}\left[\frac{1}{2}\int_{-\Delta}^{0} d\varepsilon_k\; D_\downarrow^2(\varepsilon_k) + \frac{1}{4}\sum_\sigma \int_{-V/2}^{V/2} d\varepsilon_k\; D_\sigma^2(\varepsilon_k) + \frac{1}{4}\int_{-\Delta-V/2}^{V/2} d\varepsilon_k\; D_\downarrow^2(\varepsilon_k)\right] \\ &= \frac{15\pi}{32}(\nu J)^2\left[\Delta + \frac{26}{3}\frac{\pi\nu K}{\Gamma}\Delta^2 + O(\Delta^3)\right] + O(J^3). \qquad (5.4)\end{aligned}$$

We find $\gamma_{2\sigma}(V = \Delta) \approx 2\gamma_{2\sigma}(\Delta, V = 0)$ underlining the fact that the finite bias voltage favors the decoherence of the Kondo state.

5.1.3 Numerical result

The evolution with the magnetic field of the density of states in the dot calculated from Eq. (2.48) is shown in Fig. 5.1. At equilibrium (Fig. 5.1(a)), the Kondo resonance,

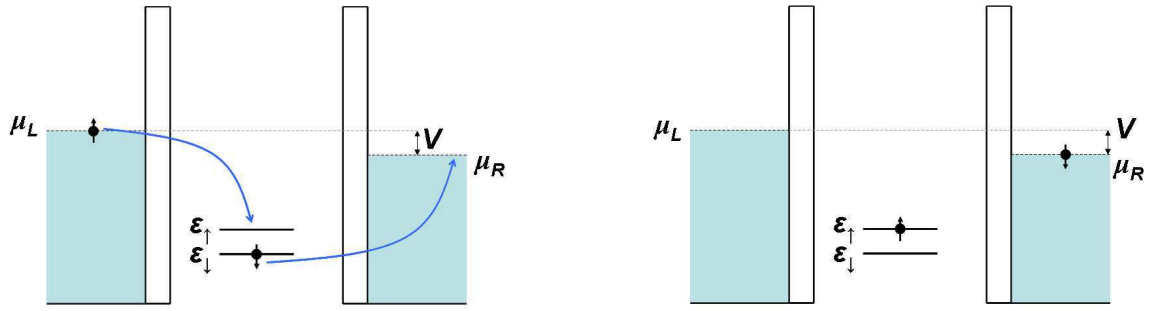

Figure 5.2: Schematic representation of the non-equilibrium co-tunneling process trough a quantum dot under a magnetic field. A spin-down electron leaves the dot to the right lead while a spin-up electron from the left lead simultaneously enters the central region. This process is energetically allowed when the bias voltage V becomes larger than the Zeeman splitting $\Delta = \varepsilon_\uparrow - \varepsilon_\downarrow$ between energy levels in the dot.

initially located at the chemical potential of the leads, is shifted to the right for spin-up electrons, and to the left for spin-down electrons. When the magnetic field is increased, the decoherence rate $\gamma_{2\sigma}$ in Eq. (5.3) increases and induces a broadening of the peaks and a reduction of their height. Their position is located around the renormalized Zeeman energy $\Delta^* < \Delta$, as we concluded from Eq. (5.2).

On the figure 5.1(b), we show the total density of states $\rho_d(\omega) = \rho_\uparrow(\omega) + \rho_\downarrow(\omega)$ out of equilibrium. The two-peak structure discussed previously evolves to a 4-peak structure, with maximums around $\pm\Delta^* + \mu_\alpha$, as the spin-flip scattering processes can now happen through tunneling with two leads carrying different chemical potentials. The decoherence is stronger than at equilibrium because of the combined effect of the magnetic field and the bias voltage (see Eq. (5.4)).

5.2 Splitting of the Kondo peak in the differential conductance

A finite magnetic field induces a strong decrease of the linear conductance in the Kondo regime because the spin-flip of an electron inside the dot becomes an inelastic process, costing an energy Δ. This energy can be provided by the outside environment in a non-equilibrium setup by applying a bias voltage between two leads connecting the dot, as represented schematically on Fig. 5.2. A spin-down electron can leave the dot to the lead that carries the lowest chemical potential while an spin-up electron from the other lead enters the dot at the same time. The energy balance between the initial and final states is fulfilled if

$$\varepsilon_{Lk\uparrow} + \varepsilon_d - \frac{\Delta}{2} = \varepsilon_{Rk\downarrow} + \varepsilon_d + \frac{\Delta}{2}.$$

For conduction electrons at the Fermi edge, we have $\varepsilon_{Lk\uparrow} = \mu_L$ and $\varepsilon_{Rk\downarrow} = \mu_R$, implying

$$\mu_L - \mu_R = \Delta.$$

Therefore, the bias voltage $V = \mu_L - \mu_R$ probes the Zeeman splitting in the dot, and a new channel opens up for electron transport at $V \geq \Delta$.

We derive analytically the differential conductance at zero temperature, for a symmetric coupling to the leads $\Gamma_{\alpha\sigma} = \Gamma/4$ and a symmetric bias voltage $[\mu_L, \mu_R] = [V/2, -V/2]$.[1] In order to get an analytical expression that can be compared easily to experiments, we keep only the lowest orders in the Kondo exchange coupling J,[2] which should be reasonable as the system is driven into the weak coupling regime by the magnetic field and bias voltage (see Sec. 4.3). The differential conductance can be obtained by Eq. (1.7), which simplifies under the symmetric case to

$$\frac{dI}{dV} = \frac{2e^2}{\hbar}\frac{\Gamma}{4}\sum_\sigma \left[\frac{1}{2}\rho_\sigma(V/2) + \frac{1}{2}\rho_\sigma(-V/2) + \frac{1}{e}\int_{-V/2}^{V/2} d\omega \frac{\partial \rho_\sigma(\omega, V)}{\partial V}\right]. \tag{5.5}$$

The two first terms involve the probing of the density of states at the chemical potentials of the leads while the third one accounts for the dependence of the density of states, and indirectly of the Kondo resonance, on the bias voltage. In order to determine this last term, let us calculate the derivative of the Green's function $\partial \mathcal{G}_\sigma(\varepsilon, V)/\partial V$: recalling Eq. (2.48)

$$\mathcal{G}_\sigma(\omega, V) = \frac{u_{2\sigma}(\omega) - \langle n_{\bar\sigma}\rangle - \Pi_\sigma(\omega, V)}{u_{1\sigma}(\omega)u_{2\sigma}(\omega) + \Xi_\sigma(\omega, V)},$$

we get

$$\begin{aligned}\frac{\partial \mathcal{G}_\sigma(\omega, V)}{\partial V} &= \frac{-\partial\Pi_\sigma(\omega, V)/\partial V}{u_{1\sigma}(\omega)u_{2\sigma}(\omega) + \Xi_\sigma(\omega, V)} - \frac{u_{2\sigma}(\omega) - \langle n_{\bar\sigma}\rangle - \Pi_\sigma(\omega, V)}{\left(u_{1\sigma}(\omega)u_{2\sigma}(\omega) + \Xi_\sigma(\omega, V)\right)^2}\partial\Xi_\sigma(\omega, V)/\partial V \\ &= -\tilde{D}_\sigma(\omega)\frac{\partial\Pi_\sigma(\omega, V)}{\partial V} - \mathcal{G}_\sigma(\omega)\tilde{D}_\sigma(\omega)\frac{\partial\Xi_\sigma(\omega, V)}{\partial V} + O(J^2).\end{aligned} \tag{5.6}$$

The functions $\Pi_\sigma(\omega, V)$ and $\Xi_\sigma(\omega, V)$ in Eq. (2.49) depend on the bias voltage through the Fermi distribution under the integral. At zero temperature, this can be computed

[1] In experiments, the bias voltage is usually asymmetric ($[\mu_L, \mu_R] = [V, 0]$), but this has little influence on the low-energy features as the corrections are of the order $O(V/\varepsilon_d)$.

[2] Our calculation is done from the general Anderson model, but we derive low-energy results in series in J, as defined in Eq. (A.25), for a better comparison with results from the Kondo model. The effect of the terms beyond the Kondo model will be disscussed.

analytically

$$\begin{aligned}\frac{\partial\Pi_\sigma(\omega,V)}{\partial V} =& \frac{\Gamma}{4\pi}\frac{1}{2}\left[\frac{\mathcal{G}^*_{\bar\sigma}(V/2)}{\omega - V/2 - \Delta^*\sigma + i\gamma_{2\sigma}} - \frac{\mathcal{G}^*_{\bar\sigma}(-V/2)}{\omega + V/2 - \Delta^*\sigma + i\gamma_{2\sigma}}\right] \\ &+ \frac{\Gamma}{4\pi}\frac{1}{2}\left[-\frac{\mathcal{G}_{\bar\sigma}(V/2)}{\omega + V/2 - 2\varepsilon_d - U + i\gamma_{3\sigma}} + \frac{\mathcal{G}_{\bar\sigma}(-V/2)}{\omega - V/2 - 2\varepsilon_d - U + i\gamma_{3\sigma}}\right]. \\ \frac{\partial\Xi_\sigma(\omega,V)}{\partial V} =& -\frac{\Gamma}{4\pi}\frac{1}{2}\left[\frac{1}{\omega - V/2 - \Delta^*\sigma + i\gamma_{2\sigma}} - \frac{1}{\omega + V/2 - \Delta^*\sigma + i\gamma_{2\sigma}}\right] \\ &- \frac{\Gamma}{4\pi}\frac{1}{2}\left[\frac{1}{\omega + V/2 - 2\varepsilon_d - U + i\gamma_{3\sigma}} - \frac{1}{\omega - V/2 - 2\varepsilon_d - U + i\gamma_{3\sigma}}\right] \\ &- i\Gamma\frac{\partial\Pi_\sigma(\omega,V)}{\partial V},\end{aligned}$$

Neglecting the real part of the dot Green's function around the Fermi level, which should be close to zero because of the Friedel sum rule [54], we obtain at lowest order in t

$$\begin{aligned}\int_{-V/2}^{V/2} d\omega \frac{\partial\rho_\sigma(\omega,V)}{\partial V} &\approx D_\sigma(0)\frac{\Gamma}{8\pi}\left[\rho_{\bar\sigma}(V/2)\ln\left(\frac{\Delta^{*2}+\gamma_{2\sigma}^2}{(V+\Delta^*\sigma)^2+\gamma_{2\sigma}^2}\right)\right. \\ &\left. +\rho_{\bar\sigma}(-V/2)\ln\left(\frac{\Delta^{*2}+\gamma_{2\sigma}^2}{(V-\Delta^*\sigma)^2+\gamma_{2\sigma}^2}\right)\right] \qquad (5.7)\end{aligned}$$

Introducing this result in Eq. (5.5), the differential conductance can be reduced to two terms

$$\begin{aligned}\frac{dI}{dV} \approx \frac{2e^2}{\hbar}\frac{\Gamma_L\Gamma_R}{\Gamma_L+\Gamma_R}\sum_\sigma &\left[\frac{1}{2}\rho_\sigma(V/2)\left(1+\frac{\nu J}{4}\ln\left(\frac{\Delta^{*2}+\gamma_{2\sigma}^2}{(V-\Delta^*\sigma)^2+\gamma_{2\sigma}^2}\right)\right)\right. \\ &\left. +\ \frac{1}{2}\rho_\sigma(-V/2)\left(1+\frac{\nu J}{4}\ln\left(\frac{\Delta^{*2}+\gamma_{2\sigma}^2}{(V+\Delta^*\sigma)^2+\gamma_{2\sigma}^2}\right)\right)\right], \qquad (5.8)\end{aligned}$$

and we have to compute the density of states in the dot at the chemical potentials of the leads ($\rho_\sigma(\pm V/2)$). For the simplicity of the calculations, we consider the infinite U limit ($U\to\infty$). We also send the dot level down to infinity ($\varepsilon_d/\Gamma\to-\infty$) while keeping the ratio $\varepsilon_d/U\to 0$. Within these approximations, the dot Green's function simplifies to

$$\mathcal{G}_\sigma(\omega) \approx \frac{1/2}{u_{1\sigma}(\omega)u_{2\sigma}(\omega)+\Xi_\sigma(\omega)}.$$

At order J^3, the density of states is

$$\rho_\sigma(\omega) = \frac{1}{\pi}\frac{1/2}{\left(u_{1\sigma}(\omega)u_{2\sigma}(\omega)\right)^2}\left(\mathrm{Im}\Xi_\sigma(\omega)+\Gamma/2\right)\left(1-2\frac{\mathrm{Re}\Xi_\sigma(\omega)}{u_{1\sigma}(\omega)u_{2\sigma}(\omega)}\right)+O(J^4/U).$$

Only $\rho_\uparrow(V/2)$ and $\rho_\downarrow(-V/2)$ give a sensible contribution to the differential conductance in Eq. (5.8), while $\rho_\uparrow(-V/2)$ and $\rho_\downarrow(V/2)$ just contribute to a small constant term. In addition, due to the particle-hole symmetry at low energy, we have $\rho_\uparrow(V/2) = \rho_\downarrow(-V/2)$ and we are left with the calculation of $\rho_\downarrow(-V/2)$.[3] We find

$$\begin{aligned}\rho_\downarrow(\omega) &= \frac{1}{\pi^2}\frac{\Gamma}{8}D_\downarrow(\omega)^2\left(-\arctan\left(\frac{\omega+V/2+\Delta^*}{\gamma_2}\right)-\arctan\left(\frac{\omega-V/2+\Delta^*}{\gamma_2}\right)+3\pi\right)\\ &\quad\times\left(1-2\frac{\Gamma}{4\pi}D_\downarrow(\omega)\frac{1}{2}\ln\left(\frac{(V-\Delta^*)^2+\gamma_2^2}{W^2}\right)\right)+O(J^4/U).\end{aligned}$$

According to scaling theory, the conduction-electron bandwidth W can be renormalized down to the Zeeman energy Δ. For $V \approx \Delta^*$ and $\Delta^* \gg \gamma_{2\sigma}$, the Eq. (5.8) for the differential conductance becomes

$$\frac{dI}{dV} \approx \frac{2e^2}{h}\frac{\pi^2}{16}(\nu J)^2\left[5+\frac{2}{\pi}\arctan\left(\frac{V-\Delta^*}{\gamma_2}\right)\right]\left(1+\frac{\nu J}{2}\ln\left(\frac{\Delta^{*2}}{(V-\Delta^*)^2+\gamma_2^2}\right)\right)+\text{cst.} \tag{5.9}$$

In the limit $\gamma_2 \to 0$, the result of Eq. (5.9) is quite similar to the expression obtained from the non-equilibrium perturbation theory at order J^3 on the Kondo model [88, 30]. From scaling theory, we know that the exchange coupling is renormalized to $\nu J = \ln^{-1}(\max(\Delta, V)/T_K)$.

The great improvement brought by the EOM approach lies in the fact that it allows for the description of the decoherence of the Kondo state out of equilibrium, which implies a smearing of the Kondo peak through the decoherence rate $\gamma_2 \neq 0$. This is different from the zero-magnetic-field case, for which the differential conductance is almost unaffected by the value of γ_2 (see Sec. 4.4). The reason for it can be understood by the fact that the Kondo resonances in the dot density of states are no longer aligned with the chemical potentials of the leads. As a consequence, the crossing between the two quantities in the calculation of the current from Eq. (1.6) happens at a well-defined bias voltage V; the associated increase of current will be all the more efficient so as the resonance in the density of states is sharp, and therefore feels the influence of the decoherence rate γ_2.

Using the Eqs. (5.9), (5.2) and (5.4) with the renormalized exchange term $\nu J = \ln^{-1}(\max(\Delta, V)/T_K)$, we compute the differential conductance for different values of the magnetic field. Two transport regimes are found depending on the relative values of the Zeeman energy and the Kondo temperature, as shown on Fig. 5.3. When the ratio Δ/T_K is much larger than one, $\nu J \ll 1$ and the main contribution comes from the arctan term, which is then equivalent to a Heaviside function with borders around Δ because $\gamma_{2\sigma} \to 0$ and $\Delta_K \to \Delta$. This regime, called the *co-tunneling regime*, can be understood by the cartoon of Fig. 5.2 and yields an adequate method to measure the bare Zeeman energy in the quantum dot [57]. The conductance is enhanced for $|V| > \Delta$

[3] We choose to calculate $\rho_\downarrow$ rather than $\rho_\uparrow$ because its resonant spin-flip scattering process involves an energy below the Fermi level, which should be better described in the electron picture (see Sec. 2.8).

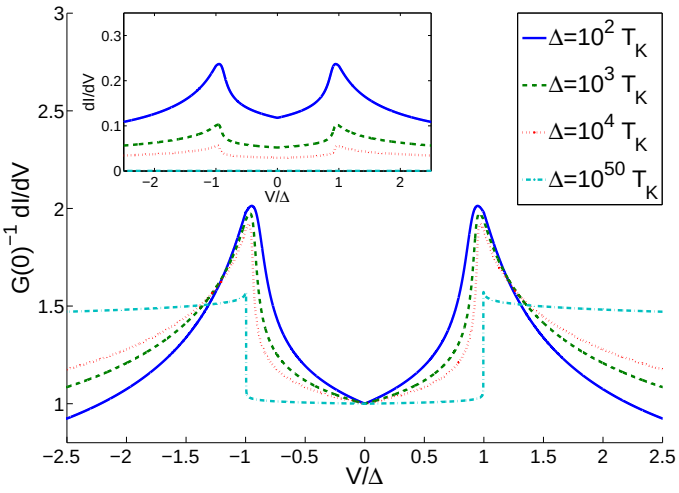

Figure 5.3: Differential conductance dI/dV as a function of the bias voltage V for different values of the Zeeman energy Δ. The curves have been scaled by the zero-bias conductance $G(0)$ at each magnetic field to allow for comparison. The inset shows the unscaled curves and the strong decrease of the conductance with the magnetic field.

as the bias voltage then provides enough energy for the transfer of an electron through a spin-flip scattering process. When the ratio Δ/T_K is decreased, higher-order spin-flip scattering processes become relevant and we enter the *Kondo regime*. As the exchange coupling constant J is no longer negligible, the log term in Eq. (5.9) becomes important and is responsible for a peaked structure around Δ^*, as shown on the three other curves of Fig. 5.3. The value of Δ^* is smaller than the bare Zeeman splitting because of the finite exchange coupling constant J. However, the actual maximum in the differential conductance, called Δ_K, is simultaneously pushed outwards by the arctan term, which gets smoothed by the finite decoherence rate $\gamma_{2\sigma}$.

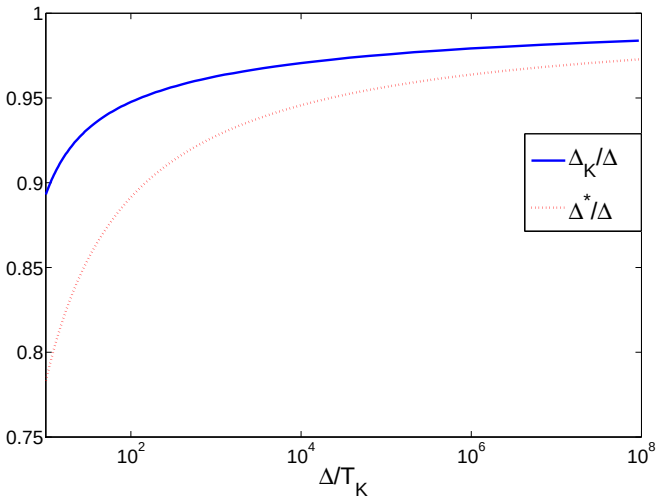

Figure 5.4: Position of the Kondo peaks in the differential conductance $V = \pm\Delta_K$ under a magnetic field (solid blue curve), compared to the position of the Kondo resonances in the density of states $V = \pm\Delta^*$ at equilibrium (dashed red curve).

We report the position $V = \pm\Delta_K$ of the Kondo peaks in the differential conductance on the solid blue curve in Fig. 5.4. We find out that the splitting Δ_K is always smaller that the bare Zeeman energy Δ, which it reaches asymptotically at high magnetic fields. It is interesting to compare that value to the renormalized Zeeman energy entering in the pole Δ^* of the Green's function $\langle\langle f^\dagger_{\bar{\sigma}} c_{k\bar{\sigma}} f_\sigma \rangle\rangle$; as can be observed, the splitting measured in the differential conductance is larger than Δ^*, and it is therefore not relevant to draw conclusions from the distance between the peaks in the equilibrium density of states. The increasing behavior of Δ_K with the magnetic field is in agreement with perturbation theory and the experiment by Liu et al [57], but we do not find any region where $\Delta_K > \Delta$.

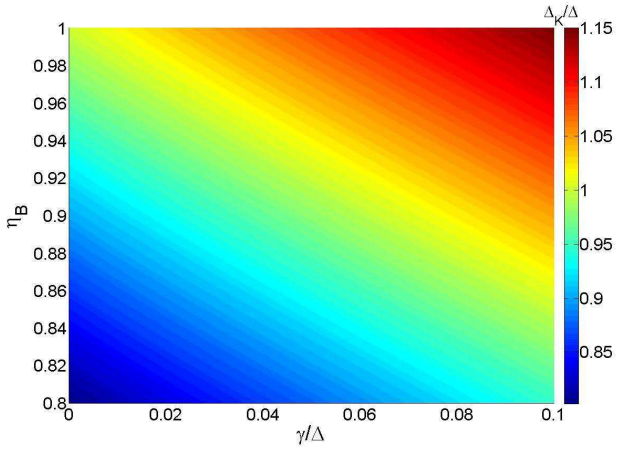

(a)

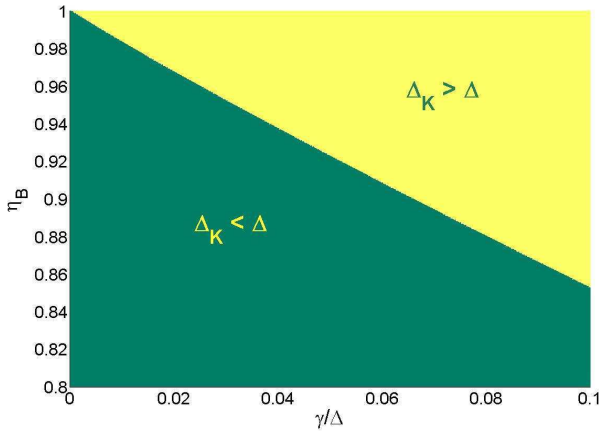

(b)

Figure 5.5: (a) Ratio Δ_K/Δ of the position of the Kondo peaks in the differential conductance $V = \pm\Delta_K$ on the Zeeman energy, as a function of the decoherence rate $\gamma_{2\sigma}$ and the renormalization of the position of the Kondo resonance at equilibrium $\eta_B = \Delta^*/\Delta$. (b) Phase diagram showing the couples of parameters $(\gamma_{2\sigma}, \eta_B)$ for which the splitting of the Kondo peaks in the differential conductance is lower than 2Δ ($\Delta_K < \Delta$) or larger than 2Δ ($\Delta_K > \Delta$).

As the actual position Δ_K depends on the interplay between the renormalization $\eta_B = \Delta^*/\Delta$ of the pole of $\langle\langle f^\dagger_\sigma c_{k\bar{\sigma}} f_\sigma \rangle\rangle$ and the associated decoherence rate $\gamma_{2\sigma}$, it is tempting to study the ratio Δ_K/Δ as a function of the parameters $\gamma_{2\sigma}$ and η_B. The result is presented in the color plot in Fig. 5.5. As expected, the ratio Δ_K/Δ is small when η_B and/or $\gamma_{2\sigma}$ go to zero, while there are chances to get Δ_K larger than Δ when η_B approaches one and $\gamma_{2\sigma}$ is large. The crossover line is found to obey the relationship

$$\Delta - \Delta^* = \frac{3}{2}\gamma_{2\sigma}. \tag{5.10}$$

The experimental results [45, 57] and the existence of couples $(\gamma_{2\sigma}, \eta_B)$ for which we find $\Delta_K > \Delta$ suggest an additional contribution to the decoherence rate $\gamma_{2\sigma}$.

However, it is dubious whether the renormalization from scaling theory applies for $\gamma_{2\sigma}$. Indeed, its bare expression (B.17) is independent of the conduction-electron bandwidth W because of the energy window $[V/2, -V/2]$ in Eq. (B.17), contrary to the second-order contribution to Δ^*. It is therefore tempting to keep the bare D function

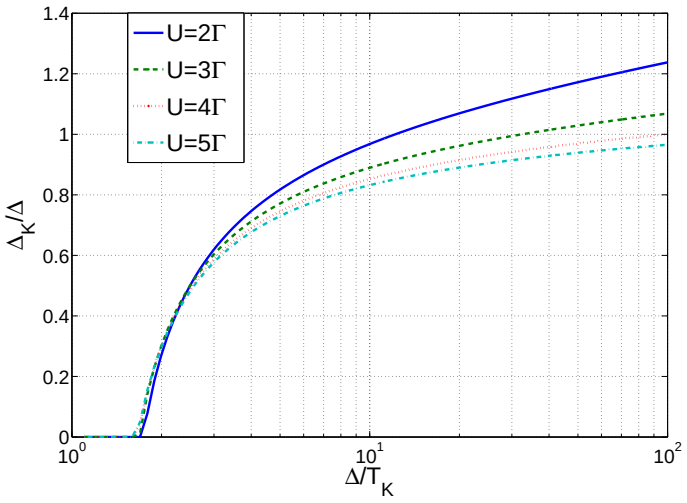

Figure 5.6: Position of the Kondo peaks in the differential conductance $V = \pm\Delta_K$. We use the bare expression for $\gamma_{2\sigma}$ for different values of U/Γ. The splitting $2\Delta_K$ increases when the ratio U/Γ decreases, eventually reaching regions where $\Delta_K > \Delta$ for small Coulomb interactions on the dot. Universality is lost at high magnetic field. At low magnetic field, a single peak is observed in the differential conductance as the Zeeman energy is too small in comparison with the width of the peaks.

for the fourth-order decoherence rate. The result is shown in Fig. 5.6 for different values of the ratio U/Γ.

When the magnetic field is smaller than the width of the zero-bias peak in the differential conductance (of the order of T_K), no splitting is observed as the two different peaks are not resolved, and $\Delta_K = 0$. When the magnetic field is increased, the two peaks are eventually separated and the distance between them quickly reaches a value of the order of 2Δ. On the contrary to Fig. 5.4, we observe a transition from $\Delta_K < \Delta$ to $\Delta_K > \Delta$ by increasing the magnetic field, as it was observed in the experiment by Liu et al. (see Fig. 5.7). This crossover happens more easily when the Coulomb repulsion on the dot is weak, which was the case in their measurement. This calls for reproducing the experiment for a much larger ratio U/Γ, which can be achieved in carbon nanotubes for instance.

In addition, we observe that the universality is destroyed at high magnetic field because of the decoherence rate $\gamma_{2\sigma}$. The relationship between the regime $\Delta_K > \Delta$ and the non-universality was discussed in [57]. However, a clear link has not yet been established and more evidence should be looked for.

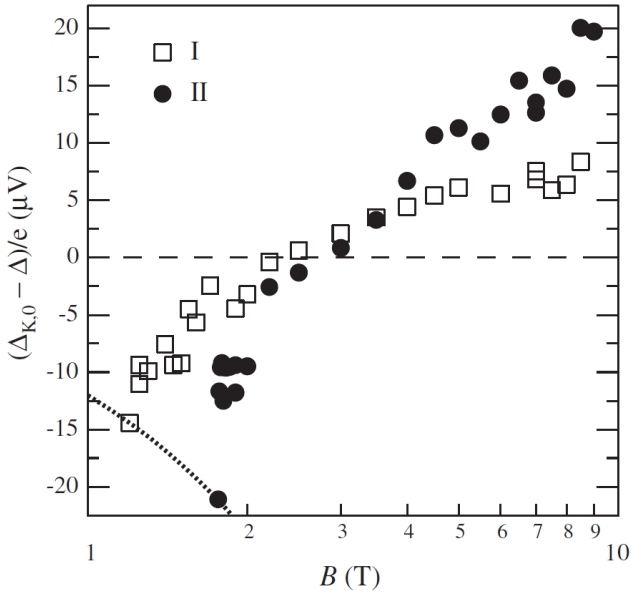

Figure 5.7: Experimental results for the position of the Kondo peaks in the differential conductance $V = \pm\Delta_K$ (Liu et al. [57]). The data were obtained at the particle-hole symmetric point for $U/\Gamma \approx 2.6$ (I) and $U/\Gamma \approx 2$ (II).

5.3 Probing the splitting in the density of states through a three-terminal experiment

In the previous section, we discussed the influence of the decoherence rate $\gamma_{2\sigma}$ on the value of the peak splitting in the differential conductance by a magnetic field. We observed that additional contributions to $\gamma_{2\sigma}$ modify the picture in agreement with experimental results, calling for a more elaborate expression [95].

On the other hand we discussed the smearing the resonance in the density of states in the dot by the decoherence rate in Sec. 5.1.2. This motivates a new experimental setup; let us now consider a three-terminal system, in which one lead has a much weaker tunneling rate to the dot (let us choose $\Gamma_3 \ll \Gamma_1 = \Gamma_2$). The third (weakly coupled) lead does not influence the Kondo effect as the Kondo temperature is proportional to the total coupling $\Gamma = \sqrt{\sum \Gamma_\alpha^2} \approx \Gamma_1 + \Gamma_2$ to the leads, and does not introduce any relevant contribution to the decay rate because $\gamma_{2\sigma}$ is proportional to the dot-lead couplings Γ_α. Therefore, we can assume that the dot density of states is unchanged in comparison with the two-terminal experiment. Interestingly, we can access this density of states experimentally in a three-terminal experiment by measuring the differential conductance dI_3/dV_{13}, as demonstrated in [56]

$$\frac{dI_3}{dV_{13}} = -\frac{4e^2\Gamma_3}{\hbar\Gamma}(\Gamma_1 + \Gamma_2)\int_{-W}^{W} d\varepsilon\, \rho_d(\varepsilon + \mu_3)\,\frac{\partial f}{\partial \varepsilon}. \tag{5.11}$$

At zero temperature, the differential conductance dI_3/dV_{13} is proportional to $\rho_d(\mu_3)$.

Experimentally, the main difficulty lies in the fact that the ratio Γ_3/Γ has to be small, which implies that the measured signal is weak. This three-terminal setup can be used to indirectly measure the decoherence rate $\gamma_{2\sigma}$ and compare it with the analytical result of Eq. (5.3).

We apply a magnetic field on the quantum dot at zero temperature and at pseudo-equilibrium $\mu_1 = \mu_2$ in such a way that the decoherence rate induced by the magnetic field is much larger than the Kondo temperature $\gamma_{2\sigma} \gg T_K$ (the weakly-coupled lead puts the system out of equilibrium, but this does not affect the Kondo effect that tkes place with the strongly coupled leads). In that case, we sit in the weak-coupling regime and the solution should be given by the lowest orders in t. At low frequency $\omega \ll \max(|\varepsilon_\sigma|, \varepsilon_\sigma + U)$, we the functions Π_σ and Ξ_σ appearing in Eq. (2.48) can be approximated by

$$\begin{aligned}
\Pi_\sigma(\omega) &\approx \frac{\Gamma_{\bar\sigma}}{\pi}\mathcal{G}^*_{\bar\sigma}(\omega - \Delta^*\sigma)\int \frac{f(\varepsilon_k) - 1/2}{\omega_{:k} - \Delta^*\sigma + i\gamma_{2\sigma}} \\
&\quad -\frac{\Gamma_{\bar\sigma}}{\pi}\mathcal{G}_{\bar\sigma}(2\varepsilon_d + U - \omega)\int \frac{f(\varepsilon_k) - 1/2}{\omega_{k:} - 2\varepsilon_d - U + i\gamma_{3\sigma}}, \\
\Xi_\sigma(\omega) &\approx i\Gamma_{\bar\sigma} - \frac{\Gamma_{\bar\sigma}}{\pi}\int \frac{f(\varepsilon_k) - 1/2}{\omega_{:k} - \Delta^*\sigma + i\gamma_{2\sigma}} - \frac{\Gamma_{\bar\sigma}}{\pi}\int \frac{f(\varepsilon_k) - 1/2}{\omega_{k:} - 2\varepsilon_d - U + i\gamma_{3\sigma}} - i\Gamma\Pi_\sigma(\omega),
\end{aligned}$$

where $f(\varepsilon_k)$ was changed to $f(\varepsilon_k) - 1/2$ before taking the Green's function out of the integral in order to respect particle-hole symmetry [27].

We are interested in finding the density of states in the dot at the resonance $\omega = \Delta^*\sigma$. Using the expressions above, we can infer that it is related to the decoherence rate $\gamma_{2\sigma}$ through solving the system of equations at the particle-hole symmetric point ($\varepsilon_d = -U/2$). We obtain for the Green's function

$$\mathcal{G}_\sigma(\Delta^*\sigma) = \frac{-i\frac{3}{2U}\pi\nu J + \nu J/2\,\mathcal{G}^*_{\bar\sigma}(0)\ln|\gamma_{2\sigma}/\gamma_{3\sigma}|}{1 + i\pi\nu J/2 + \nu J/2\,[1 + i\Gamma\mathcal{G}^*_{\bar\sigma}(0)]\ln|\gamma_{2\sigma}/\gamma_{3\sigma}|}, \tag{5.12}$$

with $\mathcal{G}^*_{\bar\sigma}(0) \approx i3\pi\nu J/2U$ at lowest order. At order J^2, we find for the density of states at the resonance

$$\rho_\sigma(\Delta^*\sigma) = \frac{3}{2U}\nu J\,[1 - \nu J\ln|\gamma_{2\sigma}/\gamma_{3\sigma}|] + O(J^3/U).$$

Similarly, we establish that the dot Green's function for the opposite spin is

$$\rho_{\bar\sigma}(\Delta^*\sigma) = \frac{3}{2U}\nu J\,[1 - \nu J\ln|2\Delta^*/\gamma_{3\sigma}|] + O(J^3/U).$$

The dot density of states at the maximum of the resonance is therefore

$$\rho_d(\pm\Delta^*) = \frac{3}{2U}\nu J\,[2 - \nu J\ln|\gamma_{2\sigma}/2\Gamma| - \nu J\ln|\Delta^*/\Gamma|] + O(J^3/U). \tag{5.13}$$

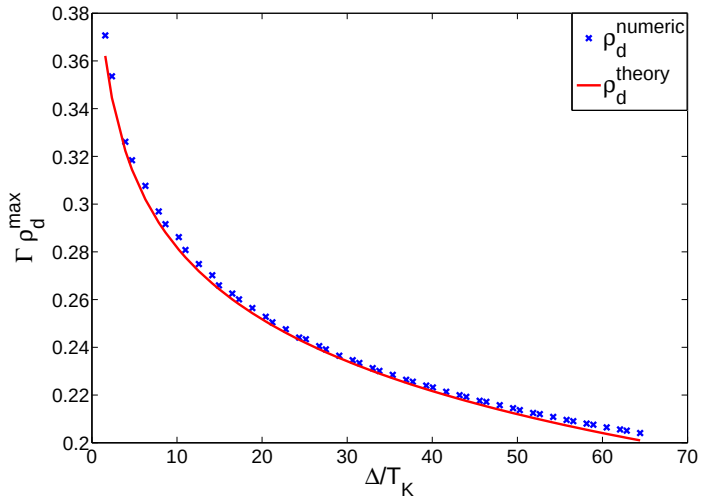

Figure 5.8: Height of the peak in the dot density of states as a function of the magnetic field for $U = 6\Gamma$ (circles). The data obtained from the numerical solution of the EOM (dots) are fitted with the formula $\rho_d(\pm\Delta) = a\nu J + b(\nu J)^2 \ln|\Delta/\Gamma|$ (solid line). The values obtained from the fit are $a = 0.0946/\Gamma$ and $b = -0.0463/\Gamma$.

The expression (5.13) can be used to measure the evolution of $\gamma_{2\sigma}$ with the magnetic field by probing the maximum of the density of states in the dot, which should be compared with the theoretical prediction for the decoherence rate in Eq. (5.3). If the decoherence rate $\gamma_{2\sigma}$ is proportional to the Zeeman energy Δ, the height of the peak should evolve as

$$\rho_d(\pm\Delta) = a\nu J + b(\nu J)^2 \ln|\Delta/\Gamma| + O(J^3/U), \tag{5.14}$$

with a, b two parameters independent of the magnetic field. Fitting the maximum in the density of states with this formula could bring information on a possible additional contribution to the decoherence rate $\gamma_{2\sigma}$ that would be of higher order in Δ. In Fig. 5.8, we show the comparison between this formula and the numerical result from the equations-of-motion. The lowest-order approximation in Eq. (5.14) provides an expression for the maximum in the density of states giving close results to the complete numerical curve, suggesting that it is accurate enough to discriminate an additional contribution in experiments.

Conclusion and Perspectives

Understanding non-equilibrium phenomena in strongly correlated systems poses fundamental challenges in theoretical physics supported by an intense experimental activity. During my Ph.D., I have tried to take up those challenges in order to unveil some of the mysteries in this new field. In this document, I have attempted to put on paper the different ideas that came up after many try-and-errors, and fruitful discussions with collaborators. My focus here has been on structuring those ideas so that they could be transfered to anyone willing to read this thesis carefully.

The interest for the Kondo effect, as several other many-particle effects in condensed matter physics, lies in its intrinsic quantum nature and its strong consequences at low energy on the dependence of any observable on external parameters. It is a fantastic effect for studying the correlations between particles in strongly-correlated systems, and requests sophisticated theoretical methods beyond mean-field approximations. One of those mathematical tools is the equations-of-motion technique, developed short after Kondo's explanation for the low-temperature minimum of the resistivity in dilute magnetic alloys. It has been extensively applied at equilibrium using a large set of approximation schemes that I summarized in Chap. 2, but few non-equilibrium extensions have been proposed and none of them has been able to give an explanation for the bias-induced decoherence of the processes involved in the Kondo effect. The new experiments in quantum dots driven out of equilibrium and the lack of exact theory to describe them have called for more elaborate approximations. In Chap. 2, a new decoupling scheme was motivated that builds on the Lacroix approximation while resumming higher-order terms that are relevant for our focus.

At equilibrium, I showed that the new method that we developed cures strong pathologies of the Lacroix approximation and extends the range of applicability to any parameter set, in particular to the particle-hole symmetric point. A comparison with approximation schemes at lower order was given for the density of states in the dot and the linear conductance. While Kondo features start to show up in truncations at second order in the tunneling coefficient t, the results are more stable within the fourth order extension developed in this work by resumming the terms related to spin-flip scattering processes (in particular it applies to the whole parameter range). The linear conductance reaches the unitary limit $G = 2e^2/h$ at zero temperature in the Kondo regime (i.e. when the total occupation number in the dot is one) while it goes to zero in even-occupancy regions because of the Coulomb blockade. We saw that a

finite temperature destroys the Kondo effect, and therefore produces a decrease of the conductance in the single-occupancy region.

More importantly, previous decoupling schemes considered the excitations involved in the spin-flip scattering process to have an infinite lifetime. This is true for a coherent spin-flip scattering but we know that it is a wrong statement out of equilibrium or under a magnetic field. In the latter case, the excitations acquire a decay rate reflecting the decoherence of the Kondo Ground State. The new decoupling scheme allowed for the investigation of problems out of equilibrium, as a decoherence rate was found within the EOM framework by resumming higher-order terms related to the spin-flip scattering processes. In Chap. 4, this decoherence rate was shown to play a crucial role in the applicability of the equations-of-motion out of equilibrium by driving the system from a strong-coupling regime, where the perturbative corrections are large and resummations poorly controllable, to a weak-coupling regime, where the series are convergent. I showed that the latter regime could also be reached by increasing the temperature or the magnetic field[4]. Experimentally, the main relevant quantity is the differential conductance, which is shown to be a universal function of the renormalized bias voltage V/T_K in the Kondo regime. We demonstrated that the method developed in this paper covers the whole parameter range on the qualitative level by representing the conductance in a three-dimensional figure as a function of the bias voltage and the gate voltage, in complete agreement with experiments.

Eventually, I studied the effect of a magnetic field in Chap. 5. An analytical formula was derived for the differential conductance at zero temperature; its expression is similar to results obtained by renormalized perturbation theory, with the difference that the EOM result also includes the dependence on the decoherence rate induced by both the bias voltage and the magnetic field. The differential conductance develops two peaks approximately separated by twice the Zeeman energy Δ. The actual value of the splitting lies at the center of an intense debate between theory and experiment since a value greater than 2Δ has been measured in a high-field regime. I have given a phenomenological explanation to this experiment, based on the dependence of the splitting on the decoherence rate. In order to check the validity of this assumption, an experimental setup has been proposed aimed at the measurement of the decoherence rate. The result of such experiments should shed light on the decoherence of the spin-flip scattering processes by the magnetic field and on possible additional contributions to those discussed in this thesis. In particular, the role of charge fluctuations inside the dot and on the particle-hole asymmetry deserve further theoretical study.

This work opens new perspectives as the flexibility of the EOM method makes it a good candidate for the study of many other problems. First, as it recovers the unitary limit at the particle-hole symmetric point, it is a good candidate as a numerically-efficient solver in Dynamical Mean Field Theory (DMFT) problems, where it would solve pathologies of the Lacroix approximation [29]. On the other hand, I showed that

[4]The magnetic-field-induced crossover to the weak-coupling regime has not been presented explicitly, but its mechanism corresponds to that described in Sec. 4.3, knowing that the magnetic-field also yields a finite decoherence rate, as expressed by Eq. (5.3).

the method is well-adapted to the study of transport problems through quantum dots, and the results could be extended without great difficulty to more exotic setups such as dots connected to ferromagnetic leads or hybrid systems. Transport in the presence of superconducting leads could also be studied but the extension of the present derivations is less straightforward because it would require to decouple pairs with two creation (resp. destruction) operators. The EOM could also be applied to multiple-dot systems or dots carrying many quantum numbers (for instance systems with a $SU(4)$ symmetry). However the complexity of the decoupling scheme explodes with the cardinal of the Hilbert space in the dot, and focusing on a particular electron occupation number in the dot would probably be wiser. I nevertheless believe that a general treatment of such systems is also possible by identifying the relevant processes and symmetries of the system, as it has been done in this work for the computation of higher-order terms. Finally great improvements deserve to be looked for on a technical side, in order to recover the exact Kondo temperature or the Fermi-liquid relationships at low temperature. I gave some indications for a study in this direction in Chap. 2 following the early work by Nagaoka [73]. A success in such a project would in my opinion be a giant leap for the EOM and their use to study strongly-correlated physics.

Appendix A

The Schrieffer-Wolff transformation

For the Kondo effect to take place, the single-level quantum dot must by singly occupied and charge fluctuations have to be weak. As the Kondo effect takes place only on low-energy scales, it is tempting to find a canonical transformation that projects the Anderson Hamiltonian on an effective low-energy Hamiltonian in which the transitions to the empty or doubly occupied states can happen only virtually. In this section, we reproduce the derivation of such a transformation, as was proposed by Schrieffer and Wolf in 1966 [96].

Let us decompose the Anderson Hamiltonian for a single-level quantum dot coupled in two terms

$$\mathcal{H} = \mathcal{H}_0 + \mathcal{H}_1, \tag{A.1}$$

with

$$\mathcal{H}_0 = \sum_{k\sigma} \varepsilon_k n_{k\sigma} + \sum_{\sigma} \varepsilon_\sigma n_\sigma + U n_\sigma n_{\bar{\sigma}}, \tag{A.2}$$

$$\mathcal{H}_1 = \sum_{k\sigma} t_\sigma c^\dagger_{k\sigma} f_\sigma + H.c. \tag{A.3}$$

We consider the region where $\varepsilon_d << \varepsilon_F$ and $\varepsilon_F << \varepsilon_d + U$, which implies the dot is singly occupied. Any canonical transformation can be written

$$\mathcal{H}_{eff} = \exp(-iS) H \exp(iS) = \mathcal{H}_0 + \mathcal{H}_1 + [iS, \mathcal{H}_0] + \frac{1}{2!}[iS, [iS, \mathcal{H}_0]] + \frac{1}{2!}[iS, [iS, \mathcal{H}_1]] + \cdots . \tag{A.4}$$

We are looking for a transformation that cancels out the tunneling term $\mathcal{H}_1$, since it couples states with different occupation numbers on the dot. In order to get the effective Hamiltonian $\mathcal{H}_{eff}$ of second order in t_σ, the operator S should satisfy

$$[iS, \mathcal{H}_0] = -\mathcal{H}_1. \tag{A.5}$$

Under that condition, the development becomes

$$\mathcal{H}_{eff} = \mathcal{H}_0 + \frac{1}{2}[iS, \mathcal{H}_1] + O(t^3). \tag{A.6}$$

Now we want to find S from Eq. (A.5). As H is hermitian, let us first notice the property

$$[iS, \mathcal{H}_0] = -\mathcal{H}_1 = -\mathcal{H}_1^\dagger = \left[\mathcal{H}_0^\dagger, -iS^\dagger\right] = \left[iS^\dagger, \mathcal{H}_0\right] \quad \Rightarrow \quad S = S^\dagger. \tag{A.7}$$

We write S under the form

$$iS = \sum_{k\sigma} t_\sigma \hat{A}_{k\sigma} c_{k\sigma}^\dagger f_\sigma + H.c., \tag{A.8}$$

where $\hat{A}_{k\sigma}$ is chosen to commute with $\mathcal{H}_0$. Then, the condition (A.5) becomes

$$\left[\sum_{k\sigma} t_\sigma \hat{A}_{k\sigma} c_{k\sigma}^\dagger f_\sigma + h.c., \mathcal{H}_0\right] = -\mathcal{H}_1, \tag{A.9}$$

which can be achieved with

$$\hat{A}_{k\sigma}\left[c_{k\sigma}^\dagger f_\sigma, \mathcal{H}_0\right] = -c_{k\sigma}^\dagger f_\sigma \tag{A.10}$$

$$\Rightarrow \hat{A}_{k\sigma}\left(-\varepsilon_k + \varepsilon_\sigma + U\hat{n}_{\bar{\sigma}}\right) c_{k\sigma}^\dagger f_\sigma = -c_{k\sigma}^\dagger f_\sigma \tag{A.11}$$

We find

$$\hat{A}_{k\sigma} = \left(\varepsilon_k - \varepsilon_\sigma - U\hat{n}_{\bar{\sigma}}\right)^{-1} \tag{A.12}$$

and

$$iS = \sum_{k\sigma} t_\sigma \left(\varepsilon_k - \varepsilon_\sigma - U\hat{n}_{\bar{\sigma}}\right)^{-1} \left(c_{k\sigma}^\dagger f_\sigma - f_\sigma^\dagger c_{k\sigma}\right). \tag{A.13}$$

However, this is not the most convenient expression since it contains an operator in the denominator. Therefore, we project $\hat{A}_{k\sigma}$ on $1 - \hat{n}_{\bar{\sigma}}$ and $\hat{n}_{\bar{\sigma}}$ and making two Taylor expansions (valid for $\varepsilon_k > \varepsilon_\sigma$ and $\varepsilon_k < \varepsilon_\sigma + U$)

$$\begin{aligned}
\frac{1 - \hat{n}_{\bar{\sigma}} + \hat{n}_{\bar{\sigma}}}{\varepsilon_k - \varepsilon_\sigma - U\hat{n}_{\bar{\sigma}}} &= (1 - \hat{n}_{\bar{\sigma}})\left(\varepsilon_k - \varepsilon_\sigma - U\hat{n}_{\bar{\sigma}}\right)^{-1} + \hat{n}_{\bar{\sigma}}\left(\varepsilon_k - \varepsilon_\sigma - U(\hat{n}_{\bar{\sigma}} - 1) - U\right)^{-1} \\
&= (1 - \hat{n}_{\bar{\sigma}})\left\{(\varepsilon_k - \varepsilon_\sigma)^{-1} + O(\hat{n}_{\bar{\sigma}})\right\} + \hat{n}_{\bar{\sigma}}\left\{(\varepsilon_k - \varepsilon_\sigma - U)^{-1} + O(1 - \hat{n}_{\bar{\sigma}})\right\} \\
&= \frac{1 - \hat{n}_{\bar{\sigma}}}{\varepsilon_k - \varepsilon_\sigma} + \frac{\hat{n}_{\bar{\sigma}}}{\varepsilon_k - \varepsilon_\sigma - U}.
\end{aligned} \tag{A.14}$$

We stress that there is no approximation here as we simply used the identity $\hat{n}_{\bar{\sigma}}^2 = \hat{n}_{\bar{\sigma}} \Rightarrow (1 - \hat{n}_{\bar{\sigma}})\hat{n}_{\bar{\sigma}} = 0$. Finally, the S operator can be written

$$iS = \sum_{k\sigma} t_\sigma \left[\frac{1 - \hat{n}_{\bar{\sigma}}}{\varepsilon_k - \varepsilon_\sigma} + \frac{\hat{n}_{\bar{\sigma}}}{\varepsilon_k - \varepsilon_\sigma - U}\right]\left(c_{k\sigma}^\dagger f_\sigma - f_\sigma^\dagger c_{k\sigma}\right) = iS^+ - iS^-. \tag{A.15}$$

The first term accounts for the virtual transitions to the empty state, while the second one describes the transitions to the doubly-occupied state. The operator S^- describes events in which the electron of spin σ tunnels from the dot to the leads, while S^+ describes the events in which a lead electron of spin σ enters the dot. Similarly, we decompose H_1 into $H_1^+ = \sum_{k\sigma} t_\sigma f_\sigma^\dagger c_{k\sigma}$ and $H_1^- = \sum_{k\sigma} t_\sigma c_{k\sigma}^\dagger f_\sigma$.

From now on, we only consider tunneling of lead electrons close to the Fermi level in comparison with the energy parameters in the dot. We use the limit $\varepsilon_\sigma << \varepsilon_k << \varepsilon_\sigma + U$ and neglect the ε_k dependence in the denominators. We evaluate the commutator $[iS, \mathcal{H}_1]$ by focusing on the states of single occupancy in the dot, and discard terms containing contributions like $f_\sigma f_{\bar\sigma}$ or $f_\sigma^\dagger f_{\bar\sigma}^\dagger$. This gives

$$\begin{aligned}
\left[iS^+, \mathcal{H}_1^-\right] &= \left[-\sum_{k\sigma} t_\sigma \left[\frac{1-\hat n_{\bar\sigma}}{\varepsilon_\sigma} + \frac{\hat n_{\bar\sigma}}{\varepsilon_\sigma + U}\right] c_{k\sigma}^\dagger f_\sigma, \sum_{k'\sigma'} t_{\sigma'}^* f_{\sigma'}^\dagger c_{k'\sigma'}\right] \\
&= \left[-\sum_{k\sigma} t_\sigma \left\{\frac{1}{+\varepsilon_\sigma} c_{k\sigma}^\dagger f_\sigma + \left[-\frac{1}{\varepsilon_\sigma} + \frac{1}{\varepsilon_\sigma + U}\right] \hat n_{\bar\sigma} c_{k\sigma}^\dagger f_\sigma\right\}, \sum_{k'\sigma'} t_{\sigma'}^* f_{\sigma'}^\dagger c_{k'\sigma'}\right].
\end{aligned}$$

As

$$\begin{aligned}
\left[c_{k\sigma}^\dagger f_\sigma, f_{\sigma'}^\dagger c_{k'\sigma'}\right] &= c_{k\sigma}^\dagger c_{k'\sigma'}\delta_{\sigma\sigma'} - \hat n_\sigma \delta_{kk'}\delta_{\sigma\sigma'}, \\
\left[\hat n_{\bar\sigma} c_{k\sigma}^\dagger f_\sigma, f_{\sigma'}^\dagger c_{k'\sigma'}\right] &= \hat n_{\bar\sigma} c_{k\sigma}^\dagger c_{k'\sigma'}\delta_{\sigma\sigma'} - f_{\bar\sigma} f_\sigma^\dagger c_{k\sigma}^\dagger c_{k'\bar\sigma}\delta_{\bar\sigma\sigma'},
\end{aligned}$$

we find

$$\begin{aligned}
\left[iS^+, \mathcal{H}_1^-\right] &= -\sum_{k\sigma} |t_\sigma|^2 \frac{1}{\varepsilon_\sigma}\left(\sum_{k'} c_{k\sigma}^\dagger c_{k'\sigma} - \hat n_\sigma\right) \\
&\quad + \sum_{k\sigma}\sum_{k'} t_\sigma \left[\frac{1}{\varepsilon_\sigma} - \frac{1}{\varepsilon_\sigma + U}\right]\left(t_\sigma^* \hat n_{\bar\sigma} c_{k\sigma}^\dagger c_{k'\sigma} - t_{\bar\sigma}^* f_{\bar\sigma}^\dagger f_\sigma c_{k\sigma}^\dagger c_{k'\bar\sigma}\right).
\end{aligned}$$

By symmetry, we have $\left[-iS^-, \mathcal{H}_1^+\right] = \left[-iS^{+\dagger}, \mathcal{H}_1^{-\dagger}\right] = \left[\mathcal{H}_1^-, -iS^+\right]^\dagger = \left[iS^+, \mathcal{H}_1^-\right]^\dagger$, which implies that

$$\begin{aligned}
\left[-iS^-, \mathcal{H}_1^+\right] &= -\sum_{k\sigma} |t_\sigma|^2 \frac{1}{\varepsilon_\sigma}\left(\sum_{k'} c_{k'\sigma}^\dagger c_{k\sigma} - \hat n_\sigma\right) \\
&\quad + \sum_{k\sigma}\sum_{k'} t_\sigma \left[\frac{1}{\varepsilon_\sigma} - \frac{1}{\varepsilon_\sigma + U}\right]\left(t_\sigma^* \hat n_{\bar\sigma} c_{k'\sigma}^\dagger c_{k\sigma} - t_{\bar\sigma}^* f_\sigma^\dagger f_{\bar\sigma} c_{k'\bar\sigma}^\dagger c_{k\sigma}\right).
\end{aligned}$$

Finally, because of the single occupancy on the dot, $\left[iS^+, \mathcal{H}_1^+\right] = \left[iS^-, \mathcal{H}_1^-\right] = 0$, and the correction to the effective Hamiltonian is

$$\begin{aligned}
[iS, \mathcal{H}_1] &= -2\sum_{k\sigma} |t_\sigma|^2 \frac{1}{\varepsilon_\sigma}\sum_{k'} c_{k\sigma}^\dagger c_{k'\sigma} + 2\sum_{k\sigma}\sum_{k'} |t_\sigma|^2 \left[\frac{1}{\varepsilon_\sigma} - \frac{1}{\varepsilon_\sigma + U}\right] \hat n_{\bar\sigma} c_{k\sigma}^\dagger c_{k'\sigma} \\
&\quad - \sum_{k\sigma}\sum_{k'} t_\sigma t_{\bar\sigma}^* \left[\frac{1}{\varepsilon_\sigma} - \frac{1}{\varepsilon_\sigma + U}\right]\left(f_{\bar\sigma}^\dagger f_\sigma c_{k\sigma}^\dagger c_{k'\bar\sigma} + f_\sigma^\dagger f_{\bar\sigma} c_{k'\bar\sigma}^\dagger c_{k\sigma}\right).
\end{aligned}$$

We neglected the term containg only a $\hat{n}_{\bar{\sigma}}$ operator as it leads only to an unimportant shift of the energy levels (which are sent to infinite). Using $n_\sigma = 1/2 + (n_\sigma - n_{\bar{\sigma}})/2$, we re-write the commutator under the form

$$\begin{aligned}
[iS, \mathcal{H}_1] &= -\sum_{k\sigma}\sum_{k'} |t_\sigma|^2 \left[\frac{1}{\varepsilon_\sigma} + \frac{1}{\varepsilon_\sigma + U}\right] c^\dagger_{k\sigma} c_{k'\sigma} \\
&\quad + \sum_{k\sigma}\sum_{k'} |t_\sigma|^2 \left[\frac{1}{\varepsilon_\sigma} - \frac{1}{\varepsilon_\sigma + U}\right] (\hat{n}_{\bar{\sigma}} - \hat{n}_\sigma)\, c^\dagger_{k\sigma} c_{k'\sigma} \\
&\quad - \sum_{k\sigma}\sum_{k'} t_\sigma t^*_{\bar{\sigma}} \left[\frac{1}{\varepsilon_\sigma} - \frac{1}{\varepsilon_\sigma + U}\right] \left(f^\dagger_{\bar{\sigma}} f_\sigma c^\dagger_{k\sigma} c_{k'\bar{\sigma}} + f^\dagger_\sigma f_{\bar{\sigma}} c^\dagger_{k'\bar{\sigma}} c_{k\sigma}\right). \quad \text{(A.16)}
\end{aligned}$$

This new expression is interesting in the sense that it highlights the spin-spin in interactions between the electron on the dot and the conduction electrons. In order to make this clear, let us remind the representation of a spin 1/2 operator in second quantization (see, for instance, [15], p.22); the expressions for the dot electron spin $\vec{S}_d$ and the conduction electron spin $\vec{S}_{kk'}$ are

$$\begin{aligned}
\vec{S}_d &= \frac{\hbar}{2} \sum_{\sigma\sigma'} \langle\sigma'| \left(\tau^x, \tau^y, \tau^z\right) |\sigma\rangle\, f^\dagger_{\sigma'} f_\sigma = \frac{\hbar}{2} \sum_{\sigma\sigma'} \vec{\tau}_{\sigma\sigma'} f^\dagger_{\sigma'} f_\sigma, \quad \text{(A.17)} \\
\vec{S}_{kk'} &= \frac{\hbar}{2} \sum_{\sigma\sigma'} \langle\sigma'| \left(\tau^x, \tau^y, \tau^z\right) |\sigma\rangle\, c^\dagger_{k'\sigma'} c_{k\sigma} = \frac{\hbar}{2} \sum_{\sigma\sigma'} \vec{\tau}_{\sigma\sigma'} c^\dagger_{k'\sigma'} c_{k\sigma}, \quad \text{(A.18)} \\
& \quad \text{(A.19)}
\end{aligned}$$

where $\vec{\tau}$ are the Pauli matrices

$$\vec{\tau} = \left\{ \begin{pmatrix} 0 & 1 \\ 1 & 0 \end{pmatrix}, \begin{pmatrix} 0 & -i \\ i & 0 \end{pmatrix} \begin{pmatrix} 1 & 0 \\ 0 & -1 \end{pmatrix} \right\}. \quad \text{(A.20)}$$

The components of the dot spin are for example

$$(S^x_d, S^y_d, S^z_d) = \frac{\hbar}{2} \left(\left[f^\dagger_\downarrow f_\uparrow + f^\dagger_\uparrow f_\downarrow\right], i\left[f^\dagger_\downarrow f_\uparrow - f^\dagger_\uparrow f_\downarrow\right], \left[f^\dagger_\uparrow f_\uparrow - f^\dagger_\downarrow f_\downarrow\right] \right). \quad \text{(A.21)}$$

Therefore, a spin-spin interaction between the electrons on the dot and in the leads is

expressed by (taking $\hbar = 1$)

$$\begin{aligned}
\vec{S}_d.\vec{S}_{kk'} &= \frac{1}{4}\sum_{\sigma\sigma'}\vec{\tau}_{\sigma\sigma'}f^\dagger_{\sigma'}f_\sigma.\sum_{\sigma_1\sigma'_1}\vec{\tau}_{\sigma_1\sigma'_1}c^\dagger_{k'\sigma'_1}c_{k\sigma_1} \\
&= \frac{1}{4}\sum_{\sigma\sigma'}\sum_{\sigma_1\sigma'_1}\left(\tau^x_{\sigma\sigma'}\tau^x_{\sigma_1\sigma'_1}+\tau^y_{\sigma\sigma'}\tau^y_{\sigma_1\sigma'_1}+\tau^z_{\sigma\sigma'}\tau^z_{\sigma_1\sigma'_1}\right)f^\dagger_{\sigma'}f_\sigma c^\dagger_{k'\sigma'_1}c_{k\sigma_1} \\
&= \frac{1}{4}\left[\left(f^\dagger_\uparrow f_\downarrow+f^\dagger_\downarrow f_\uparrow\right)\left(c^\dagger_{k'\uparrow}c_{k\downarrow}+c^\dagger_{k'\downarrow}c_{k\uparrow}\right)+i^2\left(-f^\dagger_\uparrow f_\downarrow+f^\dagger_\downarrow f_\uparrow\right)\left(-c^\dagger_{k'\uparrow}c_{k\downarrow}+c^\dagger_{k'\downarrow}c_{k\uparrow}\right)\right. \\
&\quad \left.+\left(f^\dagger_\uparrow f_\uparrow-f^\dagger_\downarrow f_\downarrow\right)\left(c^\dagger_{k'\uparrow}c_{k\uparrow}-c^\dagger_{k'\downarrow}c_{k\downarrow}\right)\right] \\
&= \frac{1}{4}\left[2\left(f^\dagger_\uparrow f_\downarrow c^\dagger_{k'\downarrow}c_{k\uparrow}+f^\dagger_\downarrow f_\uparrow c^\dagger_{k'\uparrow}c_{k\downarrow}\right)+\left(f^\dagger_\uparrow f_\uparrow-f^\dagger_\downarrow f_\downarrow\right)\left(c^\dagger_{k'\uparrow}c_{k\uparrow}-c^\dagger_{k'\downarrow}c_{k\downarrow}\right)\right] \\
&= \frac{1}{4}\sum_\sigma\left[2f^\dagger_\sigma f_{\bar\sigma}c^\dagger_{k'\bar\sigma}c_{k\sigma}+\left(n_\sigma-n_{\bar\sigma}\right)c^\dagger_{k'\sigma}c_{k\sigma}\right] \qquad \text{(A.22)}
\end{aligned}$$

Hence, in the absence of magnetic field ($\varepsilon_\sigma = \varepsilon_{\bar\sigma} = \varepsilon_d$), and for spin independent tunneling ($t_\sigma = t_{\bar\sigma} = t$), we identify

$$[iS,\mathcal{H}_1] = -|t|^2\left[\frac{1}{\varepsilon_d}+\frac{1}{\varepsilon_d+U}\right]\sum_{kk'}\sum_\sigma c^\dagger_{k\sigma}c_{k'\sigma}-4|t|^2\left[\frac{1}{\varepsilon_d}-\frac{1}{\varepsilon_d+U}\right]\sum_{kk'}\vec{S}_d.\vec{S}_{kk'}$$

The effective Hamiltonian at second order in t can be written under the form

$$\mathcal{H}^{(2)}_{eff} = K\sum_{kk'\sigma}c^\dagger_{k\sigma}c_{k'\sigma}+J\sum_{kk'}\vec{S}_d.\vec{S}_{kk'}, \qquad \text{(A.23)}$$

with

$$K = -\frac{1}{2}|t|^2\left[\frac{1}{\varepsilon_d}+\frac{1}{\varepsilon_d+U}\right], \qquad \text{(A.24)}$$

$$J = -2|t|^2\left[\frac{1}{\varepsilon_d}-\frac{1}{\varepsilon_d+U}\right] = 2|t|^2 D_\sigma(0) > 0. \qquad \text{(A.25)}$$

As the dot operators are summed in an effective spin operator, we can focus on the behavior of the conduction electrons the the total Hamiltonian writes

$$\mathcal{H}_{eff} = \sum_{kk'\sigma}\left(\varepsilon_k\delta_{kk'}+K\right)c^\dagger_{k\sigma}c_{k'\sigma}+J\sum_{kk'}\vec{S}_d.\vec{S}_{kk'}. \qquad \text{(A.26)}$$

The constant K represents the energy for potential scattering between the conduction electrons while J defines the exchange scattering between a conduction electron and the spin of the impurity. As $J > 0$, the spin-spin interaction is anti-ferromagnetic, meaning that the energy of the system is minimized when the spins are in an anti-parallel configuration.

The development of the Schrieffer-Wolff transformation can be easily generalized to the case of a dot coupled to many leads (with the same density of states ν). At the particle-hole symmetric point, the potential scattering term vanishes ($K = 0$), and we find the effective Kondo Hamiltonian

$$\mathcal{H}_{Kondo} = \sum_{\alpha k\sigma} \varepsilon_k c^\dagger_{\alpha k\sigma} c_{\alpha k\sigma} + J \sum_{kk'} \vec{S}_d . \vec{S}_{kk'}, \tag{A.27}$$

with the spin operator for the conduction electrons

$$\vec{S}_{kk'} = \frac{\hbar}{2} \sum_{\alpha\alpha'} \sum_{\sigma\sigma'} \vec{\tau}_{\sigma\sigma'} c^\dagger_{\alpha' k'\sigma'} c_{\alpha k\sigma}. \tag{A.28}$$

Let us stress that the Kondo Hamiltonian is a simplification of the Anderson model as it was derived from it by reducing the Hilbert space on the dot to two states $|\uparrow\rangle$ and $|\downarrow\rangle$.

Appendix B

Calculation of the coefficients for the resummations of the EOM

In this Appendix, we derive the coefficients that relate the Green's functions in Eqs. (2.46) at second order in t. In addition, the coefficient $\Sigma_{2\sigma}$ is calculated at fourth order in t because its second order expression turns out to have a zero imaginary part at resonance in the Kondo regime.

We call *self-energies* the coefficients that correct the energy terms in the denominators of the Green's functions in Eqs. (2.46) and *cross-coefficients* those which relate the different Green's functions integrally (see Fig. 2.1).

B.1 Coefficients at second order in t

B.1.1 Self-energy of $\langle\langle n_{\bar\sigma} c_{k\sigma}\rangle\rangle$ ($\Sigma_{1\sigma}(\omega_{:k})$)

The equations-of-motion for $\langle\langle n_{\bar\sigma} c_{k\sigma}\rangle\rangle$ is given by Eq. (2.28a):

$$\begin{aligned}\omega_{:k}\langle\langle n_{\bar\sigma} c_{k\sigma}\rangle\rangle &= t_\sigma\langle\langle n_{\bar\sigma} f_\sigma\rangle\rangle + \sum_{k_1} t_{\bar\sigma}\left[\langle\langle f^\dagger_{\bar\sigma} c_{k_1\bar\sigma} c_{k\sigma}\rangle\rangle - \langle\langle c^\dagger_{k_1\bar\sigma} f_{\bar\sigma} c_{k\sigma}\rangle\rangle\right] \\ &= \Sigma_{1\sigma}(\omega_{:k})\langle\langle n_{\bar\sigma} c_{k\sigma}\rangle\rangle + \cdots .\end{aligned}$$

We want to re-sum all the processes that loop back to $\langle\langle n_{\bar\sigma} c_{k\sigma}\rangle\rangle$ at second order in t, which define the self-energy $\Sigma_{1\sigma}(\omega_{:k})$. On the right-hand-side, we have to consider the EOM for the Green's functions of higher order in t, namely $\langle\langle f^\dagger_{\bar\sigma} c_{k_1\bar\sigma} c_{k\sigma}\rangle\rangle$ and $\langle\langle c^\dagger_{k_1\bar\sigma} f_{\bar\sigma} c_{k\sigma}\rangle\rangle$. The first one gives

$$\begin{aligned}\omega_{\bar\sigma:kk_1}\langle\langle f^\dagger_{\bar\sigma} c_{k_1\bar\sigma} c_{k\sigma}\rangle\rangle &= -t_{\bar\sigma}\sum_{k_2}\langle\langle c^\dagger_{k_2\bar\sigma} c_{k_1\bar\sigma} c_{k\sigma}\rangle\rangle + t_{\bar\sigma}\langle\langle n_{\bar\sigma} c_{k\sigma}\rangle\rangle \\ &\quad + t_\sigma\langle\langle f^\dagger_{\bar\sigma} c_{k_1\bar\sigma} f_\sigma\rangle\rangle + U\langle\langle f^\dagger_\sigma{:}f^\dagger_{\bar\sigma} c_{k_1\bar\sigma} c_{k\sigma}{:}f_\sigma\rangle\rangle,\end{aligned}$$

where the second term on the right-hand-side is the original Green's function $\langle\langle n_{\bar\sigma} c_{k\sigma}\rangle\rangle$. We put the vertical dots to remind the decoupling done at the order of Lacroix. The

other terms do not provide any way back to $\langle\langle n_{\bar\sigma} c_{k\sigma}\rangle\rangle$ at second order in t (in particular, there is no decoupling possible of $\langle\langle f^\dagger_\sigma{:}f^\dagger_{\bar\sigma} c_{k_1\bar\sigma} c_{k\sigma}{:}f_\sigma\rangle\rangle$ at second order that leaves the operator $c_{k\sigma}$ inside the Green's function, and we can therefore not come back to $\langle\langle n_{\bar\sigma} c_{k\sigma}\rangle\rangle$). We conclude that the only second-order process that comes back to $\langle\langle n_{\bar\sigma} c_{k\sigma}\rangle\rangle$ is

$$\langle\langle n_{\bar\sigma} c_{k\sigma}\rangle\rangle \to \langle\langle f^\dagger_{\bar\sigma} c_{k_1\bar\sigma} c_{k\sigma}\rangle\rangle \to \langle\langle n_{\bar\sigma} c_{k\sigma}\rangle\rangle.$$

After re-summation on the corresponding coefficients and energy propagators, we get the following contribution to the self-energy

$$\Sigma_{1\sigma}(\omega_{:k})\big|_{\langle\langle n_{\bar\sigma} c_{k\sigma}\rangle\rangle\to\langle\langle f^\dagger_{\bar\sigma} c_{k_1\bar\sigma} c_{k\sigma}\rangle\rangle} = \sum_{k_1} t^2_{\bar\sigma} \frac{1}{\omega_{\bar\sigma:kk_1}} = -i\Gamma_{\bar\sigma}.$$

The correction for the processes starting with $\langle\langle n_{\bar\sigma} c_{k\sigma}\rangle\rangle \to \langle\langle c^\dagger_{k_1\bar\sigma} f_{\bar\sigma} c_{k\sigma}\rangle\rangle$ can be obtained by symmetry by making the transformation

$$\Sigma_\sigma(\omega_{:k})\big|_{\langle\langle n_{\bar\sigma} c_{k\sigma}\rangle\rangle\to\langle\langle c^\dagger_{k_1\bar\sigma} f_{\bar\sigma} c_{k\sigma}\rangle\rangle} \to -\,\Sigma^*_\sigma(-\omega_{:k})\big|_{\langle\langle n_{\bar\sigma} c_{k\sigma}\rangle\rangle\to\langle\langle f^\dagger_{\bar\sigma} c_{k_1\bar\sigma} c_{k\sigma}\rangle\rangle}.$$

The total self-energy at second order in t is

$$\Sigma^{(2)}_{1\sigma}(\omega_{:k}) = -2i\Gamma_{\bar\sigma}. \tag{B.1}$$

B.1.2 Self-energy of $\langle\langle f^\dagger_{\bar\sigma} c_{k\bar\sigma} f_\sigma\rangle\rangle$ $(\Sigma_{2\sigma}(\omega_{:k}))$

The EOM for $\langle\langle f^\dagger_{\bar\sigma} c_{k\bar\sigma} f_\sigma\rangle\rangle$ is given by Eq. (2.28b):

$$\omega_{\bar\sigma:k\sigma}\langle\langle f^\dagger_{\bar\sigma} c_{k\bar\sigma} f_\sigma\rangle\rangle \;=\; \langle f^\dagger_{\bar\sigma} c_{k\bar\sigma}\rangle + t_{\bar\sigma}\langle\langle n_{\bar\sigma} f_\sigma\rangle\rangle + \sum_{k_1}\Big[t_\sigma\langle\langle f^\dagger_{\bar\sigma} c_{k\bar\sigma} c_{k_1\sigma}\rangle\rangle - t_{\bar\sigma}\langle\langle c^\dagger_{k_1\bar\sigma} c_{k\bar\sigma} f_\sigma\rangle\rangle\Big].$$

Again, we have to look for the expansion of $\langle\langle f^\dagger_{\bar\sigma} c_{k\bar\sigma} c_{k_1\sigma}\rangle\rangle$ and $\langle\langle c^\dagger_{k_1\bar\sigma} c_{k\bar\sigma} f_\sigma\rangle\rangle$. We proceed in a similar way as in Sec. B.1.1 and indicate only the processes relevant for contributions to $\Sigma_{2\sigma}(\omega_{:k})$. Let us concentrate on the Green's function $\langle\langle c^\dagger_{k_1\bar\sigma} c_{k\bar\sigma} f_\sigma\rangle\rangle$ and focus on the processes coming back to $\langle\langle f^\dagger_{\bar\sigma} c_{k\bar\sigma} f_\sigma\rangle\rangle$ at second order in t. These are

1. $\langle\langle f^\dagger_{\bar\sigma} c_{k\bar\sigma} f_\sigma\rangle\rangle \to \langle\langle c^\dagger_{k_1\bar\sigma} c_{k\bar\sigma} f_\sigma\rangle\rangle \to \langle\langle f^\dagger_{\bar\sigma} c_{k\bar\sigma} f_\sigma\rangle\rangle$.

   This process leads to the following correction:

   $$\sum_{k_1} t^2_{\bar\sigma} \frac{1}{w_{k_1:k\sigma}} = -i\Gamma_{\bar\sigma}$$

2. $\langle\langle f^\dagger_{\bar\sigma} c_{k\bar\sigma} f_\sigma\rangle\rangle \to \langle\langle c^\dagger_{k_1\bar\sigma} c_{k\bar\sigma} f_\sigma\rangle\rangle \to -U\langle\langle f^\dagger_{\bar\sigma}{:}c^\dagger_{k_1\bar\sigma} c_{k\bar\sigma} f_\sigma{:}f_{\bar\sigma}\rangle\rangle \to \langle\langle f^\dagger_{\bar\sigma}{:}c^\dagger_{k_1\bar\sigma} c_{k\bar\sigma} f_\sigma{:}c_{k_2\bar\sigma}\rangle\rangle \to \langle c^\dagger_{k_1\bar\sigma} c_{k_2\bar\sigma}\rangle\langle\langle f^\dagger_{\bar\sigma} c_{k\bar\sigma} f_\sigma\rangle\rangle$,

where the vertical dots to remind the decoupling already done at lower order. For $\langle c^\dagger_{k_1\bar\sigma} c_{k_2\bar\sigma}\rangle = f(\varepsilon_{k_1})\delta_{k_1k_2}$, this process leads to the following correction:

$$\sum_{k_1}\sum_{k_2} \frac{-t_{\bar\sigma}}{w_{k_1:k\sigma}} \frac{-U}{w_{k_1:k\sigma}-U} t_{\bar\sigma}\langle c^\dagger_{k_1\bar\sigma} c_{k_2\bar\sigma}\rangle = -t^2_{\bar\sigma}\sum_{k_1} D_\sigma(\omega_{k_1:k}) f(\varepsilon_{k_1}),$$

where the function $D_\sigma(\omega)$ is defined by

$$D_\sigma(\omega) = -U\frac{1}{\omega-\varepsilon_\sigma}\frac{1}{\omega-\varepsilon_\sigma-U}. \tag{B.2}$$

It can be replaced by a dressed expression in order to resum on all the intermediate processes starting from $\langle\langle c^\dagger_{k_1\bar\sigma} c_{k\bar\sigma} f_\sigma\rangle\rangle$ and $\langle\langle f^\dagger_{\bar\sigma}\vdots c^\dagger_{k_1\bar\sigma} c_{k\bar\sigma} f_\sigma\vdots f_{\bar\sigma}\rangle\rangle$, as those Green's functions acquire the same corrections on the denominator as $\langle\langle f_\sigma\rangle\rangle$ and $\langle\langle n_{\bar\sigma} f_\sigma\rangle\rangle$ (see Sec. 2.7.1),

$$\tilde D_\sigma(\omega) = \frac{1}{u_{1\sigma}(\omega)u_{2\sigma}(\omega)+\Xi_\sigma(\omega)}. \tag{B.3}$$

On the opposite, the average value $\langle c^\dagger_{k_1\bar\sigma} c_{k_2\bar\sigma}\rangle$ can *not* be computed self-consistently because it would involve a double counting with the decoupling of $\langle f^\dagger_{\bar\sigma} c_{k\bar\sigma}\rangle$ in the Green's function $\langle\langle f^\dagger_{\bar\sigma} c_{k\bar\sigma} f_\sigma\rangle\rangle$ (see Sec. 2.7.1).

Finally, the processes starting with $\langle\langle f^\dagger_{\bar\sigma} c_{k\bar\sigma} f_\sigma\rangle\rangle \to \langle\langle f^\dagger_{\bar\sigma} c_{k\bar\sigma} c_{k_1\sigma}\rangle\rangle \to \cdots$ can be found directly by applying the following transformation to the previous results

$$\Sigma_\sigma(w_{:k}) \to -\Sigma^*_{\bar\sigma}(-w_{:k}).$$

Summing all the terms gives

$$\Sigma^{(2)}_{2\sigma}(\omega_{:k}) = -i\Gamma - t^2_{\bar\sigma}\sum_{k_1} D_\sigma(\omega_{k_1:k}) f(\varepsilon_{k_1}) + t^2_\sigma \sum_{k_1} D^*_{\bar\sigma}(-\omega_{k_1:k}) f(\varepsilon_{k_1}) + O(t^4), \tag{B.4}$$

where the $O(t^4)$ term stands for the additional contributions generated when the D_σ function is replaced by its dressed expression.

B.1.3 Self-energy of $\langle\langle c^\dagger_{k\bar\sigma} f_{\bar\sigma} f_\sigma\rangle\rangle$ $(\Sigma_{3\sigma}(\omega_{k:}))$

The EOM for $\langle\langle c^\dagger_{k\bar\sigma} f_{\bar\sigma} f_\sigma\rangle\rangle$ is given by Eq. (2.28c)

$$(\omega_{k:\sigma\bar\sigma} - U)\,\langle\langle c^\dagger_{k\bar\sigma} f_{\bar\sigma} f_\sigma\rangle\rangle \;=\; \langle c^\dagger_{k\bar\sigma} f_{\bar\sigma}\rangle - t_{\bar\sigma}\langle\langle n_{\bar\sigma} f_\sigma\rangle\rangle + \sum_{k_1}\left[t_{\bar\sigma}\langle\langle c^\dagger_{k\bar\sigma} c_{k_1\bar\sigma} f_\sigma\rangle\rangle + t_\sigma\langle\langle c^\dagger_{k\bar\sigma} f_{\bar\sigma} c_{k_1\sigma}\rangle\rangle\right].$$

The processes starting with $\langle\langle c^\dagger_{k\bar\sigma} f_{\bar\sigma} f_\sigma\rangle\rangle \to \langle\langle c^\dagger_{k\bar\sigma} c_{k_1\bar\sigma} f_\sigma\rangle\rangle$ give the following contributions:

1. $\langle\langle c^\dagger_{k\bar\sigma} f_{\bar\sigma} f_\sigma\rangle\rangle \to \langle\langle c^\dagger_{k\bar\sigma} c_{k_1\bar\sigma} f_\sigma\rangle\rangle \to \langle\langle c^\dagger_{k\bar\sigma} f_{\bar\sigma} f_\sigma\rangle\rangle$

   This process leads to the following correction:

$$\sum_{k_1} t^2_{\bar\sigma} \frac{1}{\omega_{k:k_1\sigma}} = -i\Gamma_{\bar\sigma}.$$

2. $\langle\langle c^\dagger_{k\bar\sigma} f_{\bar\sigma} f_\sigma\rangle\rangle \to \langle\langle c^\dagger_{k\bar\sigma} c_{k_1\bar\sigma} f_\sigma\rangle\rangle \to -U\langle\langle f^\dagger_{\bar\sigma} \vdots c^\dagger_{k\bar\sigma} c_{k_1\bar\sigma} f_\sigma \vdots f_{\bar\sigma}\rangle\rangle \to -\langle\langle c^\dagger_{k_2\bar\sigma} \vdots c^\dagger_{k\bar\sigma} c_{k_1\bar\sigma} f_\sigma \vdots f_{\bar\sigma}\rangle\rangle \to \langle c^\dagger_{k_2\bar\sigma} c_{k_1\bar\sigma}\rangle\langle\langle c^\dagger_{k\bar\sigma} f_{\bar\sigma} f_\sigma\rangle\rangle$

   This process leads to the following correction:

$$\sum_{k_1}\sum_{k_2} \frac{t_{\bar\sigma}}{\omega_{k:k_1\sigma}} \frac{-U}{\omega_{k:k_1\sigma} - U} (-t_{\bar\sigma}) \langle c^\dagger_{k_2\bar\sigma} c_{k_1\bar\sigma}\rangle = -t^2_{\bar\sigma} \sum_{k_1} D_\sigma(\omega_{k:k_1\sigma}) f(\varepsilon_{k_1}).$$

Again, it is possible to replace D_σ by its dressed expression. The processes starting with $\langle\langle c^\dagger_{k\bar\sigma} f_{\bar\sigma} f_\sigma\rangle\rangle \to \langle\langle c^\dagger_{k\bar\sigma} f_{\bar\sigma} c_{k_1\sigma}\rangle\rangle \to \cdots$ can be computed similarly. They can be found directly by applying the following transformation to the previous results:

$$\Sigma_\sigma(\omega_{k:}) \to \Sigma_{\bar\sigma}(\omega_{k:}).$$

Summing all the processes gives

$$\Sigma^{(2)}_{3\sigma}(\omega_{k:}) = -i\Gamma - t^2_\sigma \sum_{k_1} D_{\bar\sigma}(\omega_{k:k_1\bar\sigma}) f(\varepsilon_{k_1}) - t^2_{\bar\sigma} \sum_{k_1} D_\sigma(\omega_{k:k_1\sigma}) f(\varepsilon_{k_1}) + O(t^4). \quad \text{(B.5)}$$

B.1.4 Cross-coefficient $\langle\langle n_{\bar\sigma} c_{k_1\sigma}\rangle\rangle \to \langle\langle f^\dagger_{\bar\sigma} c_{k\bar\sigma} f_\sigma\rangle\rangle$ $(t_{12,\sigma})$

The calculation of the cross-coefficient is similar to that of the self-energies: we look for the processes that connect the Green's functions considered. At second order in t, there is only one path to go from $\langle\langle n_{\bar\sigma} c_{k_1\sigma}\rangle\rangle$ to $\langle\langle f^\dagger_{\bar\sigma} c_{k\bar\sigma} f_\sigma\rangle\rangle$:

$\langle\langle n_{\bar\sigma} c_{k_1\sigma}\rangle\rangle \to \langle\langle f^\dagger_{\bar\sigma} c_{k\bar\sigma} c_{k_1\sigma}\rangle\rangle \to \langle\langle f^\dagger_\sigma \vdots f^\dagger_{\bar\sigma} c_{k\bar\sigma} c_{k_1\sigma} \vdots f_\sigma\rangle\rangle \to \langle\langle c^\dagger_{k_2\sigma} \vdots f^\dagger_{\bar\sigma} c_{k\bar\sigma} c_{k_1\sigma} \vdots f_\sigma\rangle\rangle$
$\to \langle c^\dagger_{k_2\sigma} c_{k_1\sigma}\rangle\langle\langle f^\dagger_{\bar\sigma} c_{k\bar\sigma} f_\sigma\rangle\rangle.$

The corresponding amplitude is given by

$$t_{12,\sigma}(\omega, k_1, k) = t_{\bar\sigma} \frac{U}{w_{\bar\sigma:kk_1}} \frac{-t_\sigma}{w_{\bar\sigma:kk_1} + U} \sum_{k_2} \langle c^\dagger_{k_2\sigma} c_{k_1\sigma}\rangle.$$

As in the previous sections, we must take the bare average value $\langle c^\dagger_{k_2\sigma} c_{k_1\sigma}\rangle = f(\varepsilon_{k_1})\delta_{k_1k_2}$ in order to avoid double counting, we have

$$t_{12,\sigma}(\omega, k_1, k) = t_\sigma t_{\bar\sigma} D^*_{\bar\sigma}(-\omega_{:kk_1}) f(\varepsilon_{k_1}) + O(t^4). \quad \text{(B.6)}$$

B.1.5 Cross-coefficient $\langle\langle n_{\bar\sigma} c_{k_1\sigma}\rangle\rangle \to \langle\langle c^\dagger_{k\bar\sigma} f_{\bar\sigma} f_\sigma\rangle\rangle$ $(t_{13,\sigma})$

The process $\langle\langle n_{\bar\sigma} c_{k_1\sigma}\rangle\rangle \to \langle\langle c^\dagger_{k\bar\sigma} f_{\bar\sigma} f_\sigma\rangle\rangle$ at second order in t is

$\langle\langle n_{\bar\sigma} c_{k_1\sigma}\rangle\rangle \to \langle\langle c^\dagger_{k\bar\sigma} f_{\bar\sigma} c_{k_1\sigma}\rangle\rangle \to \langle\langle f^\dagger_\sigma \vdots c^\dagger_{k\bar\sigma} f_{\bar\sigma} c_{k_1\sigma} \vdots f_\sigma\rangle\rangle \to \langle\langle c^\dagger_{k_2\sigma} \vdots c^\dagger_{k\bar\sigma} f_{\bar\sigma} c_{k_1\sigma} \vdots f_\sigma\rangle\rangle$
$\to \langle c^\dagger_{k_2\sigma} c_{k_1\sigma}\rangle \langle\langle c^\dagger_{k\bar\sigma} f_{\bar\sigma} f_\sigma\rangle\rangle$.

The corresponding amplitude is

$$t_{13,\sigma}(\omega, k_1, k) \;=\; (-t_{\bar\sigma}) \frac{-U}{w_{k_1:k\bar\sigma}} \frac{-t_\sigma}{w_{k_1:k\bar\sigma} - U} \sum_{k_2} \langle c^\dagger_{k_2\sigma} c_{k_1\sigma}\rangle.$$

Taking $\langle c^\dagger_{k_2\sigma} c_{k_1\sigma}\rangle = f(\varepsilon_{k_1})\delta_{k_1k_2}$, we obtain

$$t_{13,\sigma}(\omega, k_1, k) \;=\; t_\sigma t_{\bar\sigma} D_{\bar\sigma}(\omega_{k:k_1}) f(\varepsilon_{k_1}) + O(t^4). \tag{B.7}$$

B.1.6 Cross-coefficient $\langle\langle f^\dagger_{\bar\sigma} c_{k_1\bar\sigma} f_\sigma\rangle\rangle \to \langle\langle c^\dagger_{k\bar\sigma} f_{\bar\sigma} f_\sigma\rangle\rangle$ $(t_{23,\sigma})$

The process $\langle\langle f^\dagger_{\bar\sigma} c_{k_1\bar\sigma} f_\sigma\rangle\rangle \to \langle\langle c^\dagger_{k\bar\sigma} f_{\bar\sigma} f_\sigma\rangle\rangle$ at second order in t is

$\langle\langle f^\dagger_{\bar\sigma} c_{k_1\bar\sigma} f_\sigma\rangle\rangle \to \langle\langle c^\dagger_{k\bar\sigma} c_{k_1\bar\sigma} f_\sigma\rangle\rangle \to \langle\langle f^\dagger_{\bar\sigma} \vdots c^\dagger_{k\bar\sigma} c_{k_1\bar\sigma} f_\sigma \vdots f_{\bar\sigma}\rangle\rangle \to \langle\langle c^\dagger_{k_2\bar\sigma} \vdots c^\dagger_{k\bar\sigma} c_{k_1\bar\sigma} f_\sigma \vdots f_{\bar\sigma}\rangle\rangle$
$\to \langle c^\dagger_{k_2\bar\sigma} c_{k_1\bar\sigma}\rangle \langle\langle c^\dagger_{k\bar\sigma} f_{\bar\sigma} f_\sigma\rangle\rangle$.

The corresponding amplitude is

$$t_{23,\sigma}(\omega, k_1, k) \;=\; (-t_{\bar\sigma}) \frac{-U}{w_{k:k_1\sigma}} \frac{-t_{\bar\sigma}}{w_{k:k_1\sigma} - U} \sum_{k_2} \langle c^\dagger_{k_2\sigma} c_{k_1\sigma}\rangle.$$

Taking $\langle c^\dagger_{k_2\sigma} c_{k_1\sigma}\rangle = f(\varepsilon_{k_1})\delta_{k_1k_2}$, we obtain

$$t_{23,\sigma}(\omega, k_1, k) \;=\; t^2_{\bar\sigma} D_\sigma(\omega_{k:k_1}) f(\varepsilon_{k_1}) + O(t^4). \tag{B.8}$$

B.1.7 Cross-coefficient$\langle\langle c^\dagger_{k_1\bar\sigma} f_{\bar\sigma} f_\sigma\rangle\rangle \to \langle\langle f^\dagger_{\bar\sigma} c_{k\bar\sigma} f_\sigma\rangle\rangle$ $(t_{32,\sigma})$

The process $\langle\langle c^\dagger_{k_1\bar\sigma} f_{\bar\sigma} f_\sigma\rangle\rangle \to \langle\langle f^\dagger_{\bar\sigma} c_{k\bar\sigma} f_\sigma\rangle\rangle$ at second order in t is

$\langle\langle c^\dagger_{k_1\bar\sigma} f_{\bar\sigma} f_\sigma\rangle\rangle \to \langle\langle c^\dagger_{k_1\bar\sigma} c_{k\bar\sigma} f_\sigma\rangle\rangle \to \langle\langle f^\dagger_{\bar\sigma} \vdots c^\dagger_{k_1\bar\sigma} c_{k\bar\sigma} f_\sigma \vdots f_{\bar\sigma}\rangle\rangle \to \langle\langle f^\dagger_{\bar\sigma} \vdots c^\dagger_{k_1\bar\sigma} c_{k\bar\sigma} f_\sigma \vdots c_{k_2\bar\sigma}\rangle\rangle$
$\to \langle c^\dagger_{k_1\bar\sigma} c_{k_2\bar\sigma}\rangle \langle\langle f^\dagger_{\bar\sigma} c_{k\bar\sigma} f_{\bar\sigma}\rangle\rangle$.

The corresponding amplitude is

$$t_{32,\sigma}(\omega, k_1, k) \;=\; t_{\bar\sigma} \frac{-U}{w_{k_1:k\sigma}} \frac{t_\sigma}{w_{k_1:k\sigma} - U} \sum_{k_2} \langle c^\dagger_{k_1\bar\sigma} c_{k_2\bar\sigma}\rangle.$$

Taking $\langle c^\dagger_{k_1\bar\sigma} c_{k_2\bar\sigma}\rangle = f(\varepsilon_{k_1})\delta_{k_1k_2}$, we obtain

$$t_{32,\sigma}(\omega, k_1, k) \;=\; t_{\bar\sigma}^2 D_\sigma(\omega_{k_1:k}) f(\varepsilon_{k_1}) + O(t^4). \tag{B.9}$$

B.1.8 Effective couplings $\langle\langle n_{\bar\sigma} f_\sigma\rangle\rangle \to \langle\langle f^\dagger_{\bar\sigma} c_{k\bar\sigma} f_\sigma\rangle\rangle$ ($t_{2\sigma}$) and $\langle\langle n_{\bar\sigma} f_\sigma\rangle\rangle \to \langle\langle c^\dagger_{k\bar\sigma} f_{\bar\sigma} f_\sigma\rangle\rangle$ ($t_{3\sigma}$)

The coefficients $t_{ij,\sigma}$ connect the three Green's functions $\langle\langle n_{\bar\sigma} c_{k\sigma}\rangle\rangle$, $\langle\langle f^\dagger_{\bar\sigma} c_{k\bar\sigma} f_\sigma\rangle\rangle$ and $\langle\langle c^\dagger_{k\bar\sigma} f_{\bar\sigma} f_\sigma\rangle\rangle$ between each other. By summing up all paths leading to those functions, we obtain the effective couplings $t_{2\sigma}$ for all processes $\langle\langle n_{\bar\sigma} f_\sigma\rangle\rangle$ to $\langle\langle f^\dagger_{\bar\sigma} c_{k\bar\sigma} f_\sigma\rangle\rangle$ and $t_{3\sigma}$ for all processes $\langle\langle n_{\bar\sigma} f_\sigma\rangle\rangle \to \langle\langle c^\dagger_{k\bar\sigma} f_{\bar\sigma} f_\sigma\rangle\rangle$ (see Fig. 2.1).

The effective coefficients are obtained by solving the self-consistent equations

$$\begin{aligned} t_{2\sigma}(\omega_{:k}) \;&=\; t_{\bar\sigma} + t_\sigma \sum_{k_1} \frac{1}{\omega_{:k_1} - \Sigma_{1\sigma}(\omega_{:k_1})} t_{12,\sigma}(\omega, k_1, k) \\ &\quad + \sum_{k_1} t_{3\sigma}(\omega_{k_1:}) \frac{1}{\omega_{k_1:\sigma\bar\sigma} - U - \Sigma_{3\sigma}(\omega_{k_1:})} t_{32,\sigma}(\omega, k_1, k). \end{aligned} \tag{B.10a}$$

$$\begin{aligned} t_{3\sigma}(\omega_{:k}) \;&=\; -t_{\bar\sigma} + t_\sigma \sum_{k_1} \frac{1}{\omega_{:k_1} - \Sigma_{1\sigma}(\omega_{:k_1})} t_{13,\sigma}(\omega, k_1, k) \\ &\quad + \sum_{k_1} t_{2\sigma}(\omega_{:k_1}) \frac{1}{\omega_{\bar\sigma:k_1\sigma} - \Sigma_{2\sigma}(\omega_{:k_1})} t_{23,\sigma}(\omega, k_1, k). \end{aligned} \tag{B.10b}$$

As $t_{21,\sigma} = t_{31,\sigma} = 0$, the coefficient relating the Green's functions $\langle\langle n_{\bar\sigma} f_\sigma\rangle\rangle \to \langle\langle n_{\bar\sigma} c_{k\sigma}\rangle\rangle$ keeps its bare expression $t_{1\sigma} = t_\sigma$.

B.2 Self-energy $\Sigma_{2\sigma}(w_{:k})$ at fourth order in t

The second-order expressions for the self-energies are studied in Sec. 3.1. It turns out the the imaginary part of $\Sigma_{2\sigma}(\omega_{:k})$ is zero at the resonance point $\omega_{:k} = \Delta\sigma$. The corresponding diverging terms in the dot Green's function therefore remain, and we recover the Kondo features at equilibrium and for zero temperature.

However, we expect that the diverging terms should be smeared out when there is decoherence of the Kondo Ground State, for instance when a bias voltage is applied between the leads. As this feature is not present inside $\Sigma^{(2)}_{2\sigma}$, it gives a motivation to look for the fourth-order contribution.

B.2.1 Fourth-order processes for $\Sigma_{2\sigma}(w_{:k})$

As in the previous sections, we list the relevant processes.

1. A first process is given by
$\langle\langle f^\dagger_{\bar\sigma} c_{k\bar\sigma} f_\sigma\rangle\rangle \to \langle\langle c^\dagger_{k_1\bar\sigma} c_{k\bar\sigma} f_\sigma\rangle\rangle \to -U\langle\langle f^\dagger_{\bar\sigma}\vdots c^\dagger_{k_1\bar\sigma} c_{k\bar\sigma} f_\sigma\vdots f_{\bar\sigma}\rangle\rangle \to \langle\langle f^\dagger_{\bar\sigma}\vdots c^\dagger_{k_1\bar\sigma} c_{k\bar\sigma} c_{k_2\sigma}\vdots f_{\bar\sigma}\rangle\rangle \to$
$\langle\langle f^\dagger_{\bar\sigma}\vdots c^\dagger_{k_1\bar\sigma} c_{k\bar\sigma} c_{k_2\sigma}\vdots c_{k_3\bar\sigma}\rangle\rangle \to -U\langle\langle f^\dagger_{\sigma}\vdots f^\dagger_{\bar\sigma}\vdots c^\dagger_{k_1\bar\sigma} c_{k\bar\sigma} c_{k_2\sigma}\vdots c_{k_3\bar\sigma}\vdots f_\sigma\rangle\rangle$
$\to \langle\langle c^\dagger_{k_4\sigma}\vdots f^\dagger_{\bar\sigma}\vdots c^\dagger_{k_1\bar\sigma} c_{k\bar\sigma} c_{k_2\sigma}\vdots c_{k_3\bar\sigma}\vdots f_\sigma\rangle\rangle \to +\langle c^\dagger_{k_1\bar\sigma} c_{k_3\bar\sigma}\rangle\langle c^\dagger_{k_4\sigma} c_{k_2\sigma}\rangle\langle\langle f^\dagger_{\bar\sigma} c_{k\bar\sigma} f_\sigma\rangle\rangle$

   where the second set of vertical dots avoids double-counting with the decouplings done at second order. The corresponding contribution to the self-energy is given by

$$\sum_{k_1k_2k_3k_4} \frac{-t_{\bar\sigma}}{\omega_{k_1:k\sigma}} \frac{-U}{\omega_{k_1:k\sigma}-U} \frac{t_\sigma}{\omega_{k_1:kk_2}} \frac{t_{\bar\sigma}}{\omega_{k_1\bar\sigma:kk_2k_3}} \frac{U}{\omega_{k_1\bar\sigma:kk_2k_3}+U} (-t_\sigma) \langle c^\dagger_{k_1\bar\sigma} c_{k_3\bar\sigma}\rangle\langle c^\dagger_{k_4\sigma} c_{k_2\sigma}\rangle$$
$$= -t_\sigma^2 t_{\bar\sigma}^2 \sum_{k_1} D_\sigma(\omega_{k_1:k}) f(\varepsilon_{k_1}) \sum_{k_2} \frac{1}{\omega_{k_1:kk_2}} D^*_{\bar\sigma}(-\omega_{:kk_2}) f(\varepsilon_{k_2}).$$

2. A second process is given by
$\langle\langle f^\dagger_{\bar\sigma} c_{ik\bar\sigma} f_\sigma\rangle\rangle \to \langle\langle c^\dagger_{k_1\bar\sigma} c_{ik\bar\sigma} f_\sigma\rangle\rangle \to -U\langle\langle f^\dagger_{\bar\sigma}\vdots c^\dagger_{k_1\bar\sigma} c_{ik\bar\sigma} f_\sigma\vdots f_{\bar\sigma}\rangle\rangle \to \langle\langle c^\dagger_{k_2\bar\sigma}\vdots c^\dagger_{k_1\bar\sigma} c_{ik\bar\sigma} f_\sigma\vdots f_{\bar\sigma}\rangle\rangle \to$
$\langle\langle c^\dagger_{k_2\bar\sigma}\vdots c^\dagger_{k_1\bar\sigma} c_{ik\bar\sigma} f_\sigma\vdots c_{k_3\bar\sigma}\rangle\rangle \to -U\langle\langle f^\dagger_{\bar\sigma}\vdots c^\dagger_{k_2\bar\sigma}\vdots c^\dagger_{k_1\bar\sigma} c_{ik\bar\sigma} f_\sigma\vdots c_{k_3\bar\sigma}\vdots f_{\bar\sigma}\rangle\rangle$
$\to \langle\langle f^\dagger_{\bar\sigma}\vdots c^\dagger_{k_2\bar\sigma}\vdots c^\dagger_{k_1\bar\sigma} c_{ik\bar\sigma} f_\sigma\vdots c_{k_3\bar\sigma}\vdots c_{k_4\bar\sigma}\rangle\rangle \to \langle c^\dagger_{k_1\bar\sigma} c_{k_3\bar\sigma}\rangle\langle c^\dagger_{k_2\bar\sigma} c_{k_4\bar\sigma}\rangle\langle\langle f^\dagger_{\bar\sigma} c_{ik\bar\sigma} f_\sigma\rangle\rangle$

   The corresponding self-energy is

$$\sum_{k_1k_2k_3k_4} \frac{-t_{\bar\sigma}}{\omega_{k_1:k\sigma}} \frac{-U}{\omega_{k_1:k\sigma}-U} \frac{-t_{\bar\sigma}}{\omega_{k_1k_2:k\sigma\bar\sigma}-U} \frac{t_{\bar\sigma}}{\omega_{k_1k_2:kk3\sigma}} \frac{-U}{\omega_{k_1k_2:kk3\sigma}-U} t_{\bar\sigma} \langle c^\dagger_{k_1\bar\sigma} c_{k_3\bar\sigma}\rangle\langle c^\dagger_{k_2\bar\sigma} c_{k_4\bar\sigma}\rangle$$
$$= t_{\bar\sigma}^4 \sum_{k_1} D_\sigma(\omega_{k_1:k}) f(\varepsilon_{k_1}) \sum_{k_2} \frac{1}{\omega_{k_1k_2:k\sigma\bar\sigma}-U} D_\sigma(\omega_{k_2:k}) f(\varepsilon_{k_2})$$

3. Finally, the remaining processes start with
$\langle\langle f^\dagger_{\bar\sigma} c_{k\bar\sigma} f_\sigma\rangle\rangle \to \langle\langle f^\dagger_{\bar\sigma} c_{k\bar\sigma} c_{k_1\sigma}\rangle\rangle \to \cdots$

   These processes can be computed similarly. They can be found directly by applying the following transformation to the previous results:

$$\Sigma_{2\sigma}(w_{:k}) \to -\Sigma^*_{2\bar\sigma}(-w_{:k}).$$

Summing all the terms gives

$$\begin{aligned}\Sigma^{(4)}_{2\sigma}(\omega_{:k}) &= -t_\sigma^2 t_{\bar\sigma}^2 \sum_{k_1} D_\sigma(\omega_{k_1:k}) f(\varepsilon_{k_1}) \sum_{k_2} \frac{1}{\omega_{k_1:kk_2}} D^*_{\bar\sigma}(-\omega_{:kk_2}) f(\varepsilon_{k_2}) \\ &\quad + t_\sigma^2 t_{\bar\sigma}^2 \sum_{k_1} D^*_{\bar\sigma}(-\omega_{:kk_1}) f(\varepsilon_{k_1}) \sum_{k_2} \frac{1}{-\omega^*_{k_2:kk_1}} D_\sigma(\omega_{k_2:k}) f(\varepsilon_{k_2}) \\ &\quad + t_{\bar\sigma}^4 \sum_{k_1} D_\sigma(\omega_{k_1:k}) f(\varepsilon_{k_1}) \sum_{k_2} \frac{1}{\omega_{k_1k_2:k\sigma\bar\sigma} - U} D_\sigma(\omega_{k_2:k}) f(\varepsilon_{k_2}) \\ &\quad - t_\sigma^4 \sum_{k_1} D^*_{\bar\sigma}(-\omega_{:kk_1}) f(\varepsilon_{k_1}) \sum_{k_2} \frac{1}{-\omega^*_{\sigma\bar\sigma:kk_1k_2} - U} D^*_{\bar\sigma}(-\omega_{:kk_2}) f(\varepsilon_{k_2}).\end{aligned} \tag{B.11}$$

Unfortunately, this expression does not involve only convolutions, on the contrary to all the second-order coefficients. Numerically, we can no longer use a linear scale for a complete self-consistent treatment (see App. C). One option is to use a logarithmic scale, the other is to calculate the value of $\Sigma^{(4)}_{2\sigma}$ analytically without any re-summing on $D_\sigma(\omega)$.

However, for our concerns, it is not important to find the energy-dependence of the fourth-order self-energy, but rather its expression at the pole of $\langle\langle f^\dagger_{\bar\sigma} c_{k\bar\sigma} f_\sigma \rangle\rangle$. At resonance, $w_{:k} = \Delta\sigma$, we find

$$\begin{aligned}\Sigma^{(4)}_{2\sigma}(\Delta\sigma) \approx & -t_\sigma^2 t_{\bar\sigma}^2 \sum_{k_1} D_\sigma(\varepsilon_{k_1} + \Delta\sigma) f(\varepsilon_{k_1}) \sum_{k_2} \frac{1}{\varepsilon_{k_1} - \varepsilon_{k_2} + \Delta\sigma + i\delta} D^*_{\bar\sigma}(\varepsilon_{k_2} - \Delta\sigma) f(\varepsilon_{k_2}) \\ & + t_\sigma^2 t_{\bar\sigma}^2 \sum_{k_1} D^*_{\bar\sigma}(\varepsilon_{k_1} - \Delta\sigma) f(\varepsilon_{k_1}) \sum_{k_2} \frac{1}{\varepsilon_{k_1} - \varepsilon_{k_2} - \Delta\sigma + i\delta} D_\sigma(\varepsilon_{k_2} + \Delta\sigma) f(\varepsilon_{k_2}) \\ & + t_{\bar\sigma}^4 \sum_{k_1} D_\sigma(\varepsilon_{k_1} + \Delta\sigma) f(\varepsilon_{k_1}) \sum_{k_2} \frac{1}{\varepsilon_{k_1} + \varepsilon_{k_2} - 2\varepsilon_{\bar\sigma} - U + i\delta} D_\sigma(\varepsilon_{k_2} + \Delta\sigma) f(\varepsilon_{k_2}) \\ & - t_\sigma^4 \sum_{k_1} D^*_{\bar\sigma}(\varepsilon_{k_1} - \Delta\sigma) f(\varepsilon_{k_1}) \sum_{k_2} \frac{1}{\varepsilon_{k_1} + \varepsilon_{k_2} - 2\varepsilon_\sigma - U + i\delta} D^*_{\bar\sigma}(\varepsilon_{k_2} - \Delta\sigma) f(\varepsilon_{k_2}),\end{aligned} \tag{B.12}$$

which is now a convolution product that can be treated numerically without difficulty.

B.2.2 Simplification of fourth-order terms at resonance

In addition to the bare fourth order contribution $\Sigma^{(4)}_{2\sigma}$ obtained in Eq. (B.12), we have to consider the fourth order terms generated by $\Sigma^{(2)}_{2\sigma}$ when we put the dressed $\tilde D_\sigma$ propagator. Recalling Eq. (B.4)

$$\Sigma^{(2)}_{2\sigma}(\omega_{:k}) = -i\Gamma - t_{\bar\sigma}^2 \sum_{k_1} \tilde D_\sigma(\omega_{k_1:k}) f(\varepsilon_{k_1}) + t_\sigma^2 \sum_{k_1} \tilde D^*_{\bar\sigma}(-\omega_{k_1:k}) f(\varepsilon_{k_1}), \tag{B.13}$$

where we expand the dressed propagator

$$\tilde{D}_\sigma(\omega) = \frac{1}{u_{1\sigma}(\omega)u_{2\sigma}(\omega)+\Xi_\sigma(\omega)} = \frac{1}{u_{1\sigma}(\omega)u_{2\sigma}(\omega)} - \Xi^{(2)}_\sigma(\omega)\frac{1}{u^2_{1\sigma}(\omega)u^2_{2\sigma}(\omega)} + O(t^4). \tag{B.14}$$

where $\Xi^{(2)}_\sigma(\omega)$ corresponds to the second order terms inside $\Xi_\sigma(\omega)$:

$$\Xi^{(2)}_\sigma(\omega) = -t^2_{\bar\sigma}\sum_k \left[\frac{f(\varepsilon_k)}{\omega_{:k}-\Delta\sigma} + \frac{f(\varepsilon_k)}{\omega_{k:}-2\varepsilon_d-U}\right]. + O(t^4) \tag{B.15}$$

Introducing Eqs. (B.14) and (B.15) inside Eq. (B.13) gives the following fourth order contribution at resonance $w_{:k} = \Delta\sigma$

$$\begin{aligned}
&-t^4_{\bar\sigma}\sum_{k_1} D^2_\sigma(\varepsilon_{k_1}+\Delta\sigma)f(\varepsilon_{k_1})\sum_{k_2}\frac{f(\varepsilon_{k_2})}{\varepsilon_{k_1}-\varepsilon_{k_2}+i\delta}\\
&-t^4_{\bar\sigma}\sum_{k_1} D^2_\sigma(\varepsilon_{k_1}+\Delta\sigma)f(\varepsilon_{k_1})\sum_{k_2}\frac{f(\varepsilon_{k_2})}{\varepsilon_{k_1}-\varepsilon_{k_2}-2\varepsilon_{\bar\sigma}-U+i\delta}\\
&+t^4_{\sigma}\sum_{k_1} D^{*2}_{\bar\sigma}(-\varepsilon_{k_1}-\Delta\sigma)f(\varepsilon_{k_1})\sum_{k_2}\frac{f(\varepsilon_{k_2})}{-\varepsilon_{k_1}+\varepsilon_{k_2}+i\delta}\\
&+t^4_{\sigma}\sum_{k_1} D^{*2}_{\bar\sigma}(-\varepsilon_{k_1}-\Delta\sigma)f(\varepsilon_{k_1})\sum_{k_2}\frac{f(\varepsilon_{k_2})}{-\varepsilon_{k_1}+\varepsilon_{k_2}-2\varepsilon_{\sigma}-U+i\delta}.
\end{aligned} \tag{B.16}$$

Interestingly, the contributions from the poles of the D functions inside Eq. (B.12) cancel out with contributions of Eq. (B.16). Summing the imaginary part of all the contributions for spin-independent tunneling, we get, after some long but straightforward calculations, the fourth order decoherence rate $\gamma^{(4)}_{2\sigma} = -\mathrm{Im}\Sigma^{(4)}_{2\sigma}(\Delta\sigma)$

$$\gamma^{(4)}_{2\sigma} = \sum_{\alpha_1\alpha_2}\sum_{\sigma_1\sigma_2}\frac{\Gamma_{\alpha_1\sigma_1}\Gamma_{\alpha_2\sigma_2}}{\pi}\int_{-W}^{W} d\varepsilon_k f(\varepsilon_k-\mu_{\alpha_1})\left[1-f(\varepsilon_k-\mu_{\alpha_2}+\varepsilon_{\sigma_1}-\varepsilon_{\sigma_2})\right]\ D^2_{\sigma_2}(\varepsilon_k), \tag{B.17}$$

where lead indexes α were re-introduced alongside the k numbers. As we can see from Eq. (B.17), we obtain a finite decoherence rate as soon as either the temperature or the bias voltage or the magnetic field is finite. Those three effects are discussed in the thesis.

Appendix C

Numerical computation

While the derivation of the equations-of motion (EOM) is completely analytical, their solution for the Green's function requires solving self-consistently a system of integral equations (2.48). Using the atomic limit expression (2.18) as a starting point, each iteration calculates the next order in dot-lead tunneling rate Γ (or more precisely in exchange coupling νJ given by Eq. (A.25)) for the integral terms. In the weak-coupling regime, corrections are small and an analytical treatment at lowest-order in νJ should be satisfactory, as we did in Chap. 5. However when corrections grow larger a numerical treatment is required.

Fortunately the integrals involve convolution products only, allowing for the use of *Discrete Fourier Transforms* (DFT[1]) that reduce the numerical complexity of the summation from N^2 to $N\log(N)$, where N is the number of points used for the discretization. However the algorithm that enables such a reduction in complexity requires a linear discretization step that suits poorly to the Kondo physics where one deals with terms containing logarithmic divergences around the Fermi level. To circumvent this, a logarithmic discretization is proposed that 'zooms' on the resonance, allowing for a smaller number of points.

C.1 Linear energy-scale

C.1.1 Relations after Fourier transform

For simplicity we consider the infinite U Lacroix approximation as its numerical treatment can directly be extended to more sophisticated schemes. The Green's function is obtained from the self-consistent equation

$$\mathcal{G}_\sigma(\omega) = \frac{1 - \langle n_{\bar\sigma}\rangle - \sum_\alpha \frac{\Gamma_{\alpha\bar\sigma}}{\pi}\int d\varepsilon_k \frac{1}{\omega_{\bar\sigma:k\sigma} + i\delta}\, f(\varepsilon_k)\mathcal{G}^*_{\bar\sigma}(\varepsilon_k)}{w - \varepsilon_\sigma + i\Gamma_\sigma - \sum_\alpha \frac{\Gamma_{\alpha\bar\sigma}}{\pi}\int d\varepsilon_k \frac{1}{\omega_{\bar\sigma:k\sigma} + i\delta}\, f(\varepsilon_k)\left[1 + i\Gamma\mathcal{G}^*_{\bar\sigma}(\varepsilon_k)\right]}. \tag{C.1}$$

[1] Do not confuse with 'Density Functional Theory'.

The Green's functions couple integrally to each other inside a convolution product. We define the two functions

$$\mathcal{H}_\sigma(\omega) \equiv f(\omega)\mathcal{G}_\sigma(\omega), \tag{C.2}$$

$$\mathcal{A}_\sigma(\omega) \equiv \sum_\alpha \frac{\Gamma_{i\sigma}}{\pi} \int dw' \frac{1}{w - w' + i\delta}\, \mathcal{H}^*_{i\sigma}(w'). \tag{C.3}$$

The Fourier transform of $\mathcal{H}_\sigma(\omega)$ reads

$$\mathcal{H}_\sigma(\omega) = \int_{-\infty}^{\infty} dt e^{-iwt} H_{i\sigma}(t), \tag{C.4a}$$

$$H_{i\sigma}(t) = \frac{1}{2\pi} \int_{-\infty}^{\infty} dw e^{iwt} \mathcal{H}_\sigma(\omega). \tag{C.4b}$$

The functions $\mathcal{H}_\sigma$ and $\mathcal{A}_\sigma$ are related by Eq. (C.1). The Fourier-transform of $\mathcal{A}_\sigma(\omega)$ in Eq. (C.3) is given by

$$A_\sigma(t) = 2\pi \sum_\alpha \frac{\Gamma_{i\sigma}}{\pi} H^*_{i\sigma}(-t).\left[-ie^{\delta t}\Theta(-t)\right] = -2i \sum_\alpha \Gamma_{i\sigma} H^*_{i\sigma}(-t) e^{\delta t}\Theta(-t). \tag{C.5}$$

Notice that $A_\sigma(t)$ is zero for $t > 0$. This is expected as it is related to the advanced Green's function $\mathcal{G}^*_{\bar{\sigma}}(\varepsilon_k)$.

Proof of Eq. (C.5)

We demonstrate the equality (C.5) by taking the Fourier transform of $A_\sigma(t)$.

$$\begin{aligned}
\mathcal{A}_\sigma(\omega) &= -2i \sum_\alpha \Gamma_{i\sigma} \int_{-\infty}^{\infty} dt e^{-iwt} H^*_{i\sigma}(-t) e^{\delta t}\Theta(-t) \\
&= -2i \sum_\alpha \Gamma_{i\sigma} \int_0^{\infty} dt e^{iwt} H^*_{i\sigma}(t) e^{-\delta t} \\
&= -2i \sum_\alpha \Gamma_{i\sigma} \int_0^{\infty} dt e^{iwt} e^{-\delta t} \left[\frac{1}{2\pi} \int_{-\infty}^{\infty} dw' e^{iw't} \mathcal{H}_\sigma(w')\right]^* \\
&= -\frac{i}{\pi} \sum_\alpha \Gamma_{i\sigma} \int_{-\infty}^{\infty} dw' \mathcal{H}^*_\sigma(w') \int_0^{\infty} dt\, e^{i(w-w')t} e^{-\delta t} \\
&= -\frac{i}{\pi} \sum_\alpha \Gamma_{i\sigma} \int_{-\infty}^{\infty} dw' \mathcal{H}^*_\sigma(w') \underbrace{\left[\frac{e^{i(w-w')t} e^{-\delta t}}{i(w-w') - \delta}\right]_0^{\infty}}_{-\frac{1}{i}\frac{1}{w-w'+i\delta}} \\
&= \sum_\alpha \frac{\Gamma_{i\sigma}}{\pi} \int_{-\infty}^{\infty} dw' \mathcal{H}^*_\sigma(w') \frac{1}{w - w' + i\delta}.
\end{aligned}$$

Notice the importance of the finite convergence factor δ when we put $e^{-\delta t} \to 0$ for $t \to \infty$; had we put $\delta = 0$, the integral was badly defined. The actual value that has to be chosen for the numerical computations to converge is given in Sec. C.1.2.

C.1.2 Linear discretization

On a linear scale, the DFT can be computed by means of a very efficient algorithm called *Fast-Fourier-Transform* (FFT) and numerical computations will gain a lot of efficiency (with an optimum when $N = 2^n$, where n is an integer) allowing for the use of large numbers of points (typically $N = 10^6$). We show how the expression from the EOM can be mapped on such a scale by discretizing the energy variable $\omega \to \omega_k$ $(k = 0, \cdots, N-1)$ in the Green's function. We write $\mathcal{H}_\sigma[w_k] = \mathcal{H}_{k;\sigma}$ the sequence of the discretized values of the analytical function $\mathcal{H}_\sigma(\omega)$.

The Discrete Fourier Transform is defined by

$$\begin{aligned} \mathcal{H}_{k;\sigma} &= \sum_{n=0}^{N-1} H_{n;\sigma} e^{-\frac{2\pi i}{N}kn}, \\ H_{n;\sigma} &= \frac{1}{N}\sum_{k=0}^{N-1} \mathcal{H}_{k;\sigma} e^{\frac{2\pi i}{N}kn}. \end{aligned}$$

The phase factor is zero for the first term of the sequence, while for the continuous Fourier Transform this happens at $\omega = 0$. We therefore have to care for the phase factor by discretizing the integral carefully. We discretize the frequency space symmetrically around the Fermi level

$$\omega \to \omega_k = -W\left(\frac{N-1}{N}\right) + \frac{2W}{N}k \qquad (k = 0, \cdots, N-1); \tag{C.6}$$

the origin $\omega_k = 0$ can be reached only for N odd (for $k = (N-1)/2$), to the cost of a longer computation time. After discretization of the integral, the continuous Fourier transform becomes

$$\begin{aligned} H_\sigma(t) &= \frac{1}{2\pi}\lim_{W\to\infty}\int_{-W}^{W} dw\, e^{iwt}\,\mathcal{H}_\sigma(\omega) \\ &= \frac{1}{2\pi}\frac{2W}{N}\sum_{k=0}^{N-1} e^{i\omega_k t}\,\mathcal{H}_\sigma[\omega_k] = \frac{W}{\pi N}\, e^{-iD\frac{N-1}{N}t}\sum_{k=0}^{N-1} e^{i\frac{2W}{N}kt}\,\mathcal{H}_{k;\sigma}, \end{aligned}$$

where the bandwidth W is of course chosen large but finite. The time t has to be discretized as well by setting

$$t_n = -\frac{\pi}{2W}(N-1) + \frac{\pi n}{W} \qquad (n = 0, \cdots N-1). \tag{C.7}$$

We obtain

$$H_\sigma[t_n] = \frac{W}{\pi N}\, e^{i\pi\frac{(N-1)^2}{2N}}\, e^{-i\pi\frac{N-1}{N}n}\sum_{k=0}^{N-1} e^{i\frac{2\pi}{N}kn}\, e^{-i\pi\frac{N-1}{N}k}\,\mathcal{H}_{k;\sigma}, \tag{C.8}$$

and find $A_\sigma[t_n]$ according to Eq. (C.5)

$$\begin{aligned} A_\sigma[t_n] = A_{n;\sigma} &= -2i\sum_\alpha \Gamma_{\alpha\sigma} e^{\delta t_n} H^*_\sigma[-t_n]\Theta(-t_n) \\ &= -2i\frac{W}{\pi N}\, e^{i\pi\frac{(N-1)^2}{2N}}\, e^{\delta\frac{\pi}{2W}(2n-N+1)}\,\Theta(N-1-2n)\, e^{-i\pi\frac{N-1}{N}n} \\ &\quad \times \sum_{k=0}^{N-1} e^{i\frac{2\pi}{N}kn}\, e^{-i\pi\frac{N-1}{N}k} \sum_\alpha \Gamma_{\alpha\sigma}\mathcal{H}^*_{k;i\sigma}. \end{aligned}$$

We see that $A_{n;\sigma}$ is the result of the DFT of a function proportional to $\mathcal{H}^*_{k;\sigma}$ multiplied by a phase factor.

The last step is to transform back in frequency space $A_{k;\sigma} = A_\sigma[\omega_k]$. Discretizing the inverse Fourier transform in a very similar way as previously and introducing the result for $A_{n;\sigma}$, we obtain

$$\begin{aligned} A_{k;\sigma} &= \int_{-\infty}^{\infty} dt e^{-i\omega_k t} A_\sigma(t) \\ &\approx \frac{\pi}{W}\sum_{n=0}^{N-1} e^{-i\frac{\pi}{2N}(-N+1+2k)(-N+1+2n)} A_{n;\sigma} \\ &= \frac{\pi}{W} e^{-i\pi\frac{(N-1)^2}{2N}} e^{i\pi\frac{N-1}{N}k} \sum_{n=0}^{N-1} e^{i\pi\frac{N-1}{N}n} e^{-i\frac{2\pi}{N}kn} A_{n;\sigma} \\ &= -2ie^{i\pi\frac{N-1}{N}k}\left\{\sum_{n=0}^{N-1} e^{-i\frac{2\pi}{N}kn}\,\left[e^{\delta\frac{\pi}{2W}(2n-N+1)}\,\Theta(N-1-2n)\right.\right. \\ &\quad \left.\left.\frac{1}{N}\sum_{k'=0}^{N-1} e^{i\frac{2\pi}{N}k'n}\left(e^{-i\pi\frac{N-1}{N}k'}\sum_\alpha \Gamma_{\alpha\sigma}\mathcal{H}^*_{k';i\sigma}\right)\right]\right\} \end{aligned}$$

We see clearly the sequence of two DFT. Notice that $A_{k;\sigma}$ is not the DFT of $A_{n;\sigma}$ because of the additional phase factors.

A last important issue is the value we choose for δ. As we saw in the continuous regime, it cannot be strictly zero, otherwise the integral would be badly defined . We have to cover all the information in our time range, which is the case if

$$e^{-\delta\pi N/2W} << 1 \quad \Leftrightarrow \quad \delta >> \frac{2W}{\pi N}. \tag{C.9}$$

Of course, if we want to describe the Kondo physics, we also need our energy resolution to be smaller than T_K. This has to be achieved playing on N, to the price of an increasing computation time.

The non-zero value of δ has an influence on the low-energy results which are therefore sensitive to a purely numerical issue. However, within our approximation scheme at fourth-order in t, the pole in Eq. (C.3) gets smeared by the decoherence rate $\gamma_{2\sigma}$ that is

non-zero as soon as either the temperature or the bias voltage or the magnetic field is non-zero, and δ is then replaced by a quantity that has a physical origin. It is therefore possible to obtain results independent on numerical issues as soon as $\gamma_{2\sigma} >> 2W/\pi N$, which sets the application range of the linear discretization for the EOM (or, reversing the problem, allows to take smaller number of points when $\gamma_{2\sigma}$ is large).

C.2 Logarithmic energy-scale

As the Kondo effect exhibits a narrow resonance at low energy, it makes sense to have a discretization which is finer in regions where the density of states has strong variations.

C.2.1 Logarithmic discretization for a single resonance

At equilibrium $V = 0$, we only have to zoom on the central peak that shows a logarithmic divergence around $\omega = 0$ (the non-zero magnetic field is discussed later on). In order to optimize the number of points needed to compute the Green's function, it is relevant to use a logarithmic scale for ω. This can be defined by

$$\omega_n = \begin{cases} \omega_{min}\, a^{n-N/2-1} & \text{for} \quad n \geq \frac{N}{2}+1 \\ -\omega_{min}\, a^{N/2-n} & \text{for} \quad n \leq \frac{N}{2} \end{cases}, \tag{C.10}$$

where ω_{min} and a are 2 parameters, and N is the number of points which is much smaller than for the linear scale as the numerical complexity now turned to N^2 (typically $N = 10^3$).

How to choose ω_{min} and a? First there is a boundary condition that fixes the bandwidth W:

$$W = \omega_{min}\, a^{N/2-1}. \tag{C.11}$$

The other condition is more loose and has to be chosen in order to make a compromise between having ω_{min} very small in order to describe the Kondo peak very accurately, and having a the closest to 1 in order to keep the precision on the high-energy physics (we remind that there are two high-energy peaks around ε_d and $\varepsilon_d + U$). Notice that the relative difference between to successive points depends only on a:

$$\frac{d\omega}{\omega} = \left| \frac{\omega_n - \omega_{n-1}}{\omega_n} \right| = 1 - \frac{1}{a},$$

Hence, we decide to choose $d\omega/\omega = 0.1$, corresponding to $a = 1/0.9 = 1.111$. This gives a ratio $w_{min}/D \approx 10^{-23}$ for $N = 10^3$, which is much better than the linear scale for which $w_{min}/D \approx 10^{-6}$.

C.2.2 Discretization in the presence of 2 resonances

In a two-leads setup put out of equilibrium, the reservoirs carry two different chemical potentials μ_L and μ_R and as a consequence two resonances show up in the density of states, hence the need for a discretization that zooms on two different points $\omega = \mu_\alpha$. Let us consider the case of 2 resonances at p_1 and p_2; the discretization is then

$$\omega_n = \begin{cases} -\omega_{min}\, a^{N_1-n} + p_1 & \text{for} \quad n \leq N_1 \\ \omega_{min}\, a^{n-N_1-1} + p_1 & \text{for} \quad N_1+1 \leq n \leq N_1+N_2 \\ -\omega_{min}\, a^{N_1+2N_2-n} + p_2 & \text{for} \quad N_1+N_2+1 \leq n \leq N_1+2N_2 \\ \omega_{min}\, a^{n-N_1-2N_2-1} + p_2 & \text{for} \quad N_1+2N_2+1 \leq n \leq 2N_1+2N_2 \end{cases}, \quad \text{(C.12)}$$

to which the intermediate points at p_1, $(p_1+p_2)/2$ and p_2 should be added.

The parameters ω_{min}, a, N_1, N_2 have to be determined. We have the following constraints[2]:

1. Total number condition
$$N_1 + N_2 = N/2, \quad \text{(C.13)}$$
where N is the total number of points.

2. Boundary limit at high energy
$$W = \min\left(\left|-\omega_{min}\, a^{N_1-1} + p_1\right|, \omega_{min}\, a^{N_1-1} + p_2\right), \quad \text{(C.14)}$$
which leads to
$$\omega_{min}\, a^{N_1-1} = W - \min\left(-p_1, p_2\right) = W + \max\left(p_1, -p_2\right). \quad \text{(C.15)}$$
Indeed the boundary is different on the left and on the right if $p_1 + p_2 \neq 0$ (for instance in case of an asymmetric bias voltage).

3. Boundary limit at the middle of the peaks $(p_1+p_2)/2$
$$\omega_{min}\, a^{N_2-1} + p_1 \leq \frac{p_1+p_2}{2} \quad \Rightarrow \quad \omega_{min}\, a^{N_2-1} \leq \frac{p_2-p_1}{2}, \quad \text{(C.16)}$$
where N_2 is the largest integer satisfying the inequality. Notice that that if these conditions imply $(p_2-p_1)/2 < wa_{min}$, we turn back to the single-peak case.

There is still one free parameter that can be set by choosing $a = 1/0.9$ as in the previous section. The relative precision at the peaks is at worst of the order of $w_{min}/D \leq 10^{-23/2} \approx 3.10^{-12}$, which is still much better than with the linear scale.

[2]The constraints are written for $p_1 \leq 0$ and $p_2 \geq 0$.

C.2.3 The magnetic field issue

The logarithmic discretization is much more tricky in the presence of a magnetic field as it splits the Kondo resonance in the density of states. As the integrals involve a product $f(\varepsilon_k)\mathcal{G}_\sigma(\varepsilon_k)$, where the Fermi function is insensitive to the magnetic field, the number of peaks that has to be considered increases to two at equilibrium[3] (around 0 and $\Delta\sigma$) or four out of equilibrium[4] (around $\mu_{L/R}$ and $\mu_{L/R} + \Delta\sigma$). In the latter case, the precision of the energy scale at the resonances is of the order of $w_{min}/D \leq 10^{-23/4} \approx 10^{-6}$, not better than with a linear scale.

Another difficulty comes from the renormalization of the peak position by the magnetic field (see Chap. 5) that implies we do not know a priori where to zoom precisely. For those reasons, the logarithmic discretization is not adapted to the magnetic field case. A more sophisticated method involving a dynamic discretization that depends on the frequency-derivative of the density of states might overcome these problems. However, let us remind the results from Chap. 5 showing that a finite magnetic field induces a decoherence rate that smears the resonance in the density of states; as a consequence a linear scale is often satisfactory enough for most cases.

[3]In addition, the position of the peaks depends on the spin of the Green's function.

[4]It can reduce to three peaks at some symmetric points.

Appendix D

French summary (Résumé en français)

Introduction

« Il serait en effet remarquable que la Nature se soit elle-même prémunie contre de nouvelles avancées dans la connaissance en se réfugiant derrière les difficultés analytiques du problème N corps »

Max Born, 1960

La physique N corps s'intéresse à des systèmes contenant un nombre important de particules et aux corrélations présentes entre elles. Dans de nombreux cas, les interactions au niveau microscopique impliquent de fantastiques modifications du comportement du système macroscopique. La physique à N corps est par conséquent à l'origine d'un grand nombre de problèmes théoriques en physique de la matière condensée, comme par exemple celui de la supraconductivité, de la condensation de Bose-Einstein ou des liquides de Luttinger.

Un nouveau champ pour l'étude des corrélations quantiques s'est ouvert dans les années 80, quand l'amélioration des techniques expérimentales a permis d'isoler des électrons dans des zones d'une longueur typique de quelques nanomètres (quelques dizaines d'atomes), appelées boîtes quantiques. Ceci ouvrait la porte à des descriptions à l'interface entre physique microscopique et physique macroscopique. La nouvelle discipline, baptisée physique mésoscopique, étudie des objets qui contiennent un nombre important de particules, mais qui restent néanmoins sensibles aux fluctuations quantiques. Elle présente un grand intérêt dans la perspective d'applications à l'industrie électronique, qui tend vers une miniaturisation constante de la taille des transistors.

Dans ce travail, j'étudie l'effet Kondo qui résulte de l'interaction d'échange à N corps d'électrons itinérants avec un état de spin localisé. Il a d'abord été étudié dans des systèmes macroscopiques suite à la mesure d'un important accroissement de la résistivité à basse température dans des alliages magnétiques dilués dans les années 30. L'explication de cette expérience a été donnée par J. Kondo environ 30 ans plus tard [46],

et réside dans des processus de diffusion cohérents dans lesquels les spins de l'impureté et de l'électron délocalisé sont échangés, donnant lieu à des contributions logarithmiques divergentes pour la résisitivité, et fournissant par là une explication satisfaisante aux résultats expérimentaux cités ci-dessus. Pour un moment magnétique de spin 1/2, A.H. Wilson a démontré que l'impureté localisée et les électrons de conduction délocalisés sont liés dans un état fondamental singulet de spin [105].

L'intérêt pour l'effet de Kondo a connu un grand renouveau ces dix dernières années après son observation dans des boîtes quantiques couplées par effet tunnel à des réservoirs bidimensionnels d'électrons de conduction [32, 20, 94]. Quand la boîte quantique contient un nombre impair d'électrons, elle porte un spin qui interagit avec les électrons de la conduction d'une façon fort similaire à celle décrite dans les alliages magnétiques.

A basse température, les processus de spin-flip à N corps impliqués dans l'effet de Kondo permettent aux électrons de conduction de passer librement d'un réservoir à l'autre. Par conséquent, le système est complètement transparent à la température nulle et la conductance linéaire atteint le quantum de conductance $2e^2/h$ (c.à.d. la valeur maximale pour un seul canal de conductance). Grâce à l'excellent contrôle de leurs paramètres (niveaux discrets d'énergie, énergie de charge, couplage boîte-réservoir), les boîtes quantiques ont ouvert de nouveaux horizons pour l'étude de l'effet de Kondo, soulevant des questions et ouvrant de nouvelles voies à la recherche.

Au niveau théorique, l'effet de Kondo dans les boîtes quantiques est souvent décrit à l'aide d'un modèle mis au point par P.W. Anderson [7] , dans lequel le moment magnétique résulte d'une répulsion de Coulomb localisée sur la boîte. Quand les potentiels chimiques des réservoirs sont égaux, le système est à l'équilibre et la plupart de ses propriétés sont à présent bien comprises, le modèle d'Anderson ayant été résolu grâce à une série de techniques perfectionnées. Cependant, la plupart de ces dernières échouent hors d'équilibre, d'où le grand intérêt pour des méthodes susceptibles de résoudre le problème de l'effet de Kondo dans ce cas, et d'une manière plus générale pour l'étude des effets de non-équilibre dans des systèmes d'électrons fortement corrélés.

Une caractéristique importante de l'effet Kondo hors d'équilibre est la décohérence de l'état fondamental singulet de spin associé à l'effet de Kondo, qui évolue vers un état stationnaire en présence de courant électrique. Dans ce cadre-là, la description théorique de l'effet de Kondo est beaucoup plus complexe, et aucun résultat exact n'a été obtenu jusqu'à présent, ce qui laisse la porte ouverte à des recherches supplémentaires. Dans cette thèse, le système est placé hors d'équilibre par l'application d'une différence de potentiel entre les deux réservoirs connectant la boîte. Une méthode des équations du mouvement hors d'équilibre est développée pour discuter certains aspects théoriques de la décohérence et ses conséquences sur le comportement physique du système. Je discute également d'autres sources de décohérence pour les processus de retournement spin, telles que la température et le champ magnétique.

D.1 Aspects généraux de l'effect Kondo et du transport électronique à travers les boîtes quantiques

Nous étudions des systèmes composés d'une boîte quantique connectée à deux réservoirs d'électrons de conductions, et modélisée par l'Hamiltonien d'Anderson [7]

$$\mathcal{H} = \mathcal{H}_{dot} + \mathcal{H}_{leads} + \mathcal{H}_{tun}, \tag{D.1}$$

où $\mathcal{H}_{dot}$ décrit la boîte, $\mathcal{H}_{leads}$ les réservoirs, et $\mathcal{H}_{tun}$ le passage entre les deux par effet tunnel.

La boîte isolée est décrite par

$$\mathcal{H}_{dot} = \sum_{i\sigma} \varepsilon_{i\sigma} \hat{n}_{i\sigma} + \frac{U}{2} \sum_{i\sigma} \sum_{i'\sigma' \neq i\sigma} \hat{n}_{i\sigma} \hat{n}_{i'\sigma'}, \tag{D.2}$$

avec $\hat{n}_{i\sigma} = f^{\dagger}_{i\sigma} f_{i\sigma}$, où $f_{i\sigma}$ est l'opérateur d'anihilation d'un électron de spin σ sur le niveau d'énergie i dans la boîte. L'énergie de charge $2e^2/C$ pour l'ajout d'un électron est modélisée par une répulsion Coulombienne U.

Les réservoirs sont modélisés par

$$\mathcal{H}_{leads} = \sum_{\alpha k\sigma} \varepsilon_k \hat{n}_{\alpha k\sigma}, \tag{D.3}$$

où $\hat{n}_{\alpha k\sigma} = c^{\dagger}_{\alpha k\sigma} c_{\alpha k\sigma}$ and $c^{\dagger}_{\alpha k\sigma}(c_{\alpha k\sigma})$ est l'opérateur de création (annihilation) d'un électron de nombre d'onde k et de spin σ dans les réservoir $\alpha(= L,\ R)$. La distribution des électrons dans les réservoirs est donnée par la distribution de Fermi-Dirac $f_\alpha(\varepsilon_k) = f(\varepsilon_k - \mu_\alpha)$, où μ_α est le potentiel chimique du réservoir α.

Enfin, nous avons le terme de couplage

$$\mathcal{H}_{tun} = \sum_{\alpha k i\sigma} \left(t_{\alpha i\sigma} c^{\dagger}_{\alpha k\sigma} f_{i\sigma} + H.c. \right). \tag{D.4}$$

Comme je l'ai indiqué dans l'introduction, l'effet Kondo peut être observé dans les boîtes quantiques lorsque celles-ci contiennent un nombre impair d'électrons et portent par conséquence un spin non nul qui interagit avec les électrons de conduction dans les réservoirs. Il en résulte une augmentation brutale de la conductance à basse température, atteignant la limite unitaire $G = 2e^2/h$ à température nulle. La principale signature expérimentale de l'effet Kondo est liée au caractère universel du comportement des observables en fonction des paramètres extérieurs lorsque ceux-ci sont normalisés par une échelle d'énergie appelée température Kondo T_K.

D.2 Formalisme des équations du mouvement

Afin de déterminer les propriétés de transport à travers le système, nous désirons obtenir la fonction de Green dans la boîte. Pour ce faire, nous dérivons une méthode des

équations du mouvement (EOM) qui décrit une hiérarchie infinie d'équations décrivant les fonctions de Green du système. Pour une fonction de Green comprenant deux opérateurs fermioniques $\hat{A}$ et $\hat{B}$ dans l'espace des fréquences

$$\langle\langle \hat{A}, \hat{B} \rangle\rangle = -i \lim_{\delta \to 0^+} \int_0^\infty d\tau \; e^{i(\omega + i\delta)\tau} \; \langle \{ \hat{A}(\tau), \hat{B}(0) \} \rangle, \tag{D.5}$$

nous avons les EOM suivantes

$$\omega \langle\langle \hat{A}, \hat{B} \rangle\rangle = \langle \{ \hat{A}, \hat{B} \} \rangle + \langle\langle [\hat{A}, \mathcal{H}], \hat{B} \rangle\rangle. \tag{D.6}$$

La hiérarchie infinie d'équations doit être tronquée à l'aide d'un schéma de découplage adéquat. Dans cette thèse, nous présentons une méthode de troncation à l'ordre 4 en t, permettant la description de phénomènes au-delà des approximations précédentes, comme nous le décrivons dans les chapitres suivants.

D.3 Propriétés du modèle d'Anderson à l'équilibre

Il existe une littérature abondante sur le modèle d'Anderson à l'équilibre, ce qui permet une vérification de la validité de notre schéma d'approximations. Nous discutons l'amélioration amenée par notre approche en comparaison avec les découplages à l'ordre inférieur, notamment en ce qui concerne la description de l'effet Kondo au point de symétrie particule-trou. En effet, la très utilisée approximation de Lacroix (ordre 2 en t) se révèle incapable de décrire l'effet Kondo à ce point en raison de la présence d'une anti-résonance non physique dans la densité d'états en $\omega = 2\varepsilon_d + U$.

Nous décrivons également la conductance différentielle. Dans le régime Kondo (un seul électron dans la boîte), nous voyons que la conductance augmente brusquement lorsque l'on décroît la température et que l'on atteint $T = T_K$. Nous observons un comportement inverse dans les autres régions en raison du blocage de Coulomb.

Enfin, nous montrons que la résonance à basse énergie dans la densité d'états dans la boîte est atténuée lorsque l'on augmente la température. Ceci est lié au taux de décohérence $\gamma_{2\sigma}$ des états excités liés à l'effet Kondo, dont l'expression est ici

$$\gamma_{2\sigma}^{(4)}(T) = T \sum_{\sigma'\sigma''} \frac{\Gamma_{\sigma'}\Gamma_{\sigma''}}{\pi} \; D_{\sigma''}^2(0) = T \frac{\Gamma^2 U^2}{\pi \varepsilon_d^2 \left(\varepsilon_d + U\right)^2} = \left(\nu J\right)^2 \pi T, \tag{D.7}$$

où nous définissons la constante de couplage d'échange $\nu J = \Gamma U / \pi \varepsilon_d (\varepsilon_d + U)$.

D.4 Transport hors d'équilibre

Ce chapitre est dédié au transport hors d'équilibre à travers la boîte quantique en l'absence de champ magnétique. De nombreux challenges subsistent dans ce cas en raison de désaccords persistant entre théorie et expériences.

Nous discutons la division de la résonance de Kondo dans la densité d'états à l'intérieur de la boîte en présence d'une différence de potentiel et l'atténuation des pics correspondants par les taux de relaxation des excitations. Cette atténuation est reliée au taux de décohérence $\gamma_{2\sigma}$ des états excités liés à l'effet Kondo par la différence de potentiel, dont l'expression est

$$\gamma_{2\sigma}(V) = \frac{\Gamma_L\Gamma_R}{\pi} D_\sigma^2(0) V + O(t^6) = \pi \frac{\Gamma_L\Gamma_R}{\Gamma^2} (\nu J)^2 V + O(J^3 V). \tag{D.8}$$

De l'atténuation des termes divergents, on dérive un critère pour le passage du régime de couplage fort à celui de couplage faible, où les corrections perturbatives sont suffisamment faibles pour être resommées, et nous en déduisons l'applicabilité de la méthode des équations du mouvement hors d'équilibre. Le régime de couplage faible est atteint lorsque le taux de décohérence $\gamma_{2\sigma}$ est supérieur à une échelle d'énergie T^* définie par

$$T^* = \begin{cases} \sqrt{eT_K^2 - V^2/4} & : \quad |V| < \sqrt{2e}\, T_K \\ eT_K^2/V & : \quad |V| > \sqrt{2e}\, T_K \end{cases} \tag{D.9}$$

Enfin, nous donnons les résultats numériques pour la conductance différentielle, qui développe une structure piquée à faible différence de potentiel, en accord avec les résultats expérimentaux et d'autres théories. La conductance différentielle présente un comportement universel en fonction de la différence de potentiel normalisée V/T_K.

D.5 Transport sous champ magnétique

Ce Chapitre est dédié à l'influence d'un champ magnétique sur le transport hors d'équilibre à travers une boîte quantique. A partir des EOM, nous dérivons une formule analytique pour la conductance différentielle, dont l'expression est

$$\frac{dI}{dV} \approx \frac{2e^2}{h}\frac{\pi^2}{16}(\nu J)^2 \left[5 + \frac{2}{\pi}\arctan\left(\frac{V-\Delta^*}{\gamma_2}\right)\right]\left(1 + \frac{\nu J}{2}\ln\left(\frac{\Delta^{*2}}{(V-\Delta^*)^2+\gamma_2^2}\right)\right) + \text{cst}, \tag{D.10}$$

où

$$\begin{aligned} \Delta^* &= \Delta + \frac{\Gamma}{2\pi}\left\{\ln\left|\frac{\varepsilon_d + \Delta/2}{\varepsilon_d - \Delta/2}\right| - \ln\left|\frac{\varepsilon_d - \Delta/2 + U}{\varepsilon_d + \Delta/2 + U}\right|\right\} + O(\Gamma^2/U) \\ &= (1 - \nu J/2)\,\Delta + O(J^2), \end{aligned} \tag{D.11}$$

et

$$\gamma_{2\sigma}|_{(V=\Delta)} = \frac{15\pi}{32}(\nu J)^2\left[\Delta + \frac{26}{3}\frac{\pi\nu K}{\Gamma}\Delta^2 + O(\Delta^3)\right] + O(J^3). \tag{D.12}$$

Le pic à différence de potentiel nulle dans la conductance différentielle est divisé par une énergie proche du double de l'énergie Zeeman, comme observé expérimentalement. La conductance différentielle est sensible à la décohérence γ_2 de l'état fondamental singulet de spin, ce qui a des conséquences sur la distance entre les pics. Une explication est proposée pour le passage d'un régime où cette distance est inférieure au double de la division de Zeeman à un autre régime où elle y est supérieure, comme cela a été observé expérimentalement. Enfin, nous proposons un montage expérimental capable de détecter une contribution additionnelle possible au taux de décohérence et ainsi vérifier nos hypothèses.

Conclusion

La compréhension des phénomènes hors d'équilibre dans les systèmes fortement corrélés pose des défis fondamentaux en physique théorique, soutenus par une intense activité expérimentale. J'ai tenté de relever ces défis au cours de ma thèse en vue de dévoiler certains des mystères dans ce nouveau champ d'étude. Sans ce document, j'ai essayé de coucher sur le papier les différentes idées qui me sont venues après de nombreux essais et erreurs et des discussions fructueuses avec mes collaborateurs. J'ai cherché ici à structurer ces idées de façon à les rendre accessibles à quiconque désireux de lire cette thèse avec attention.

L'intérêt pour l'effet Kondo, comme c'est le cas pour beaucoup d'autres effets à N corps en physique de la matière condensée, réside dans sa nature intrinsèquement quantique et de ses fortes conséquences à basse énergie sur la dépendance de toute observable en les paramètres extérieurs. L'effet Kondo est très intéressant pour l'étude des corrélations entre les particules dans des systèmes fortement corrélés, et il appelle à des méthodes théoriques sophistiquées allant au-delà des approximations de champ moyen. L'un de ces outils mathématiques est la technique des équations du mouvement, développée peu après l'explication de Kondo de la résistivité minimale à basse température dans des alliages magnétiques dilués. Elle a été beaucoup appliquée à l'équilibre à l'aide d'une série de schémas d'approximation, résumés au chapitre 2, mais peu d'extensions hors d'équilibre ont été proposées et aucune d'entre elles n'a su donner d'explication à la décohérence induite par une différence de potentiel. Les expériences nouvelles sur les boîtes quantiques hors d'équilibre et le manque de théorie précise pour les décrire ont appelé des approximations plus élaborées. Un nouveau schéma de découplage a été motivé au chapitre 2, qui se construit sur l'approximation de Lacroix tout en re-sommant des termes d'ordre plus élevé qui sont pertinents pour notre objectif.

A l'équilibre, j'ai montré que la nouvelle méthode que nous avons développée résout d'importantes faiblesses de l'approximation de Lacroix et élargit l'éventail d'applicabilité à toute série de paramètres, en particulier au point de symétrie particule-trou. Une comparaison avec les schémas d'approximation d'ordre inférieur a été donnée pour la densité des états dans la boîte et pour la conductance linéaire. Tandis que les caractéristiques de l'effet Kondo commencent à apparaître pour les troncations au second ordre dans le

coefficient t, les résultats sont plus stables à l'intérieur de l'extension au quatrième ordre développée dans ce travail en re-sommant les termes liés aux processus de diffusion avec spin-flip. La conductance linéaire atteint la limite unitaire $G = 2e^2/h$ à température nulle dans le régime de Kondo (par exemple quand le nombre total d'occupation(s) dans la boîte est d'un), tandis qu'elle tombe sous zéro dans des régions d'occupation paire en raison du blocage de Coulomb. Nous avons vu que la température détruit l'effet de Kondo, et produit dès lors une chute de la conductance dans la région d'occupation unique.

De façon plus importante, le schémas de découplage précédents considéraient que les excitations impliquées dans le processus de diffusion avec retournement du spin avaient une durée de vie limitée. Ceci est vrai pour une diffusion cohérente du spin-flip, mais nous savons que cet énoncé s'avère faux hors d'équilibre ou sous un champ magnétique. Dans ce dernier cas, les excitations acquièrent un taux de relaxation qui reflète la décohérence de l'état fondamental Kondo. Le nouveau schéma de découplage a permis l'investigation de problèmes hors d'équilibre, un taux de décohérence ayant été trouvé dans le cadre EOM. On a montré que ce taux de décohérence joue un rôle crucial dans l'applicabilité des équations du mouvement hors d'équilibre en amenant le système d'un régime de couplage fort, où les corrections perturbatrices sont importantes et les re-sommations mal contrôlées, à un régime de couplage faible, où les séries sont convergentes. Nous avons vu montré que ce dernier régime pouvait également être atteint par une augmentation de la température ou du champ magnétique. Expérimentalement, la quantité principale est la conductance différentielle, qui s'avère être une fonction universelle de la différence de potentiel normalisée V/T_K. Enfin, nous avons montré que notre méthode s'applique à une vaste gamme de paramètres en représentant la conductance dans une figure 3D en fonction de la différence de potentiel et du potentiel de grille.

L'influence du champ mangétique a également été étudiée. Une formule analytique a été dérivée pour la conductance différentielle à température nulle ; son expression est similaire à celle obtenue par la théorie des perturbations, si ce n'est que notre expression contient également l'effet de décohérence par la différence de potentiel. La conductance différentielle présente une structure avec deux pics séparés d'une distance de l'ordre de 2Δ, où Δ représente l'énergie de Zeeman. La valeur précise de l'écart entre les pics s'avère dépendre du taux de décohérence $\gamma_{2\sigma}$ et être en accord avec l'expérience. Finalement, nous proposons un nouveau schéma expérimental pour vérifier nos hypothèses.

Bibliography

[1] A., A. A. On anomalous temperature-dependence of resistivity of non-magnetic metals with a weak concentration of magnetic impurities. *Soviet Physics JETP-USSR 21*, 3 (1965), 660–&.

[2] Affleck, I., and Ludwig, A. W. Critical theory of overscreened kondo fixed points. *Nuclear Physics B 360*, 2-3 (1991), 641 – 696.

[3] Aguado, R., and Langreth, D. C. Out-of-equilibrium kondo effect in double quantum dots. *Phys. Rev. Lett. 85*, 9 (Aug 2000), 1946–1949.

[4] Amasha, S., Gelfand, I. J., Kastner, M. A., and Kogan, A. Kondo temperature dependence of the kondo splitting in a single-electron transistor. *Phys. Rev. B 72*, 4 (Jul 2005), 045308.

[5] Andergassen, S., Feinberg, D., Florens, S., Lavagna, M., Shiau, S., Simon, P., and Van Roermund, R. New trends for the Kondo effect in nanostructures. *International Journal of Nanotechnology 7*, 4-8, Sp. Iss. SI (2010), 438–455.

[6] Anders, F. B. Steady-state currents through nanodevices: A scattering-states numerical renormalization-group approach to open quantum systems. *Phys. Rev. Lett. 101*, 6 (Aug 2008), 066804.

[7] Anderson, P. W. Localized magnetic states in metals. *Phys. Rev. 124*, 1 (Oct 1961), 41–53.

[8] Andrei, N. Diagonalization of the kondo hamiltonian. *Phys. Rev. Lett. 45*, 5 (Aug 1980), 379–382.

[9] Andrei, N. Diagonalization of the kondo hamiltonian. *Phys. Rev. Lett. 45*, 5 (Aug 1980), 379–382.

[10] Appelbaum, J. "$s-d$" exchange model of zero-bias tunneling anomalies. *Phys. Rev. Lett. 17*, 2 (Jul 1966), 91–95.

[11] Appelbaum, J. A., and Penn, D. R. Localized correlations in narrow conduction bands. i. *Phys. Rev. 188*, 2 (Dec 1969), 874–887.

[12] Appelbaum, J. A., and Penn, D. R. Localized correlations in narrow conduction bands. ii. *Phys. Rev. B 3*, 3 (Feb 1971), 942–953.

[13] Barnes, S. E. New method for the anderson model. *Journal of Physics F: Metal Physics 6*, 7 (1976), 375–1383, ISSN = 0305–4608, Unique–ID = ISI:A1976CB49400018,.

[14] Borda, L., Zaránd, G., Hofstetter, W., Halperin, B. I., and von Delft, J. Su(4) fermi liquid state and spin filtering in a double quantum dot system. *Phys. Rev. Lett. 90*, 2 (Jan 2003), 026602.

[15] Bruus, H., and Flensberg, K. *Many-body quantum theory in condensed matter physics: an introduction*. Oxford Graduate Texts, 2004.

[16] Bulla, R., Costi, T. A., and Pruschke, T. Numerical renormalization group method for quantum impurity systems. *Rev. Mod. Phys. 80*, 2 (Apr 2008), 395–450.

[17] Clerk, A. A., Ambegaokar, V., and Hershfield, S. Andreev scattering and the kondo effect. *Phys. Rev. B 61*, 5 (Feb 2000), 3555–3562.

[18] Coleman, P., Hooley, C., and Parcollet, O. Is the quantum dot at large bias a weak-coupling problem? *Phys. Rev. Lett. 86*, 18 (Apr 2001), 4088–4091.

[19] Costi, T., and Hewson, A. A new approach to the calculation of spectra for strongly correlated systems. *Physica B: Condensed Matter 163*, 1-3 (1990), 179 – 181.

[20] Cronenwett, S. M., Oosterkamp, T. H., and Kouwenhoven, L. P. A Tunable Kondo Effect in Quantum Dots. *Science 281*, 5376 (1998), 540–544.

[21] Datta, S. *Electronic transport in mesoscopic systems*. Cambridge University Press, Cambridge, 1995.

[22] de Haas, W., de Boer, J., and van dën Berg, G. The electrical resistance of gold, copper and lead at low temperatures. *Physica 1*, 7-12 (1934), 1115 – 1124.

[23] Dias da Silva, L. G. G. V., Heidrich-Meisner, F., Feiguin, A. E., Büsser, C. A., Martins, G. B., Anda, E. V., and Dagotto, E. Transport properties and kondo correlations in nanostructures: Time-dependent dmrg method applied to quantum dots coupled to wilson chains. *Phys. Rev. B 78*, 19 (Nov 2008), 195317.

[24] Doyon, B., and Andrei, N. Universal aspects of nonequilibrium currents in a quantum dot. *Phys. Rev. B 73*, 24 (Jun 2006), 245326.

[25] Dworin, L. Anderson model of localized magnetic moments. i. high-temperature behavior. *Phys. Rev. 164*, 2 (Dec 1967), 818–840.

[26] Dworin, L. Anderson model of localized magnetic moments. ii. "derivation" of the integral equation. *Phys. Rev. 164*, 2 (Dec 1967), 841–856.

[27] Entin-Wohlman, O., Aharony, A., and Meir, Y. Kondo effect in complex mesoscopic structures. *Phys. Rev. B 71*, 3 (Jan 2005), 035333.

[28] Fazio, R., and Raimondi, R. Resonant andreev tunneling in strongly interacting quantum dots. *Phys. Rev. Lett. 80*, 13 (Mar 1998), 2913–2916.

[29] Feng, Q., Zhang, Y.-Z., and Jeschke, H. O. Fast impurity solver based on equations of motion and decoupling. *Phys. Rev. B 79*, 23 (Jun 2009), 235112.

[30] Glazman, L., and Pustilnik, M. Low-temperature transport through a quantum dot. *arXiv:cond-mat/0501007 (unpublished)* (Jul 2005).

[31] Glazman, L., and Raikh, M. Resonant kondo transparency of a barrier with quasilocal impurity states. *JETP Lett. 47* (1988), 452.

[32] Goldhaber-Gordon, D., Shtrikman, H., Mahalu, D., Abusch-Magder, D., Meirav, U., and Kastner, M. Kondo effect in a single-electron transistor. *Nature 391* (Jan 1998), 156.

[33] Haldane, F. D. M. Scaling theory of the asymmetric anderson model. *Phys. Rev. Lett. 40*, 6 (Feb 1978), 416–419.

[34] Han, J. E. Nonequilibrium electron transport in strongly correlated molecular junctions. *Phys. Rev. B 81*, 11 (Mar 2010), 113106.

[35] Han, J. E., and Heary, R. J. Imaginary-time formulation of steady-state nonequilibrium: Application to strongly correlated transport. *Phys. Rev. Lett. 99*, 23 (Dec 2007), 236808.

[36] Hewson, A. *The Kondo Problem to Heavy Fermions*. Cambridge Univ. Press, Cambridge, 1993.

[37] Hewson, A. C. Theory of localized magnetic states in metals. *Phys. Rev. 144*, 2 (Apr 1966), 420–427.

[38] Świrkowicz, R., Barnaś, J., and Wilczyński, M. Nonequilibrium kondo effect in quantum dots. *Phys. Rev. B 68*, 19 (Nov 2003), 195318.

[39] Jarillo-Herrero, P., Kong, J., van der Zant, H., Dekker, C., Kouwenhoven, L., and De Franceschi, S. Orbital Kondo effect in carbon nanotubes. *Nature 434*, 7032 (MAR 24 2005), 484–488.

[40] Jeschke, H. O., and Kotliar, G. Decoupling method for dynamical mean-field theory calculations. *Phys. Rev. B 71*, 8 (Feb 2005), 085103.

[41] Kaminski, A., Nazarov, Y. V., and Glazman, L. I. Universality of the kondo effect in a quantum dot out of equilibrium. *Phys. Rev. B 62*, 12 (Sep 2000), 8154–8170.

[42] Kane, C. L., and Fisher, M. P. A. Transmission through barriers and resonant tunneling in an interacting one-dimensional electron gas. *Phys. Rev. B 46*, 23 (Dec 1992), 15233–15262.

[43] Kashcheyevs, V., Aharony, A., and Entin-Wohlman, O. Applicability of the equations-of-motion technique for quantum dots. *Phys. Rev. B 73*, 12 (Mar 2006), 125338.

[44] Knight, W. D. Nuclear magnetic resonance shift in metals. *Phys. Rev. 76*, 8 (Oct 1949), 1259–1260.

[45] Kogan, A., Amasha, S., Goldhaber-Gordon, D., Granger, G., Kastner, M. A., and Shtrikman, H. Measurements of kondo and spin splitting in single-electron transistors. *Phys. Rev. Lett. 93*, 16 (Oct 2004), 166602.

[46] Kondo, J. Resistance minimum in dilute magnetic alloys. *Progress of Theoretical Physics 32*, 1 (1964), 37–49.

[47] Konik, R. M., Saleur, H., and Ludwig, A. Transport in quantum dots from the integrability of the anderson model. *Phys. Rev. B 66*, 12 (Sep 2002), 125304.

[48] Konik, R. M., Saleur, H., and Ludwig, A. W. W. Transport through quantum dots: Analytic results from integrability. *Phys. Rev. Lett. 87*, 23 (Nov 2001), 236801.

[49] Korringa, J. Nuclear magnetic relaxation and resonnance line shift in metals. *Physica 16*, 7-8 (1950), 601 – 610.

[50] Kouwenhoven, L., Marcus, C., Mceuen, P., Tarucha, S., Westervelt, R., and Wingreen, N. Electron transport in quantum dots. In *Mesoscopic Electron Transport* (1997), Sohn, LL and Kouwenhoven, LP and Schon, G, Ed., vol. 345 of *NATO Advanced Institutes Series, Series E, Applied Sciences*, pp. 105–214.

[51] Kubo, R. Generalized cumulant expansion method. *Journal of the Physical Society of Japan 17*, 7 (1962), 1100–1120.

[52] Lacroix, C. Density of states for the anderson model. *J. Phys. F. 11* (1981), 2389.

[53] Lacroix, C. Density of states for the asymmetric anderson model. *J. Appl. Phys. 53* (1982), 2131.

[54] Langreth, D. C. Friedel sum rule for anderson's model of localized impurity states. *Phys. Rev. 150*, 2 (Oct 1966), 516–518.

[55] Langreth, D. C., and Wilkins, J. W. Theory of spin resonance in dilute magnetic alloys. *Phys. Rev. B 6*, 9 (Nov 1972), 3189–3227.

[56] Lebanon, E., and Schiller, A. Measuring the out-of-equilibrium splitting of the kondo resonance. *Phys. Rev. B 65*, 3 (Dec 2001), 035308.

[57] Liu, T.-M., Hemingway, B., Kogan, A., Herbert, S., and Melloch, M. Magnetic-field-induced crossover to a nonuniversal regime in a kondo dot. *Phys. Rev. Lett. 103*, 2 (Jul 2009), 026803.

[58] Logan, D. E., and Dickens, N. L. Field-dependent dynamics of the anderson impurity model. *Journal of Physics: Condensed Matter 13*, 43 (2001), 9713.

[59] Luo, H.-G., Ying, J.-J., and Wang, S.-J. Equation of motion approach to the solution of the anderson model. *Phys. Rev. B 59*, 15 (Apr 1999), 9710–9713.

[60] Luttinger, J. M. Fermi surface and some simple equilibrium properties of a system of interacting fermions. *Phys. Rev. 119*, 4 (Aug 1960), 1153–1163.

[61] M., G., G., R. I., M., P. R., and D., G.-G. Kondo effect in mesoscopic quantum dots. *Preprint cond-mat/0611480v1* (2006).

[62] Mahan, G. D. *Many-Particle Physics*, third ed. Kluwer Academic/Plenum Publishers, New York, 2000.

[63] Mamada, H., and Takano, F. Self-consistent treatment of anderson model and magnetic susceptibility. *Progress of Theoretical Physics 43*, 6 (1970), 1458–1479.

[64] Martinek, J., Sindel, M., Borda, L., Barnaś, J., Bulla, R., König, J., Schön, G., Maekawa, S., and von Delft, J. Gate-controlled spin splitting in quantum dots with ferromagnetic leads in the kondo regime. *Phys. Rev. B 72*, 12 (Sep 2005), 121302.

[65] Martinek, J., Sindel, M., Borda, L., Barnaś, J., König, J., Schön, G., and von Delft, J. Kondo effect in the presence of itinerant-electron ferromagnetism studied with the numerical renormalization group method. *Phys. Rev. Lett. 91*, 24 (Dec 2003), 247202.

[66] Martinek, J., Utsumi, Y., Imamura, H., Barnaś, J., Maekawa, S., König, J., and Schön, G. Kondo effect in quantum dots coupled to ferromagnetic leads. *Phys. Rev. Lett. 91*, 12 (Sep 2003), 127203.

[67] Mehta, P., and Andrei, N. Nonequilibrium transport in quantum impurity models: The bethe ansatz for open systems. *Phys. Rev. Lett. 96*, 21 (Jun 2006), 216802.

[68] Meir, Y., and Wingreen, N. S. Landauer formula for the current through an interacting electron region. *Phys. Rev. Lett. 68*, 16 (Apr 1992), 2512–2515.

[69] Meir, Y., Wingreen, N. S., and Lee, P. A. Transport through a strongly interacting electron system: Theory of periodic conductance oscillations. *Phys. Rev. Lett. 66*, 23 (Jun 1991), 3048–3051.

[70] Meir, Y., Wingreen, N. S., and Lee, P. A. Low-temperature transport through a quantum dot: The anderson model out of equilibrium. *Phys. Rev. Lett. 70*, 17 (Apr 1993), 2601–2604.

[71] Monreal, R. C., and Flores, F. Kondo resonance decoherence caused by an external potential. *Phys. Rev. B 72*, 19 (Nov 2005), 195105.

[72] Mora, C., Vitushinsky, P., Leyronas, X., Clerk, A. A., and Le Hur, K. Theory of nonequilibrium transport in the $su(n)$ kondo regime. *Phys. Rev. B 80*, 15 (Oct 2009), 155322.

[73] Nagaoka, Y. Self-consistent treatment of kondo's effect in dilute alloys. *Phys. Rev. 138*, 4A (May 1965), A1112–A1120.

[74] Ng, T.-K. ac response in the nonequilibrium anderson impurity model. *Phys. Rev. Lett. 76*, 3 (Jan 1996), 487–490.

[75] Ng, T. K., and Lee, P. A. On-site coulomb repulsion and resonant tunneling. *Phys. Rev. Lett. 61*, 15 (Oct 1988), 1768–1771.

[76] Nozières, P. A "fermi-liquid" description of the kondo problem at low temperatures. *Journal of Low Temperature Physics 17*, 1 (Oct 1974), 31–42.

[77] Nozières, P. Impuretés magnétiques et effet kondo. *Ann. Phys. Fr. 10*, 19-35 (1985), 19.

[78] Paaske, J., Rosch, A., Kroha, J., and Wölfle, P. Nonequilibrium transport through a kondo dot: Decoherence effects. *Phys. Rev. B 70*, 15 (Oct 2004), 155301.

[79] Parcollet, O., and Hooley, C. Perturbative expansion of the magnetization in the out-of-equilibrium kondo model. *Phys. Rev. B 66*, 8 (Aug 2002), 085315.

[80] Parks, J. J., Champagne, A. R., Hutchison, G. R., Flores-Torres, S., Abruña, H. D., and Ralph, D. C. Tuning the kondo effect with a mechanically controllable break junction. *Phys. Rev. Lett. 99*, 2 (Jul 2007), 026601.

[81] Poo, G. S. Magnetic field effects in the anderson model of dilute magnetic alloys. i. self-consistent solution. *Phys. Rev. B 11*, 11 (Jun 1975), 4606–4613.

[82] Pustilnik, M., and Glazman, L. Kondo effect in quantum dots. *Journal of Physics: Condensed Matter 16*, 16 (2004), R513.

[83] rd, J. N., Cobden, D., and Lindelof, P. Kondo physics in carbon nanotubes. *Nature (London) 408* (Nov 2000), 342.

[84] Roch, N., Florens, S., Bouchiat, V., Wernsdorfer, W., and Balestro, F. Quantum phase transition in a single-molecule quantum dot. *Nature 453*, 7195 (MAY 29 2008), 633–U3.

[85] Roch, N., Winkelmann, C. B., Florens, S., Bouchiat, V., Wernsdorfer, W., and Balestro, F. Kondo effects in a C-60 single-molecule transistor. *Physica Status Solidi B-Basic Solid State Physics 245*, 10, Sp. Iss. SI (OCT 2008), 1994–1997.

[86] Rosch, A., Kroha, J., and Wölfle, P. Kondo effect in quantum dots at high voltage: Universality and scaling. *Phys. Rev. Lett. 87*, 15 (Sep 2001), 156802.

[87] Rosch, A., Paaske, J., Kroha, J., and Wölfle, P. Nonequilibrium transport through a kondo dot in a magnetic field: Perturbation theory and poor man's scaling. *Phys. Rev. Lett. 90*, 7 (Feb 2003), 076804.

[88] Rosch, A., Paaske, J., Kroha, J., and Wölfle, P. Nonequilibrium transport through a kondo dot in a magnetic field: Perturbation theory and poor man's scaling. *Phys. Rev. Lett. 90*, 7 (Feb 2003), 076804.

[89] Rudin, W. *Functional Analysis*. McGraw-Hill, New York, 1973.

[90] Sarachik, M. P., Corenzwit, E., and Longinotti, L. D. Resistivity of mo-nb and mo-re alloys containing 1 *Phys. Rev. 135*, 4A (Aug 1964), A1041–A1045.

[91] Sasaki, S., De Franceschi, S., Elzerman, J., van der Wiel, W., Eto, M., Tarucha, S., and Kouwenhoven, L. Kondo effect in an integer-spin quantum dot. *Nature 405*, 6788 (JUN 15 2000), 764–767.

[92] Schiller, A., and Hershfield, S. Exactly solvable nonequilibrium kondo problem. *Phys. Rev. B 51*, 18 (May 1995), 12896–12899.

[93] Schlosshauer, M. Decoherence, the measurement problem, and interpretations of quantum mechanics. *Rev. Mod. Phys. 76*, 4 (Feb 2005), 1267–1305.

[94] Schmid, J., Weis, J., Eberl, K., and v. Klitzing, K. A quantum dot in the limit of strong coupling to reservoirs. *Physica B: Condensed Matter 256-258* (1998), 182 – 185.

[95] Schoeller, H., and Reininghaus, F. Real-time renormalization group in frequency space: A two-loop analysis of the nonequilibrium anisotropic kondo model at finite magnetic field. *Phys. Rev. B 80*, 4 (Jul 2009), 045117.

[96] Schrieffer, J. R., and Wolff, P. A. Relation between the anderson and kondo hamiltonians. *Phys. Rev. 149*, 2 (Sep 1966), 491–492.

[97] Tarucha, S., Austing, D. G., Honda, T., van der Hage, R. J., and Kouwenhoven, L. P. Shell filling and spin effects in a few electron quantum dot. *Phys. Rev. Lett. 77*, 17 (Oct 1996), 3613–3616.

[98] Theumann, A. Self-consistent solution of the anderson model. *Phys. Rev. 178*, 3 (Feb 1969), 978–984.

[99] Utsumi, Y., Martinek, J., Schön, G., Imamura, H., and Maekawa, S. Nonequilibrium kondo effect in a quantum dot coupled to ferromagnetic leads. *Phys. Rev. B 71*, 24 (Jun 2005), 245116.

[100] van der Wiel, W. G., Franceschi, S. D., Fujisawa, T., Elzerman, J. M., Tarucha, S., and Kouwenhoven, L. P. The Kondo Effect in the Unitary Limit. *Science 289*, 5487 (2000), 2105–2108.

[101] Van Roermund, R., Shiau, S.-y., and Lavagna, M. Anderson model out of equilibrium: Decoherence effects in transport through a quantum dot. *Phys. Rev. B 81*, 16 (Apr 2010), 165115.

[102] White, S. R. Density matrix formulation for quantum renormalization groups. *Phys. Rev. Lett. 69*, 19 (Nov 1992), 2863–2866.

[103] Wiegmann, P. Towards an exact solution of the anderson model. *Physics Letters A 80*, 2-3 (1980), 163 – 167.

[104] Wilhelm, U., Schmid, J., Weis, J., and v. Klitzing, K. Experimental evidence for spinless kondo effect in two electrostatically coupled quantum dot systems. *Physica E: Low-dimensional Systems and Nanostructures 14*, 4 (2002), 385 – 390.

[105] Wilson, K. G. The renormalization group: Critical phenomena and the kondo problem. *Rev. Mod. Phys. 47*, 4 (Oct 1975), 773–840.

[106] Wingreen, N. S., and Meir, Y. Anderson model out of equilibrium: Noncrossing-approximation approach to transport through a quantum dot. *Phys. Rev. B 49*, 16 (Apr 1994), 11040–11052.

[107] Wöger, W., and Zittartz, J. Impurity soin dynamics in Kondo problem. *Zeitschrift für Physik 261*, 1 (1973), 59–70.

[108] Yamada, K. Perturbation Expansion for the Anderson Hamiltonian. II. *Progress of Theoretical Physics 53* (Apr. 1975), 970–986.

[109] Zubarev, D. Double-time green functions in statistical physics. *Sov. Phys. Usp. 3* (1960), 320.